BENZODITHIOPHENE AND BENZOTRIAZOLE BEARING ALTERNATING COPOLYMERS, EFFECT OF THIOPHENE AND BITHIOPHENE π-BRIDGES ON PHOTOVOLTAIC PROPERTIES

A THESIS SUBMITTED TO
THE GRADUATE SCHOOL OF NATURAL AND APPLIED SCIENCES
OF
MIDDLE EAST TECHNICAL UNIVERSITY

BY

ÇAĞLA İSTANBULLUOĞLU

IN PARTIAL FULFILLMENT OF THE REQUIREMENTS
FOR
THE DEGREE OF MASTER OF SCIENCE
IN
CHEMISTRY

AUGUST 2016

Approval of the thesis:

BENZODITHIOPHENE AND BENZOTRIAZOLE BEARING ALTERNATING COPOLYMERS, EFFECT OF THIOPHENE AND BITHIOPHENE π-BRIDGES ON PHOTOVOLTAIC PROPERTIES

submitted by **ÇAĞLA İSTANBULLUOĞLU** in partial fulfillment of the requirements for the degree of **Master of Science in Chemistry Department, Middle East Technical University** by,

Prof. Dr. Gülbin Dural Ünver
Dean, Graduate School of **Natural and Applied Sciences** _____

Prof. Dr. Cihangir Tanyeli
Head of Department, **Chemistry** _____

Prof. Dr. Levent Toppare
Supervisor, **Chemistry Dept., METU** _____

Examining Committee Members:

Assoc. Prof. Dr. Ali Çırpan
Chemistry Dept., METU _____

Prof. Dr. Levent Toppare
Chemistry Dept., METU _____

Assoc. Prof. Dr. Yasemin Arslan Udum
Advanced Technologies Dept., Gazi University _____

Assoc. Prof. Dr. Ertuğrul Şahmetlioğlu
Chemistry and Chemistry Processing Dept., Erciyes University _____

Assist. Prof. Dr. Görkem Günbaş
Chemistry Dept., METU _____

Date: 25.08.2016

I hereby declare that all information in this document has been obtained and presented in accordance with academic rules and ethical conduct. I also declare that, as required by these rules and conduct, I have fully cited and referenced all material and results that are not original to this work.

Name, Last Name: ÇAĞLA İSTANBULLUOĞLU

Signature :

ABSTRACT

BENZODITHIOPHENE AND BENZOTRIAZOLE BEARING ALTERNATING COPOLYMERS, EFFECT OF THIOPHENE AND BITHIOPHENE π-BRIDGES ON PHOTOVOLTAIC PROPERTIES

İstanbulluoğlu, Çağla

M.S., Department of Chemistry

Supervisor : Prof. Dr. Levent Toppare

August 2016, 104 pages

In this study, two novel 1,2,3-benzotriazole and benzodithiophene bearing alternating copolymers were synthesized via Stille coupling reaction. Benzodithiophene was used as the donor moiety due to its strong electron donating ability and planar structure. Benzotriazole moiety was incorporated as the acceptor unit due to its electron deficient nature. Moreover, thiophene (P1) and bithiophene (P2) conjugated moieties were incorporated between donor and acceptor units in order to investigate the effect of π-bridge. Electrochemical, spectroelectrochemical and kinetic studies were performed. Since both polymers revealed ambipolar character, HOMO-LUMO energy levels were calculated from cyclic voltammograms. As a result of kinetic studies, good stabilities and low switching times were recorded. Moreover, bithiophene bearing copolymer showed enhanced percent transmittance and low switching time at NIR region when compared with thiophene bearing polymer.

Organic photovoltaic applications of the polymers were conducted with a device structure of ITO/PEDOT:PSS/POLYMER:$PC_{70}BM$/LiF/Al The analysis of the photovoltaic devices was performed under standard AM 1.5G illumination. Alkyl chains on the donor and acceptor moieties enhanced the solubility of the polymers in organic solvents. Thickness and morphology of the devices were examined via AFM and TEM studies. As a result of several optimization studies, power conversion efficiencies were reached to 2.12 % and 1.20 % for P1 and P2, respectively.

P1 was used as active layer for OLED applications which were constructed with a device structure of ITO/PEDOT:PSS/P1/LiF/Al. Red emissive OLED was produced with CIE coordinates (x,y) of 0.65, 0.34, respectively.

Keywords: Donor-Acceptor approach, benzotriazole, π-bridge, organic solar cells, organic light emitting diodes

ÖZ

BENZODİTİYOFEN VE BENZOTRİAZOL İÇEREN SIRALI KOPOLİMERLERDE TİYOFEN VE BİTİYOFEN π-KÖPRÜLERİNİN FOTOVOLTAİK ÖZELLİKLERE ETKİSİ

İstanbulluoğlu, Çağla

Yüksek Lisans, Kimya Bölümü

Tez Yöneticisi : Prof. Dr. Levent Toppare

Ağustos 2016 , 104 sayfa

Gerçekleştirilen bu tez çalışmasında, iki yeni benzotriazol ve benzoditiyofen içeren sıralı kopolimerler Stille kenetlenme reaksiyonu ile sentezlenmiştir. Güçlü electron verici özelliği ve yüzeysel yapısı sebebiyle benzoditiyofen ünitesi donör olarak kullanılmıştır. Elektronca eksik yapısı benzotriazol unitesini akseptör molekül olarak kullanmamızı sağlamıştır. Bunun yanı sıra, π-köprüsü etkisini incelemek için tiyofen (P1) ve bitiyofen (P2) konjüge üniteleri donör akseptör üniteleri arasına yerleştirilmiştir. Polimerlerin elektrokimyasal, spektroelektrokimyasal ve kinetik çalışmaları yapılmıştır. Polimerlerin negatif ve pozitif doplanma özelliklerini aynı anda barındırmasından dolayı, enerji seviyeleri döngüsel voltametri ile karakterize edilmiştir. Kronoamperometri çalışmalarında her iki polimer de yüksek kararlılık ve hızlı anahtarlanma zamanı gibi özelliklere sahiptir. Yakın kızılötesi bölgesinde bitiyofen unitesi içeren polimer tiyofen unitesi

içeren polimere kıyasla yüksek optik kontrast ve hızlı anahtarlanma süresine sahiptir.

Organik güneş gözelerinin yapımında ITO/PEDOT:PSS/POLİMER:$PC_{70}BM$/-LiF/METAL dizilimi izlenmiştir ve analizleri standart AM 1,5G aydınlatma ile yapılmıştır. Donör ve akseptör ünitelerindeki alkil zincirleri polimerlerin organik çözücülerdeki çözünürlüklerinin artmasını sağlamıştır. AFM ve TEM çalışmaları ile kalınlık ve morfoloji incelemeleri yapılmıştır. Birçok optimizasyon çalışmalarının sonucunda P1 ve P2 molekülleri ile üretilen güneş gözeleri sırasıyla en yüksek 2.12 % ve 1.20 % güç çevirim verimi göstermiştir.

Organik ışık saçan diyot çalışmalarında P1 aktif tabaka olarak kullanılmıştır ve kırmızı ışık yayan diyot ITO/PEDOT:PSS/P1/LiF/METAL cihaz yapısıyla elde edilmiştir. Üretilen diyotunun CIE koordinatları (x,y); 0.65, 0.34 olarak bulunmuştur.

Anahtar Kelimeler: Donör-Akseptör yaklaşımı, benzotriazol, π köprüsü, organik güneş gözeleri, organik ışık yayan diyotlar

To my lovely family and Batu...

ACKNOWLEDGMENTS

First and foremost, I would like to express my sincere gratitude to my supervisor Prof. Dr. Levent Toppare for his endless patience, encouragement, enthusiasm and continuous support throughout my time as his student. His guidance and immense knowledge helped me all the time during my Master's study. He showed me how to look at challenges from as many different aspects as possible. It was a great pleasure and honor to work with him.

A very special thank goes out to Assoc. Prof. Dr. Ali Çırpan for his support and understanding. His critical comments and suggestions on my research have been invaluable. He was always accessible and willing to help any problem I have encountered.

I must also acknowledge Assoc. Prof. Dr. Yasemin Arslan Udum and Şerife Özdemir Hacıoğlu for their contributions on electrochemical and spectroelectrochemical characterizations.

I would also like to thank Assist. Prof. Dr. Görkem Günbaş for his diligent guidance, valuable suggestions, brilliant comments and for his encouragements to my research.

I would like to thank Gönül Hızalan Özsoy for her invaluable feedbacks on my research, support and sincere encouragements that always keep me eager to work during my studies. I have learnt so many things from her enormous knowledge about organic photovoltaics. Whenever I felt desperate, I found her lovely hug right beside me and I know it will be there forever.

I am grateful to Seza Göker for her excellent guidance, caring and continuous support. I have learnt organic synthesis from her knowledge and experience. She has influenced me and supported me during this work both scientifically and personally. We have shared great moments and sleepless nights during our

synthesis. She will always be more than a friend for me.

I would especially like to thank my lovely lab-mate Ebru Işık for the wonderful times we shared and her continuous friendship whenever I was in need. She has always been a constant source of encouragement during my studies. Her contributions were the most valuable to me. It would have been a lonely lab without her.

My sincere thanks also go to my dear friend, Janset Turan, who was always ready to help me with a lovely smile. Her endless support, motivation and understanding are irreplaceable for me.

I would like to thank Melis Kesik Mancar and Seda Kutkan for coffee breaks, sharing great moments, their nice friendship, endless moral support and being thoughtful.

I would like to thank Merve İleri for her real friendship. I will always remember the excellent moments we shared while working in the lab until midnights.

I am also thankful Ece Aktaş and Şevki Can Cevher for their amazing friendship and support. We spent excellent times together. They made these years funny and endurable.

My warmest thanks go to Dr. Derya Baran who truly made a difference in my life. I have been extremely lucky to have a mentor, a friend and a sister who cared so much about both my career and my life. I know she has always been there and she will always be whenever I need.

I thank Gizem Aktaş for being always right beside me with her true friendship and endless understanding. Wherever we will go, I ensure you with no doubt that you will remain in my life.

I would like to give my special thanks to Özlem Çetin and Anıl Ulukan for being one of my best friends since undergraduate years. Their real friendship has left me precious memories and happy times. They showed me that the distance means nothing in real friendships.

I would also like to say a heartfelt thank you to my parents, to whom I owe my life for their constant love, encouragement and moral support. I have no suitable word that can fully describe my mother's everlasting love to me. I owe a lot to my precious brother Sarp İstanbulluoğlu and sister-in-law Selin Efendi İstanbulluoğlu for always believing in me and encouraging me to follow my dreams. I cannot imagine being the person I am today without such a great brother through the years.

Last but not the least, I would like to dedicate this thesis to love of my life and my best friend Batu. Even if he lives halfway around the world, the time difference has never dismayed him and he was always there for me at the cost of sleepless nights. I know that the time we spend apart will make our love grow stronger. This thesis would not have been possible without his extraordinary support, endless love and continuous encouragement.

TABLE OF CONTENTS

LIST OF TABLES

TABLES

LIST OF FIGURES

FIGURES

LIST OF ABBREVIATIONS

η	Power conversion efficiency
$(SN)_x$	Poly(sulfurnitride)
ACN	Acetonitrile
AFM	Atomic force microscopy
Alq3	Tris(8-hydroxyquinoline) aluminum
AM 1.5G	Air mass 1.5 global
BHJ	Bulk Heterojunction Solar Cell
CIE	La Commission Internationale de l'Eclairage Conducting Polymer
CV	Cyclic Voltammetry
D-A	Donor-Acceptor
DCM	Dichloromethane
DSC	Differential scanning calorimetry
E_g	Band gap
ECD	Electrochromic device
EDOT	3,4-Ethylenedioxythiophene
EL	Electroluminescence
EQE	External quantum efficiency
Fc	Ferrocene
FF	Fill factor
GPC	Gel permation chromatography
HOMO	Highest Occupied Molecular Orbital
HRMS	High Resolution Mass Spectrometer
IPCE	Incident Power to Current Efficiency
ITO	Indium Tin Oxide
J_{sc}	Short circuit current density
L, a, b	Luminance, hue, saturation
LiF	Lithium fluoride
LUMO	Lowest Unoccupied Molecular Orbital

Mn	Number average molecular weight
Mw	Weight average molecular weight
NIR	Near infrared
NMR	Nuclear Magnetic Resonance Spectrometer
OLED	Organic Light Emitting Diode
OPV	Organic Photovoltaic
PA	Polyacetylene
PCBM	[6,6]-Phenyl C 71 butyric acid methyl ester
PDI	Polydispersity Index
PEDOT	Polyethylene dioxythiophene
P_{in}	Power of the incident light
PL	Photoluminescence
P_{max}	Maximum power
PSS	Polystyrenesulfonate
RGB	Red-green-blue
$TBAPF_6$	Tetrabutylammonium hexafluorophosphate
TEM	Transmission electron microscopy
TGA	Thermal gravimetric analysis
THF	Tetrahydrofuran
TLC	Thin Layer Chromatography
UV	Ultraviolet
Vis	Visible
V_{oc}	Open circuit voltage
WF	Work Function

CHAPTER 1

INTRODUCTION

1.1 Organic Semiconductors

Organic semiconductors cover all the materials that consist of alternating single and double bonds (conjugation). In conjugated systems, sp^2 hybridized carbon atoms form σ-bonds and remaining p-orbitals delocalize on the polymeric backbone forming weak π-bonds. As a result of electron delocalization, materials become conductive. Organic semiconductors can be classified into two; high molecular weight materials (polymers) and low molecular weight materials (small molecules and oligomers).

Organic semiconductors have been under extensive research over the years because of their unique advantages such as low cost, light weight, solution processability, flexibility, simple device fabrication process and easy tunability on chemical structure [1–6]. Conducting polymers have received considerable interest as active layer materials for organic photovoltaics (OPVs) [7,8], organic light-emitting diodes (OLEDs) [9, 10], organic field effect transistors (OFETs) [11], and electrochromic devices (ECDs) [12, 13].

The discovery of supernal conductivity in perylene-iodine complex led scientists focus on organic conducting polymers in 1954. Moreover, investigation of electrical conductivity of chemically doped polyacetylene (PA) opened a new research era which is application of organic semiconductors [14].

Discovery of organic semiconductors began at the same time in two different

countries; USA and Japan. Alan J. Heeger and Alan G. MacDiarmid, in USA, polymerized sulfur nitride $(SN)_x$ from S_2N_2 crystals with an electrical conductivity of $2.5 \times 10^3\,\mathrm{S\,cm^{-1}}$. Moreover, they realized that conductivity of this inorganic polymer was enhanced with decreasing temperature (10 K). In addition to this, they increased the conductivity further from 10^4 to 10^7 by exposing reaction medium to Br_2 and I_2 vapors [15, 16].

At the same time, in Japan, Hideki Shirakawa and his students achieved to synthesize thin film polyacetylene (PA) via adding iodine vapor into polymerization set-up accidentally thousand times more than they were supposed to add which caused an injection of charges to the polymer chain and the following reaction occurred.

$$\frac{3}{2}x(I_2) + (CH)_n \longrightarrow (CH)^{+x} + x(I_3^-) \tag{1.1}$$

As a result of oxidation reaction with iodine vapor, electron vacancy on the polymer backbone; namely hole is generated hence, charge mobility can be provided on the polymer chains. This accidentally discovered overall process, later on, was called as doping process.

Infrared spectra (IR) experiments showed that temperature affects the stereochemistry of PA thin film. Trans and cis isomers of PA have different resistivities and energy gaps. The conversion between cis to trans isomers occurs irreversibly at higher temperatures around 145 °C as shown in Figure 1.1. Electronic studies of these two different forms revealed that trans PA has $1 \times 10^4\,\Omega\,\mathrm{cm}$ resistivity and 0.56 eV energy gap, whereas cis PA has $2.4 \times 10^8\,\Omega\,\mathrm{cm}$ resistivity and 0.93 eV energy gap [17, 18].

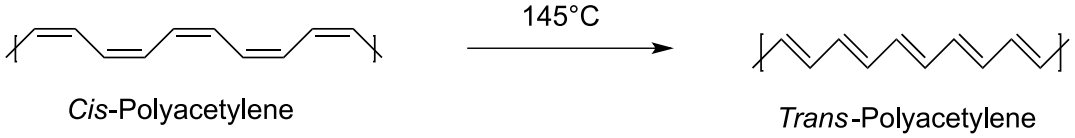

Figure 1.1: Irreversible isomerization of polyacetylene.

Later on, Heeger, MacDiarmid and Shirakawa have collaborated and started to work on polymerization of PA together. They used different halogen vapors for polymerization reactions and obtained the highest $38\,\mathrm{S\,cm^{-1}}$ conductivity at room temperature with I_2 vapor treatment [19]. After all these investigations, further developments on conducting polymers has begun with the Nobel Prize in Chemistry in 2000. In 1974, Alan J. Heeger, Alan G. MacDiarmid and Hideki Shirakawa have proved that polyacetylene can nearly be as conductive as a metal [20]. This spectacular invention has opened a unique era and usage of the organic conductive polymers has gained a big acceleration.

Although doped-polyacetylene was the first conducting polymer, further characterizations and applications of PA were limited due to its lack of solubility and high sensitivity to ambient atmospheric conditions. As a result, over the last two decades there has been huge interest to find new conjugated polymers with high conductivity and better stability. Some of the examples from literature are given in Figure 1.2.

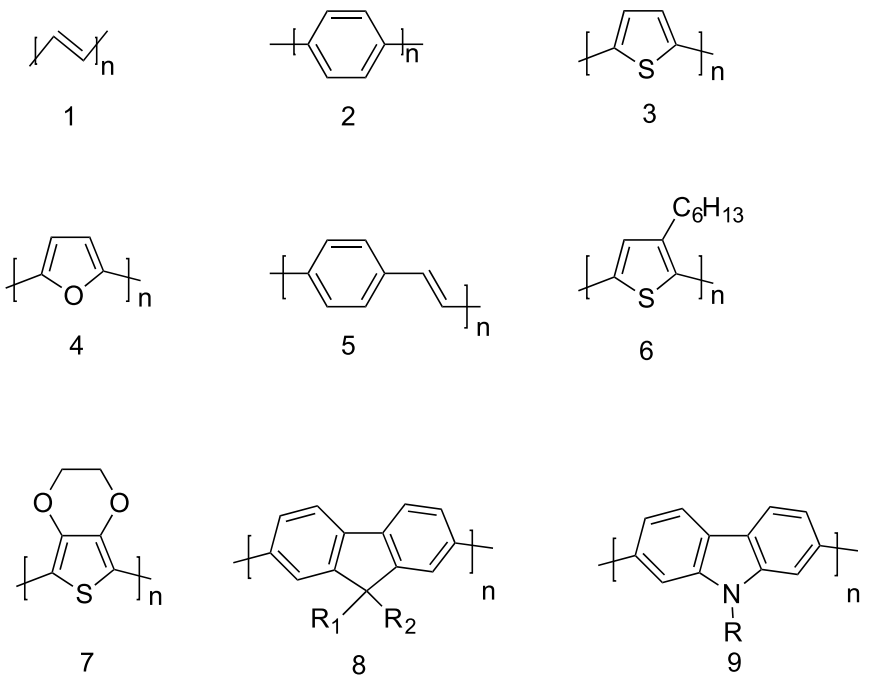

Figure 1.2: The structures of common polymers (1) polyacetylene, (2) polyparapheneylene, (3) polythiophene, (4) polyfuran, (5) poly(p-phenylenevinylene), (6) poly(3,4-ethyelenedioxy-thiophene), (7) polyethylenedioxythiophene, (8) polyfuorene, (9) polycarbazole.

1.2 Polymerization Methods

Several methods for the synthesis of semiconducting polymers have been developed such as metathesis polymerization, Grignard reaction, photochemical polymerization, ring opening metathesis polymerization, solid - state polymerization, plasma polymerization, pyrolysis. Among these methods, chemical polymerization and electropolymerization are the most performed ones. In this thesis, electropolymerization and Stille polymerization will be discussed.

1.2.1 Stille Cross Coupling

The Stille cross-coupling is 4 step cyclic reaction between organohalide and organostannes. The general mechanism was given in Figure 1.3. The first step is oxidative addition of organohalide and Pd(0) to form a Pd(II) complex. The following step is transmetallation, R group of the organostanne and halide anion of the palladium catalyst switch places. Reductive elimination is the last step forming palladium catalyst back and the cycle continues [21].

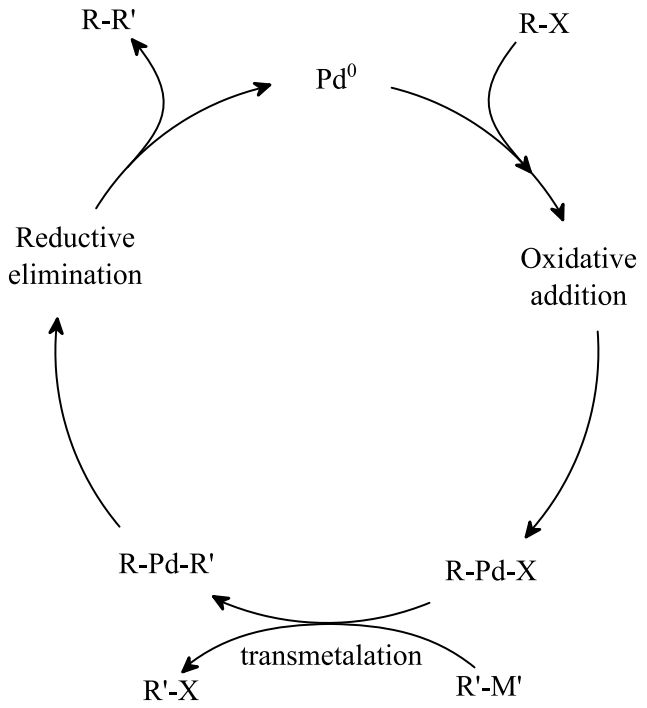

Figure 1.3: Mechanism of palladium-catalyzed cross coupling reaction.

A great variety of molecules can be synthesized via Stille cross coupling reaction because this reaction can tolerate many types of functional groups. For further studies of conducting polymers, highly soluble and high molecular weight polymers are required. The advantage of Stille coupling is to obtain polymers under mild conditions however, the only problem is toxicity of the tri-n-butyltin derivatives [22, 23].

1.2.2 Electrochemical Polymerization and Mechanism

For electrochemical polymerization, a three electrode system consisting of working, reference and counter electrodes is used. Monomer, organic solvent and supporting electrolyte containing solution are used to carry out polymerization. Appropriate voltage is applied and then polymer film is coated onto working electrode surface. Electrochemical polymerization is an easy and quick method, as well as promising since it can easily be utilized for further electrochemical, spectroelectrochemical and kinetic characterizations without any purification. Due to lack of solubility of the polymer film, gel permeation chromatography (GPC) and nuclear magnetic resonance (NMR) cannot be carried out to characterize electrochemically synthesized polymers.

General electropolymerization mechanism was given in Figure 1.4. Electropolymerization starts with the formation of radical cation by oxidation of a monomer. Electron transfer reaction is faster than the monomer diffusion from the bulk solution, resulting in the generation of high concentration of radical cations near the working electrode surface. The product can be coupled with either a second radical cation which produces dication dimer or with an another monomer that forms radical cation dimer. In the case of radical-radical coupling, by loss of two protons or rearomatization formation of dimer dication occurs. Upon applied potential, radical form of dimer is generated and process continues with additional coupling of radical dimer and monomer. In the radical cation and monomer coupling mechanism dimer is produced by losing two protons. In addition, neutral dimer goes into oxidation process and again radical cation formation occurs. Moreover, trimer is formed by coupling of radical cation dimer and monomer.

Through these steps, polymerization process continues and polymer adheres on the working electrode surface due to the decrease in its solubility [24–26].

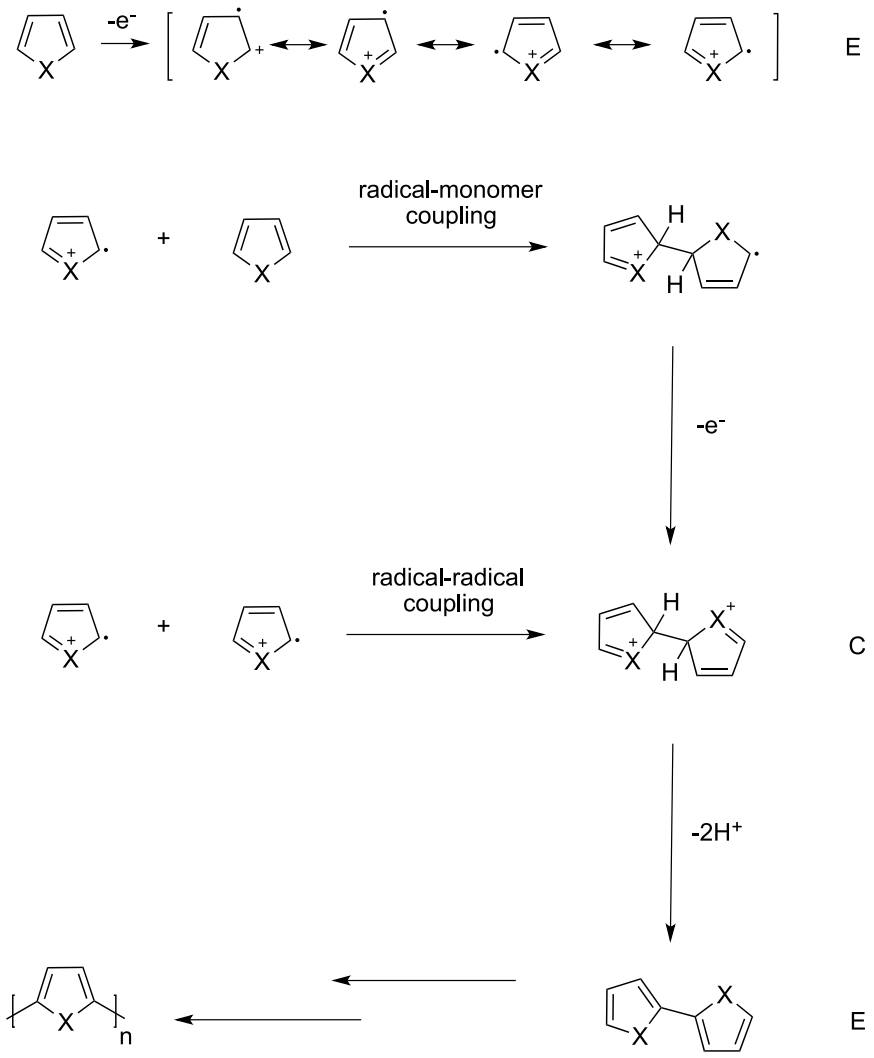

Figure 1.4: Electropolymerization mechanism of heterocycles X=O, S or N-R (ECE).

1.3 Characterization of Conducting Polymers

There are several techniques for characterization of polymers. Chemical structure of the polymer is proven with Nuclear Magnetic Resonance (NMR). Redox properties of electrochemical polymers can be analyzed by cyclic voltammetry.

HOMO and LUMO energy levels and electronic band gaps (E_g) can be calculated from single scan cyclic voltammograms. Moreover, spectroscopic characterizations are performed to investigate π-π^* electronic transition and to find optical band gap from maximum absorbance of the electro active polymer. Gel permeation chromatography is used to analyze molecular weight and polydispersity Index (PDI) of chemically synthesized polymers. For further applications, surface morphology and the roughness of the thin film polymer are analyzed by Atomic Force Microscopy (AFM) and Transmission Electron Microscopy (TEM). Degradation and glass transition temperatures are measured by Thermal Gravimetry Analysis (TGA) and Differential Scanning Calorimetry (DSC), respectively.

1.4 Chromism

Chromism is often a reversible process based on a change in the colors of the compounds. There are many types of chromisms such as thermochromism, photochromism, cathodochromism and electrochromism. Thermochromism is the most common type based on a change in the temperature. Photochromism is the isomerization between two molecular structures which are produced via light irradiation. Cathodochromism is based on irradiation of an electron beam. Lastly, upon applied potential, gaining and losing of electrons (redox properties) create electrochromism in organic compounds [27].

1.4.1 Electrochromism

Electrochromism is a reversible color change of a material upon applied external voltage or current. During electrochemical oxidation-reduction processes, optical properties of a molecule are altered due to formation of different absorption bands [28]. The most common studied electrochromic materials are metal oxides (WO_3 or IrO_2) [29], Prussian blues (iron(III)hexacyanoferrate) [30], viologens (1,1'-di-substituent-4,4'-bipyridylium) [31] and conducting polymers [32]. In the Last decades, organic conjugated polymers have gained great interest due to limitations of inorganic materials [33]. Moreover, they exhibit unique and enor-

mous properties such as multicolor feature with a subtle change in monomer form, high coloration efficiency, improvable switching time and supernal optical contrast [33–36].

When conducting polymer is in its oxidized state (p-doped state) with charge balance of counter anions, it acquires a delocalized π-electron band system and produce polarons [33–37]. These produced polarons are the major charge carriers. Reversibly, by reduction process electrochromic conducting polymers gain electrically insulating form, namely undoped-neutral form [35].

In a conjugated polymer, neutral electronic transition occurs between valence band and conduction band. The energy difference between these bands is called as band gap (E_g). External potential removes electron from valence band of the semiconducting polymer. Subsequently, a radical cation, polaronic charge carrier, is formed and charge delocalized over the polymer chains. Afterwards, semiconducting polymer relaxes from aromatic structure to quinoid structure and new electronic transitions are formed at a higher wavelength. Aromatic and quinoid forms of polythiophene were depicted in Figure 1.5. Bipolaronic charge carriers are generated with dication formation via further oxidation. This phenomena is proven with decrease in π-π^* absorption and formation of new bands between 700 - 1000 nm with external potential [33–37].

The change in color depends on the optical properties of materials. The color change can be either between two colored states or between one color and a bleached state. In the presence of multiple redox states, polyelectrochromism is observed which means various color changes at different redox states for the same material can be observed [36].

One of the most important advantages of conducting polymers is easy tunability of HOMO-LUMO energy levels via chemical modifications. Scientists have investigated the effect of repeating unit on color in neutral, oxidized or reduced states. Common polymers for electrochromic applications are followed in this section [38, 39].

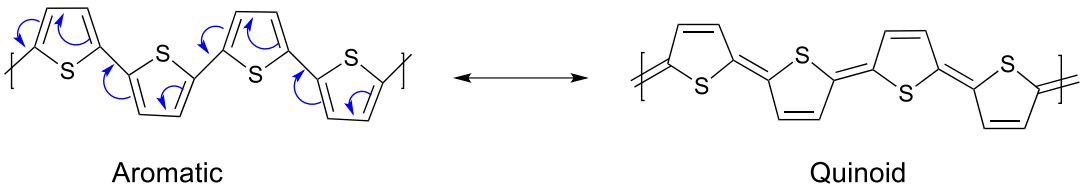

Figure 1.5: Aromatic and quinoid forms of polythiophene.

1.4.1.1 Polypyrrole(s)

Electropolymerization of pyrrole monomer in acetonitrile solution produces polypyrrole as shown in Figure 1.6. Polypyrrole exhibits blue-violet color (λ_{max} = 670 nm) in oxidized states and yellow-green color (λ_{max} = 420 nm) in reduced states. Although recursive color changing affects the polypyrrole films and causes a degradation of the film, electrochromic results of the polypyrrole are enhanced with 3,4-disubstitution [35].

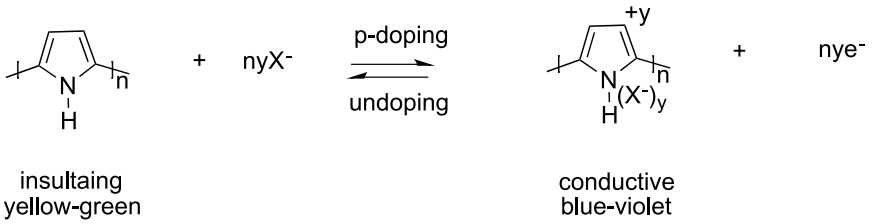

Figure 1.6: Color changes of polypyrrole upon doping/dedoping processes.

1.4.1.2 Polythiophene(s)

The first electrochemically synthesized polythiophene was reported in 1983 by Garnier et. Al. [40]. Polythiophenes are very stable character in their neutral form. In addition, ease of structural modification enables to produce substituted polythiophenes. As a result, polythiophene and substituted polythiophenes have been very promising for electrochromic device applications. Moreover, they can exhibit many different colors at their redox states as summarized in Table 1.1.

Changes on 3-methylthiophene result in tuning of color states. Reversible ox-

Table 1.1: Oxidized colors and reduced colors summary of thiophene based monomers.

	Polymer λ_{max}/nm and Color	
Monomer	Oxidized	Reduced
Thiophene	730-blue	470-red
3-Methylthiophene	750-deep blue	480-red
3,4-Dimethylthiophene	750-dark blue	620-pale brown
2,2'-Bithiophene	680-blue-grey	460-red-orange

idation and reduction of polythiophene can be obtained via substitution of an electron withdrawing group on phenyl ring which facilitates the stabilization of the n–doped states.

1.4.1.3 Polyaniline(s)

Polyaniline was produced in aqueous acid solutions with an organic medium. Letheby et. al. described first aniline electropolymerization in 1862. They exhibited excellent polyelectrochromic character with color changing from transparent yellow to green to dark blue to black [41]. Moreover, oxidized state colored polyanilines were used for electrochromic devices with complementary materials and from deep blue to green color changes was obtained.

1.5 Completing the Color Palette with Soluble Conducting Polymers

This section will briefly discuss some literature examples of conducting polymers which cover the absorption spectrum. For color displays and electrochromic window type applications, polymers must reveal one colored state and one transmissive state. To accommodate this need, researchers have designed and synthesized several types of polymers.

1.5.1 Blue to Transmissive

PEDOT (poly(3,4-ethylene-dioxythiophene)) is one of the well-known electrochromic polymer which has high conductivity and good stability in oxidized state. It has dark blue color in its neutral state and transmissive-light blue in the oxidized state [42]. The only limitation of this polymer is its low solubility. Although PEDOT shows superior electrochromic properties for device fabrication and further processes, soluble polymers that can be easily casted are desirable. In order to overcome solubility problem, PEDOT was polymerized in aqueous polyelectrolyte which is poly (styrene sulfonic acid) using oxidizing agent ($Na_2S_2O_8$) and PEDOT/PSS is produced [43]. It has low oxidation potential, highly stable oxidized state, low band gap and high conductivity. Therefore, PEDOT/PSS is very promising material for electrochromic device application for photovoltaic and LED applications [43, 44]. In order to complete color palette, solution processable and switching between colored to transmissive polymers were synthesized. In 2008, Toppare et. al. synthesized novel donor acceptor type copolymer (poly-4,7-bis(2,3-dihydrothieno[3,4-b][1,4]dioxin-5-yl)-2-dodecyl-2H-benzo [1,2,3] triazole (PBEBT)) by electropolymerization. EDOT moiety was used as a donor and benzotriazole as an acceptor moiety. These novel polymers showed superior results among PEDOT. Enhanced optical contrast like 53 % while PEDOT has 44 % and decreased switching time like 1.1 s while PEDOT has 2.2 s [45].

Moreover, benzotriazole and quinoxoline derivatives which were synthesized via D-A approach by Toppare et. al. [46, 47]. Red-green-blue(RGB) colors are synthesized for the need of full-color applications.

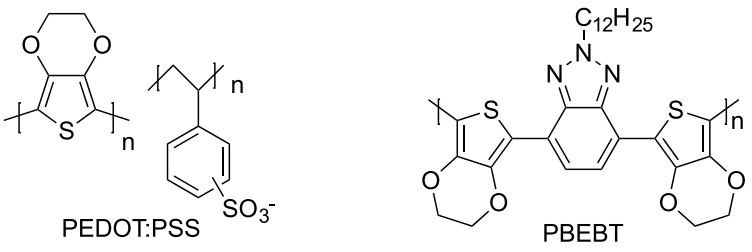

Figure 1.7: Structure of blue to transmissive polymers.

1.5.2 Red to Transmissive

Copolymer of bis(ethylhexyloxyl)-thiophene and dimethoxythiophene was synthesized (1:1) via oxidative coupling of monomers in the presence of iron(III)-chloride. It has a red neutral state color and nearly transmissive oxidized state with a low oxidation potential. Side groups enable steric hindrance and ease the elongation of conjugation length [48].

1.5.3 Orange to Transmissive

Homopolymerization of bis(ethylhexyloxyl)thiophene in the presence of iron-(III)chloride gives orange color in neutral state and transmissive color in oxidized state as shown in Figure 1.8. Directly bonded oxygens on thiophene lower the oxidation potential comparing to PEDOT. Also, solubility was enhanced with branched alkyl chains. Short conjugation length resulted in a blue shifted polymers which have 480 nm λ_{max} value [48].

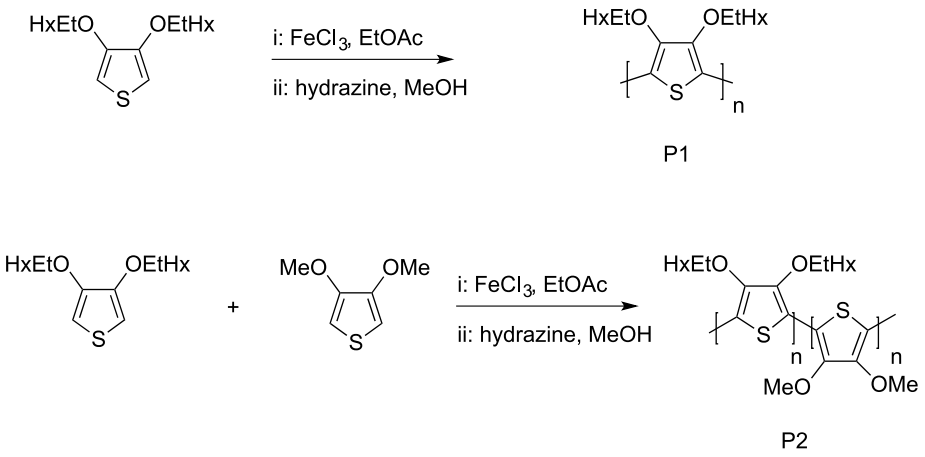

Figure 1.8: Synthesis of ECP-orange (P1) and red (P2) polymers.

1.5.4 Green to Transmissive

In order to observe green color in neutral state, it is required to have two absorption bands in red and blue regions. These bands should deplete simultaneously

when the polymer is oxidized. In 2005, Wudl and coworkers polymerized dioctyl-substituted 2,3-di(thien-3-yl)-5,7-di(thien-2-yl)thieno[3,4-b]pyrazine monomer chemically and electrochemically and obtained green in neutral state, pale brown-transmissive in oxidized state solution processable polymer [13].

In 2008, Toppare et. al. followed up Donor-Acceptor approach to obtain low band gap polymer and two absorption maxima in visible region (red and blue). They synthesized two novel polymers have green color in neutral states and excellent transmissive property in oxidized states which are poly[2,3-bis(4-tert--butylphenyl)-5,8-(2,3-dihydrothieno[3,4-b][1,4]dioxin-7yl)qui-noxaline] (PTBPEQ) and poly[2,3-diphenyl-5,8-(2,3-dihydrothieno[3,4-b][1,4]dioxin-7-yl)quinoxaline]-(PDOPEQ). They showed excellent electrochromic and physical properties such as fast switching times, high stability in oxidized states and ease of production [49].

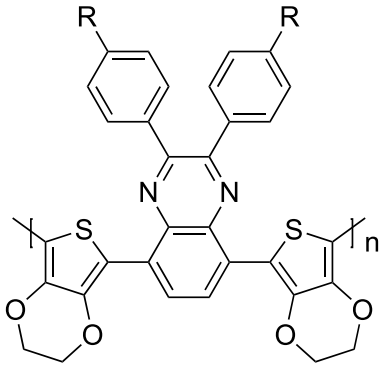

PTBPEQ: R=t-butyl

PDOPEQ: R=H

Figure 1.9: Structure of green to transmissive polymers.

1.5.5 Yellow to Transmissive

In order to complete the color wheel and obtain wide range of hue values for color display applications, cyan-magenta-yellow (CMY) and red-yellow-blue (RYB) colors can be mixed. Each color plays very important role. Series of arylene

unit containing ProDOT or copolymers of ProDOT were synthesized by Suzuki polycondensation. Cathodically colored, yellow in neutral state nearly transmissive in oxidized state polymers were synthesized successfully as demonstrated in Figure 1.10 [50].

These unique and enormous achievements in completing color palette made these polymers applicable on color display applications.

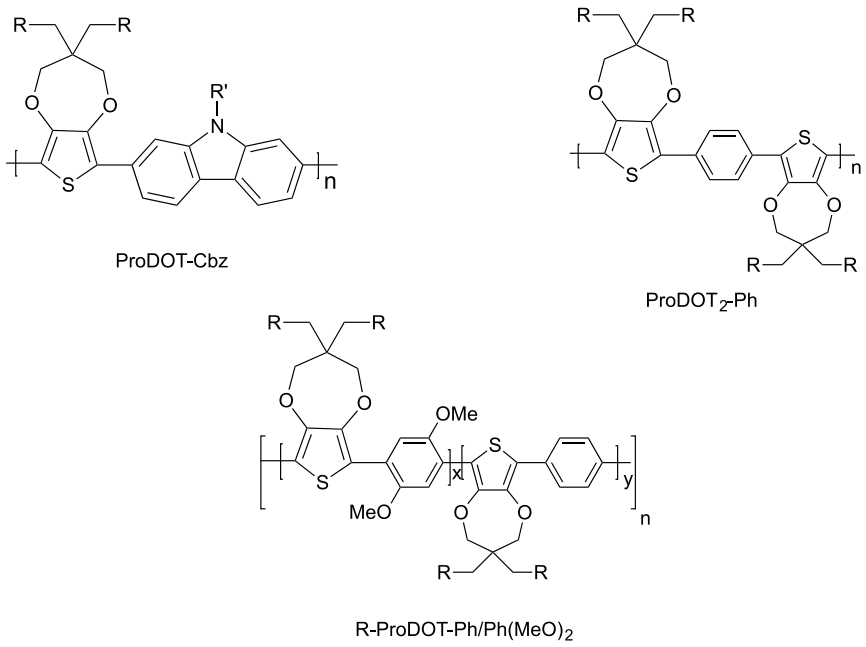

Figure 1.10: Oxidized state transmissive-neutral state yellow polymers.

1.6 Application of Conducting Polymers

After 2000 with the discovery of conductivity of PA, studies on conducting polymers have gained acceleration. These studies brought many features to literature such as flexibility, high conductivity and solution processability of conducting polymers. Due to these excellent features, conducting polymers are subjected to be used as an active layer material for electrochromic devices, photovoltaics, light emitting diodes, field effect transistors and biosensors. Some examples were

depicted in Figure 1.11.

1 2 3

Figure 1.11: 1. Electrochromic device, 2. organic photovoltaic, 3. organic light emitting diode.

1.6.1 Electrochromic Devices and Construction

Electrochromic devices have many application areas especially in industry such as rear-view mirrors and smart windows. High optical contrast value, long term stability, supernal coloration efficiency, long open circuit memory and short switching times provide many utilization areas. These devices can be established with either dual colored or colored to transmissive switching type polymers in their oxidized and reduced states [39].

Schematic illustration of electrochromic device is given in Figure 1.12. Anodically or cathodically colored electrochromic polymers are spray coated onto ITO glass working electrodes. These electrodes are sandwiched with a micrometer scale of gel electrolyte. Color changes can be observed via applying appropriate voltages according to redox states of the polymers.

Electrochromic contrast is a percent transmittance change of the thin film at a wavelength where the polymer has the highest absorbance value.

Optical memory (open-circuit memory) is defined as the time period that electrochromic device (ECD) retains at one color.

Coloration efficiency is the amount of the charges that cause optical change in electrochromic polymer film.

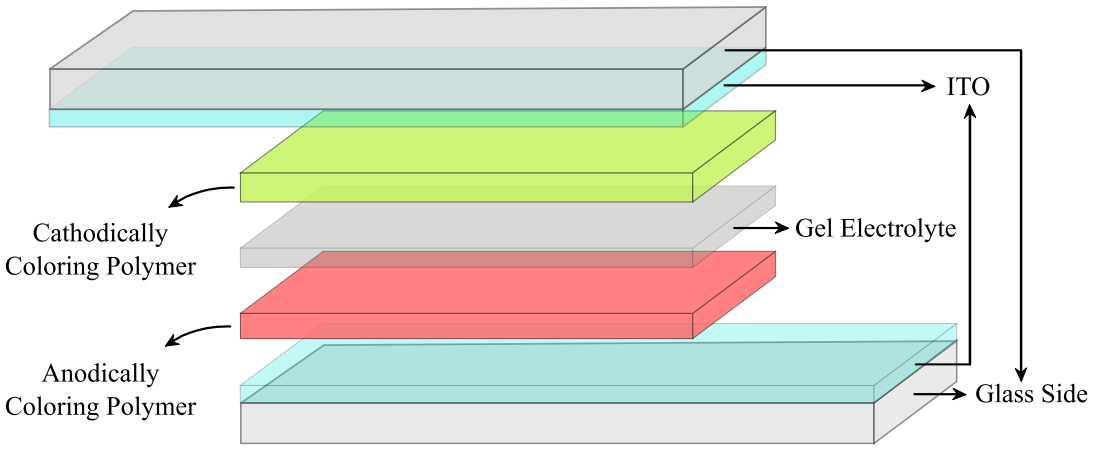

Figure 1.12: Schematic illustration of electrochromic devices.

Switching time is the time that spent between fully oxidized and bleached states of the EC material. This parameter is affected by morphology and the thickness of the thin film.

Stability is cyclic switching of ECD without significant degradation of performance. Since degradation of thin film and applying high potentials cause instability of ECD, stability is very important parameter for commercialization processes. [51].

1.6.2 Organic Solar Cells

Sun generates continuous and consistent solar power as long as it exists. Solar energy is one of the most important renewable energy due to its advantages against fossil fuels. Solar energy is clean and reliable and it does not pollute environment by releasing hazardous gases [52].

In literature three generation of solar cells have been discussed up to now. First generation solar cells use silicon wafers and have performance around 15-20 %. These type of solar cells was commercialized already and mainly seen on rooftops. Although they show high stability and good performance, they are not flexible and need a lot of energy in production process. The second generation solar cells based on amorphous silicon, CIGS, CdTe. Their performance is around 10-

15 %. Although second generation solar cells production cost is limited by use of scarce elements, compared to first generation solar cell, second generations have low manufacturing cost due to less material consumptions. However, second generation solar cells need high energy consumption due to vacuum and high temperature processes in production steps. Lastly, third generation solar cells were produced using organic materials, small molecules or polymers. Third generation covers many types of solar cells such as multijunction types which is the most efficient type solar cell whereas high production cost hinders the commercialization. Simple, quick and low cost large-scale production by roll to roll technique of polymer solar cells have great potential to commercialization [53].

The organic solar cell (OSC) is a photovoltaic device that converts sunlight into electricity. Molecular exciton formation occurs after absorption of light in the organic semiconductor material. The working principle of OSCs starts with absorption of light in the organic molecule then coulombically bound electron and hole pair (exciton) formation is followed after this exciton diffuses to donor acceptor interface and dissociate into free charge carriers and lastly charges are collected at respective electrodes.

Organic molecules can be considered as a great choice for organic solar cell applications because they bring solution processability, low production cost, flexibility and electronic tunability [54–57]. One of the important parameter for OSC and OLED construction is band gap of the material. It is defined as the energy difference between the highest occupied molecular orbital (HOMO) and the lowest unoccupied molecular orbital (LUMO). The band gap of an organic material is generally between 1.1–3.5 eV. The main advantage of organic molecules over inorganic counterparts is the ability to tune in HOMO-LUMO energy levels. As a result of this feature, optical properties of organic molecules can be controlled easily [58]. Organic molecules have a high optical absorption coefficient ($105\,\mathrm{cm}^{-1}$) compared to that of inorganic molecules; hence, polymer thin films can absorb sun light efficiently [59].

The first and the simplest organic solar cell device structure is the single layer

device construction which is shown in Figure 1.13. This type of device's working principle is based on electric field generation between anode and cathode due to their different work functions. After absorption and exciton formation in organic semiconductor layer, electric field dissociates and collects charges on the related electrodes. The most challenging issue is to keep the balance between light absorption and diffusion length of organic molecules. Exciton diffusion length of organic semiconductors is around 10 nm; however, in order to achieve reasonable amount of sunlight absorption, active layer should be thicker than 10 nm. As a result, greater part of the generated excitons is not dissociated and few number of charges are collected at the electrodes. Consequently, device efficiency of single layer type device structure is well below 1 %.

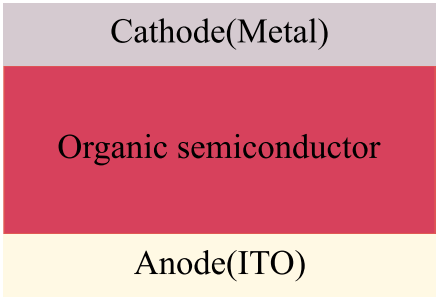

Figure 1.13: Single layer organic solar cell device configuration.

1.6.2.1 Bulk Heterojunction vs. Bilayer Device

In 1986, heterojunction formation first demonstrated by Tang et al. as a bilayer solar cell. (3). As depicted in Figure 12, a bilayer solar cell device architecture consists of an anode, electron donor (organic semiconductor), electron acceptor ($PC_{60}BM$) and cathode layer. Donor part of the active layer is responsible for sunlight absorption. The major drawback for this type of device architecture is the short exciton diffusion length which is the distance that an exciton can move without recombination. The thicknesses of donor and acceptor layers should be in a balance. When one of the layer is too thick, generated excitons will be far away from the donor-acceptor heterojunction. Another limiting point in thickness of donor and acceptor layers leads to weak absorption on active

layer. The organic semiconductors need around 80-100 nm thickness for effective sunlight harvesting. At this condition, only limited amount of excitons can reach to donor acceptor interface and be separated [60].

Due to drawbacks of bilayer device architecture, in 1995, novel concept was introduced which is called as bulk heterojunction solar cell. As depicted in Figure 1.14, active layer consists of intermixing of donor and acceptor materials in a proper solvent and the solution is coated onto anode material. By this way, active layer is comprised of many interpenetrating nanoscale networks that enhance exciton separations. As a result, absorption of sunlight increases. The donor-acceptor phase separation is around 10-20 nm for bulk heterojunction type solar cells and charge carries are transported via percolated pathways which enhances charge collection at the respective electrodes [61].

Due to these unique advantages of BHJ, over 12 % efficiency was achieved with the tandem and ternary type OSC device architectures uses polymers or small molecules as the active layer [62–65].

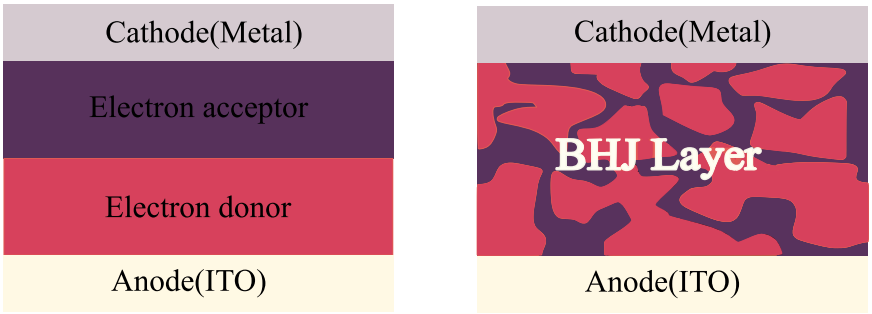

Figure 1.14: Device architecture of bilayer and bulk-heterojunction solar cell.

1.6.2.2 Operational Principles of OSCs

1.6.2.2.1 Exciton Generation

High absorption coefficients of organic semiconductors enable them to absorb large amount of sunlight with a very thin layer. Upon absorption of photon by

the organic semiconductor, an electron is excited from HOMO energy level of the molecule to the LUMO energy level. Unlike inorganic semiconductors, organic semiconductors have low dielectric constants, which results in the formation of strong coulombically bound electron and hole pair. While the binding energy of inorganic semiconductors is on the order of meV, that of organic semiconductors is between 0.1 – 1.4 eV [66].

The main concern for exciton generation is the band gap of the organic semiconductors. Most of the organic molecules have large band gap around 2 eV, which results in absorption up to 700 nm of the solar spectrum [67]. However, materials with a band gap of 1.1 eV can harvest 77 % of solar light [68].

1.6.2.2.2 Exciton Diffusion and Dissociation

Generated exciton moves to donor-acceptor interface to dissociate into free charge carriers. Exciton migration to the LUMO of the acceptor material will be energetically favorable if the difference between HOMO of the donor and LUMO of the acceptor material is lower than the exciton binding energy. As electron moves through LUMO of the acceptor molecule, hole stays at HOMO of the donor molecule. In order to obtain enhanced exciton dissociation, active layer should consist of large and sufficient donor-acceptor interface [69, 70].

1.6.2.2.3 Charge Carrier Transport

High work function anode is combined with the low work function cathode material in construction of BHJ solar cell. The difference between the work functions generates built-in electric field throughout the solar cell. Drift and diffusion currents are responsible for the charge movement through electrodes within their lifetimes. Upon applied potential, due to the change in internal electric field, drift current gets altered. Hence, the density of the generated excitons increases near the heterojunction region and they start to move through the electrodes with the help of diffusion current.

1.6.2.2.4 Charge Collection at Electrodes

Free charge carriers are extracted from active layer to the electrodes once they reach the interface. The junction between metal and the semiconductor is called as Ohmic contact. To enhance charge extraction, ohmic contact formation should also be ensured [71]. For this purpose, anode and cathode materials must carefully be chosen. As shown in Figure 1.16, in operation of organic solar cell materials should have proper band alignment for effective charge collection. Indium tin oxide (ITO) which has work function of 4.7 eV and Al which has 4.2 eV work function match well with the HOMO of the organic semiconductors and LUMO of the PCBM, respectively.

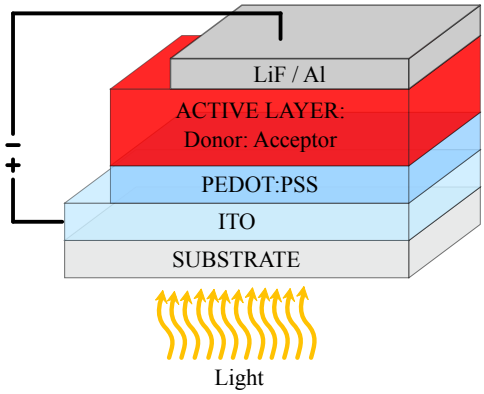

Figure 1.15: Organic solar cell device configuration.

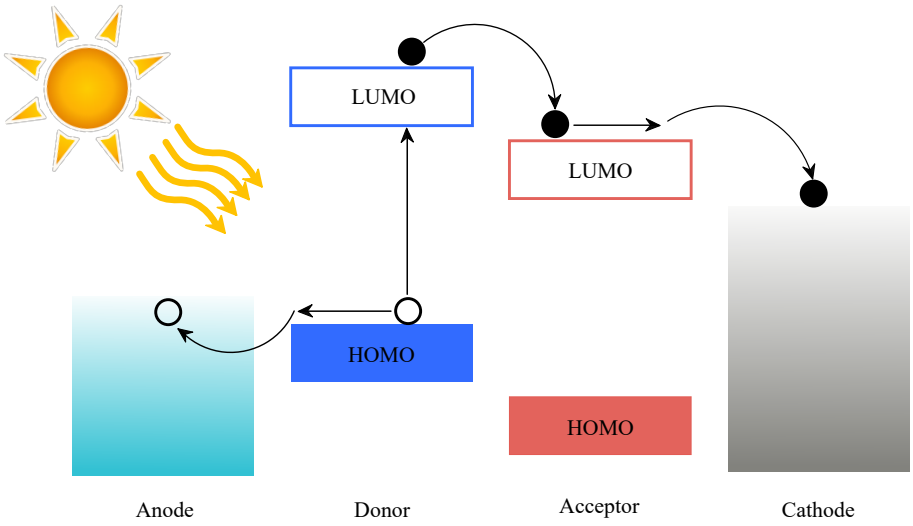

Figure 1.16: Operation principle of an organic solar cell.

1.6.2.3 Operational summary of BHJ

The overall process shown in Figure 1.16 starts with the photon absorption by an organic semiconductor then continues with generation of excitons. Generated excitons diffuse into donor-acceptor interface. Dissociation of the charges at interface takes place with the effect of electric field that is produced by reverse bias. Lastly, while the external bias gets closer to zero, free carriers are started to get extracted from the active layer to anode and cathode.

Solar cell behavior is different in dark and under illumination as shown in Figure 1.17. In both states, it follows diode behavior. In dark since there is no light absorption, there will be no photocurrent formation. In reverse bias, current flow cannot be observed due to high drift current. However, with increasing voltage, diffusion current becomes higher than the drift current and at this point the voltage called as turn on voltage. After that point, exponential increase in current is seen. Under illumination, current flows out of the solar cell and photon absorption creates charge carriers.

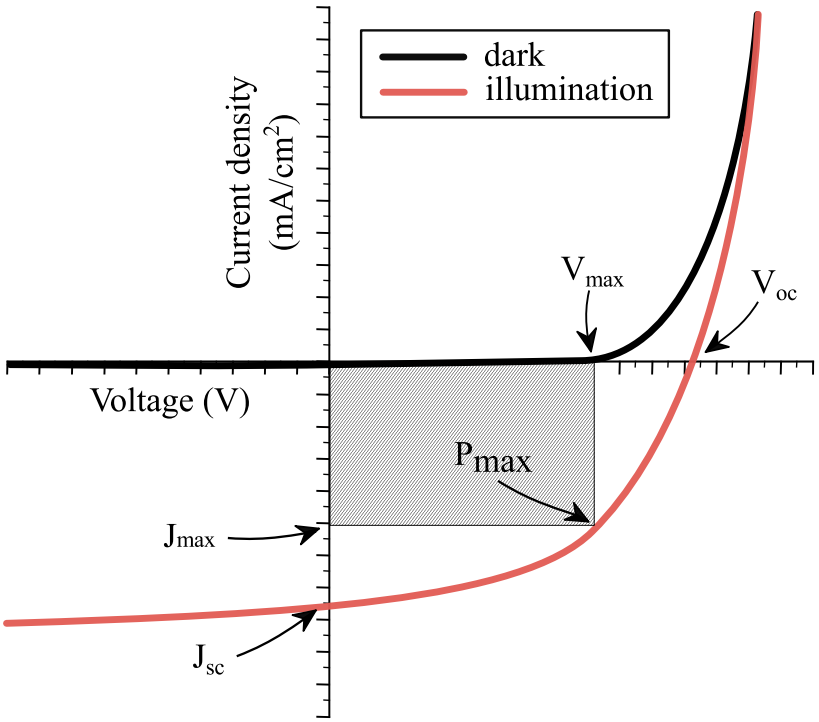

Figure 1.17: Solar cell behavior under dark and illumination of light.

1.6.2.4 Organic Solar Cell Characterization

1.6.2.4.1 Air Mass

Under standard conditions, air mass is a coefficient that is used to characterize performance of the solar cell. AM 1.5 G is a universal coefficient which depends on solar radiation angle, zenith angle. When the angle between solar irradiation and normal of the Earth is equal to 48.2°, the atmosphere thickness becomes 50 % more than the atmosphere thickness at Zenith angle and is denoted as AM 1.5. The light intensity is fixed as 100 mW cm^{-2} [72]. General overview of air mass 1.5 global standardization was demonstrated in Figure 1.18.

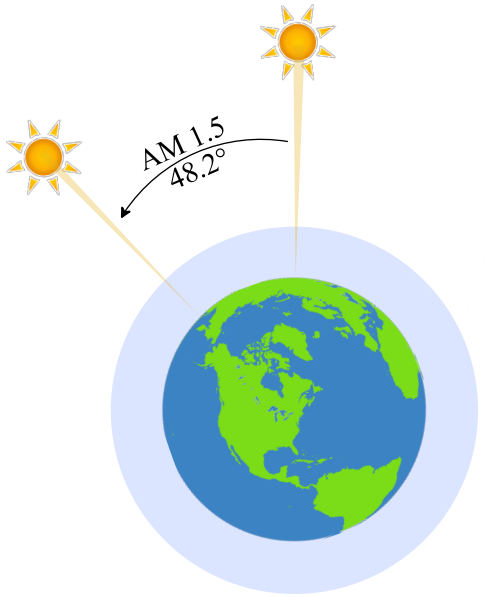

Figure 1.18: Air Mass 1.5 Global standardization.

1.6.2.4.2 Short Circuit Current (J_{sc})

When the voltage across the organic solar cell is zero, the maximum current is called short circuit current and demonstrated as J_{sc}. It is the amount of charge carriers that are produced and collected. Since J_{sc} highly depends on the photon absorption molecules should have small band gap to harvest more solar light. Hence, higher J_{sc} can be obtained [72].

1.6.2.4.3 Open Circuit Voltage (V_{oc})

V_{oc} is the maximum voltage when the current density is zero. It depends on the difference between HOMO of the donor and LUMO of the acceptor molecules [71, 72].

1.6.2.4.4 Fill factor (FF) and Power Conversion Efficiency (PCE)

Fill factor (FF) is the ratio of the maximum power to short circuit current and open circuit voltage. Power conversion efficiency is the ratio of power produced by solar cell under $100\,W/cm^2$ light intensity (Pin) [72].

$$FF = \frac{I_{mpp}V_{mpp}}{I_{sc}V_{oc}} \tag{1.2}$$

$$\eta_e = \frac{I_{mpp}V_{mpp}}{P_{in}} = \frac{I_{sc}V_{oc}FF}{P_{in}}. \tag{1.3}$$

1.6.2.4.5 External Quantum Efficiency (EQE)

EQE is defined as the conversion efficiency of photons to current, in other words it is the incident photon to current efficiency [72].

1.7 OSC Literature Survey of BDT Containing Polymers

In 1986, bilayer OPV device was firstly introduced by Tang et. al. The breakout was happened in 1995 by demonstration of polymer:fullerene and polymer:polymer blend concept which is named as BHJ by Prof. Heeger and Prof. Friend. This architecture provided enhanced donor-acceptor interface and improved charge generation and transport with nanoscale morphology [69, 70]. Besides, the design and synthesis of donor polymer play very crucial role to obtain high PCEs since active layer of OPVs must fulfill many requirements. Donor polymer should cover a broad absorption spectrum, have a nanoscale phase separation, a bicontinuous network morphology and proper HOMO and LUMO

energy levels to acquire decent driving force for charge separation with lowered energy loss [73–81].

1.7.1 Backbone Modulation

Development of OPV devices can be provided by device processing innovations, tuning of active layer blend morphology and interface engineering. One of the most used strategy is combination of Donor-Acceptor (D-A) molecules in the same polymer backbone. It is preferred to obtain broad absorption and appropriate energy levels (HOMO-LUMO). The other strategy is incorporation of π-bridge between D-A units to obtain well optimized backbone conformation and to extend π-system.

1.7.1.1 D-A Combination

Homopolymers such as MEH-PPV and P3HT [82] were used for OPV studies. However, further improvements are limited by their low absorption of light. Also, fixed HOMO energy levels reduce the J_{sc} and V_{oc} values. To overcome these limitations, D-A approach which is called as push-pull method was preferred. Hence, creating and changing the intermolecular charge transfer through donor to acceptor tune the optical and electronic properties of the polymer [83]. Electron density on the polymer backbone moves through donor to acceptor side and formation resonance structure is followed. As shown in Figure 1.19, when donor and acceptor molecules are combined in a polymer structure with covalent bonds. HOMO energy level of the resultant polymer close to the HOMO of the donor unit and LUMO energy level of it close to the acceptor moiety. As a result of this, narrowed band gap is observed with D-A approach and explained with molecular orbital hybridization.

1.7.1.1.1 BDT Based D-A Type Copolymers

In 2003, Andersson and his coworkers synthesized benzothiadiazole and fluorene containing alternating copolymer for the first time and they achieved 2.2 % PCE.

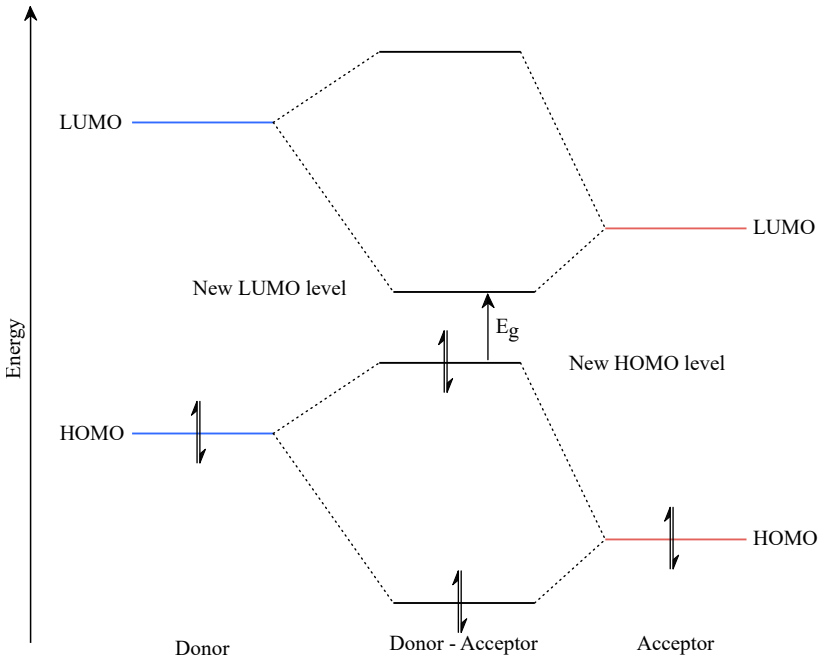

Figure 1.19: Hybridization of energy levels.

Later on, D-A type copolymers became the milestone for development of OPV industry [84].

In 2008, as shown in Figure 1.20, P1 was constructed with coupling of BDT and thiophene units and hence 1.6 % PCE was achieved [85]. After that, ester substituted thieno[3,4-b]thiophene(TT) as an acceptor moiety and BDT unit as the donor moiety were incorporated into polymer backbone by Yu. et. al. (PTB7) Consequently, stabilization of quiniodal structure was observed; and hence, a low band gap polymer was obtained namely P2 [86, 87]. In 2010, PTB7 was one of the mostly used donor molecule for its unique properties such as broad absorption ranging from 550 nm to 750 nm [88, 89].

2,1,3 Benzothiadiazole (BT) is one of the strongest acceptor molecule. BDT and BT comprising polymers showed very promising photovoltaic performance; one of the example is P3 which has impressing photovoltaic properties as shown in Figure 1.20 [90]. All results were summarized in Table 1.2.

In 1974, a very outstanding molecule, diketopyrrolopyrrole(DPP), was synthesized by Fornum and coworkers [91]. Due to high electron deficiency of DPP,

it was coupled with BDT units and hence low band gap polymers (∼1.45 eV) were obtained. PBDT-DPP is a great candidate for tandem cell applications due to its strong absorption. Yang et. al constructed inverted tandem cells and obtained PCE of 8.6 % and V_{oc} of 1.56 V [92].

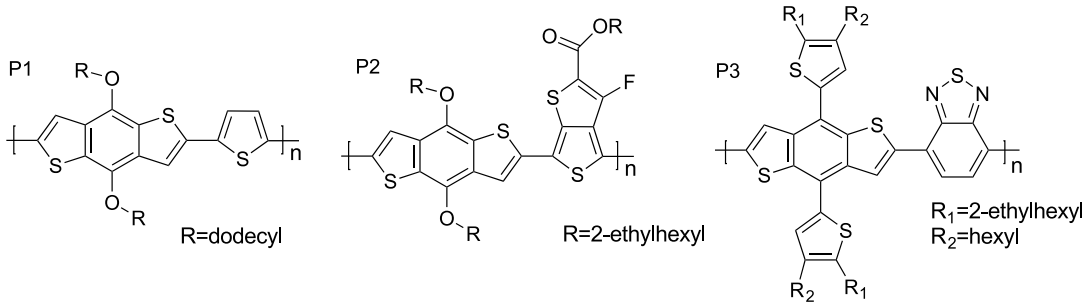

Figure 1.20: Structures of P1 P2 and P3.

Table 1.2: Summary of optical and OPV results of P1, P2 and P3.

	E_g^{op} (eV)	HOMO (eV)	V_{oc} (V)	J_{sc} (mA/cm^2)	FF (%)	PCE (%)
P1	2.06	-5.05	0.75	3.78	38	1.60
P2	1.6	-5.15	0.74	14.5	68.97	7.4
P3	1.75	-5.45	0.92	14.5	64	9.4

1.7.1.2 π-Bridge Effect

Incorporation of thiophene, selenophene or furan units between donor-acceptor molecules as a π-bridge affects the conformation of the polymer chains. As a result, optical absorption, molecular energy levels, active layer morphology and hole mobility of the conjugated polymer are changed. The angle between conjugated molecules is called connecting angle and it is affected by π-bridge units inserted into polymer backbone. On the other hand, crystallinity of the polymer is highly controlled by zigzagged or straight structure of the backbone which is affected by π-bridge units.

Hou et. al synthesized P4 with a zigzagged backbone and π-π stacking distance was determined as 3.88 Å. However, when thiophene was incorporated as a π-bridge, resulting polymer (P5) has straight-linear conformation. To the best of our knowledge it has the smallest π-π stacking distance for conjugated molecules which is 3.51 Å [93]. The structures of the copolymers were given in Figure 1.21.

Absorption properties and molecular energy levels are highly affected by backbone conformation. When π-π stacking distance between the units is decreased, HOMO energy level will be higher and absorption spectra will shift to Near IR region. The difference between HOMO energy levels were shown in Table 1.3.

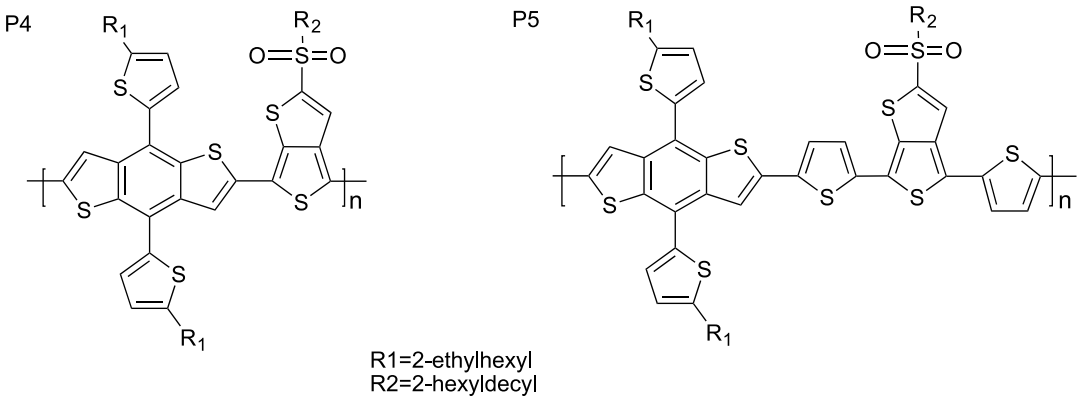

Figure 1.21: Structures of P4 and P5.

Table 1.3: Summary of optical and OPV results of P4 and P5.

	E_g^{op} (eV)	HOMO (eV)	V_{oc} (V)	J_{sc} (mA/cm^2)	FF (%)	PCE (%)
P4	1.61	-5.29	0.81	12.27	61.98	5.93
P5	1.59	-5.04	0.69	16.35	66.3	7.48

1.7.2 Optimization of Flexible Side Chain

Solubility, mobility of electrons or miscibility of different molecules are under the control of side chain optimization. Polymer-polymer and polymer-fullerene

interactions can be controlled via alkyl chain length, shape (linear or branched), position or terminal group [94, 95].

1.7.2.1 Effect of Alkyl Chain Configuration

Alkyl chain configuration affects the π-π stacking distance; therefore, it has influence on the solubility of polymers. There should be a balance between length and bulkiness of the alkyl chains to control intermolecular interactions. To illustrate, branched alkyl chain inserted polymers have larger π-π distance due to bulkiness of the side group (P6 to P7) [86]. Hou and coworkers synthesized three polymers, with different alkyl chains, octyl (P8), 2-ethylhexyl (P9), 3,7-dimethyl octyl (P10) and the structures are shown in Figure 1.22.

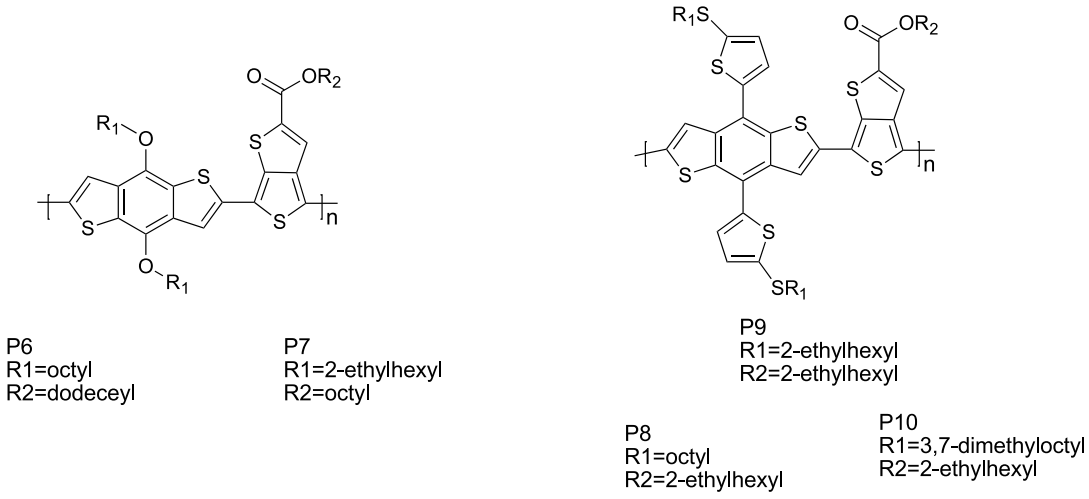

Figure 1.22: Structures of P6, P7, P8, P9 and P10.

Optical and electronic properties of the polymers did not change as depicted in Table 1.4 [96]. However, polymer with linear alkyl chain(P8) has reduced π-π stacking due to less steric hindrance of linear side chain. As a result, the highest J_{sc} belongs to P8.

Table 1.4: Summary of optical and OPV results of P6, P7, P8, P9 and P10.

	E_g^{op} (eV)	HOMO (eV)	V_{oc} (V)	J_{sc} (mA/cm^2)	FF (%)	PCE (%)
P6	1.58	-4.90	0.58	12.5	65.4	4.76
P7	1.62	-5.01	0.68	10.3	43.1	3.02
P8	1.61	-5.01	0.62	17.55	67.2	9.52
P9	1.59	5.29	0.81	16.52	62.3	8.37
P10	1.61	5.29	0.81	16.22	56	7.36

1.7.2.2 Effect of Functional Substitution

Optical and electronic properties are tunable with incorporation of electron donating or withdrawing groups. Fluorine is the most electronegative atom in the periodic table. Its small size eases modification and incorporation of it to the polymer backbone, which provides tuning the energy levels. Thienyl BDT and ester substituted TT polymer -P11 and P12 were synthesized, as shown in Figure 1.23. With incorporation of fluorine atom to the backbone, HOMO level was reduced from -5.09 to -5.22 eV and PCE enhanced from 6.21 to 9.35 through an increase in V_{oc} [97]. The results were summarized in Table 1.5.

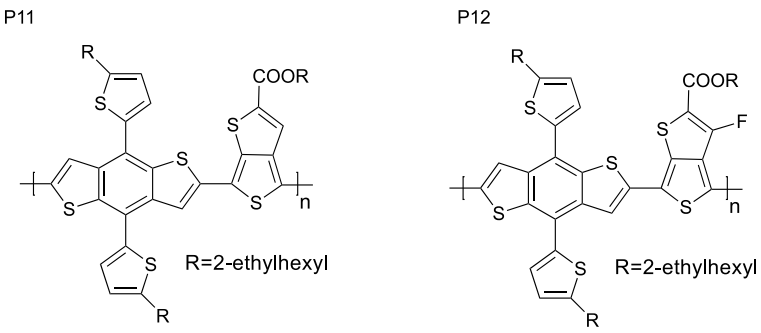

Figure 1.23: Structures of P11 and P12.

Table 1.5: Summary of optical and OPV results of P11 and P12.

	E_g^{op} (eV)	HOMO (eV)	V_{oc} (V)	J_{sc} (mA/cm^2)	FF (%)	PCE (%)
P11	1.58	-5.09	0.68	14.59	62.6	6.21
P12	1.58	-5.22	0.80	15.73	74.3	9.35

1.7.3 Benzotriazole and Benzodithiophene Containing Conjugated Polymers

Benzotriazole (Btz) derivatives can easily be modified by changing alkyl chain and enhanced solubility can be obtained. Polymers with higher HOMO energy levels can be synthesized with Btz molecules due to effect of electron rich N atom which makes Btz weaker electron acceptor. Peng and coworkers synthesized alkyl-thiol substituted BDT and fluorinated Btz comprising conjugated polymer as shown in Figure 1.24. As depicted in in Table 1.6 7.3 % PCE was achieved using polymer P13 [98].

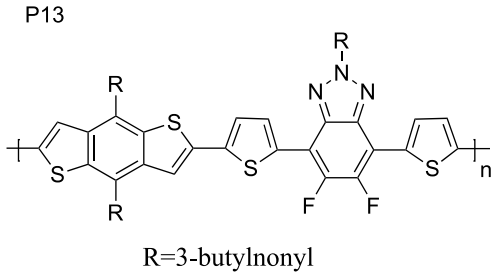

Figure 1.24: Structure of P13.

Table 1.6: Summary of optical and OPV results of P13.

	E_g^{op} (eV)	HOMO (eV)	V_{oc} (V)	J_{sc} (mA/cm^2)	FF (%)	PCE (%)
P13	2.02	-	-0.78	13.3	70.5	7.3

1.8 Organic Light Emitting Diodes

Organic light emitting diode (OLED) is a device that consists of emissive electroluminescent organic layer. Upon applied potential, OLED emits light. OLEDs are widely used for display technologies such as mobile phones, television screens, computer monitors.

Electroluminescence (EL) in organic materials was firstly discovered by Andre Bernance and coworkers applying external potential to acridine orange and quinacrine at Nancy-Universite in France however, it was not significantly developed until Ching W. Tang's study at Eastman Kodak company in 1989. Investigations on this era is very promising and has been increasing year by year. Tang et al. used Alq3 (tris(8-hydroxyquinoline) aluminum (III)) as an active layer material for the first Organic Light Emitting Diodes (OLED) application [99].

1.8.1 Luminescence

The term luminescence comes from Latin word *lumen* which means light. In 1888, Eilhord Wiedemann described the term luminescenz as a spontaneous light emission of electronically excited molecules [100]. There are several subgroups of luminescence according to type of excitation. Absorption of photons cause photoluminescence and electrical current passing through the device cause electroluminescence [101].

1.8.1.1 Photoluminescence (PL)

Photoluminescence is a spontaneous light emission with the effect of electromagnetic radiation. The relaxation process is radiative. Fluorescence and phosphorescence are the two sub-groups of photoluminescence which depend on character of excited state. Singlet and triplet states are depicted in Figure 1.25. Fluorescence is the relaxation from singlet excited state to singlet ground state which is spin allowed (Figure 1.25). The lifetime of an electron in the excited state is very short that is between 10^{-5} – 10^{-8} s which is very rapid decay. As shown

in Figure 1.25, excited electron with a same spin forms triplet excited state, emission from triplet to singlet excited state named as phosphorescence. The lifetime is between 10^{-4} – 10^{4} s which is very long compared to the former one because of forbidden energy state transition [102].

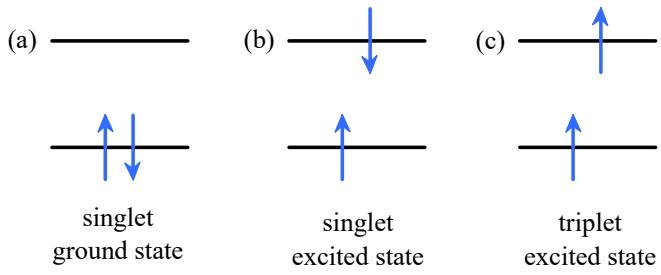

Figure 1.25: Schematic representation of singlet ground (a), excited (b) and triplet excited state (c).

1.8.1.1.1 Jablonski Diagram

Jablosnki Diagram is a vertically alignment diagram consisting of energy levels demonstrating absorption of photon, fluorescence and phosphorescence. The figure is depicted as Figure 1.26

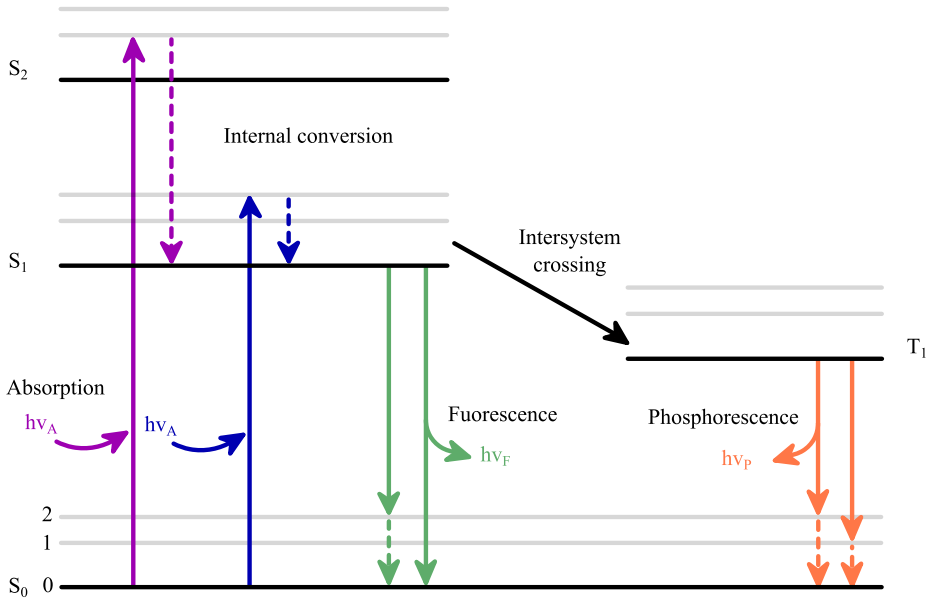

Figure 1.26: Jablonski Diagram.

1.8.1.2 Electroluminescence (EL)

If injected charge carriers (electrons and holes) combine and radiate in a semiconductor (emissive layer), this process is called as electroluminescence. In other words, it is a direct conversion of electrical energy into light emission. There are three fundamental steps; first external electrical energy is applied, according to the mode of emitting state (singlet or triplet) light generation will take place. Four different spin combination is available due to spin of hole and electrons. If the total spin of excitons is zero (antiparallel spin) it is called as singlet (S_0, S_1). In triplet state total spin of excitons is equal to one (parallel spins) (T_1). Excited electrons can produce singlet or triplet excited states in a 1:3 ratio as shown in Figure 1.27. Fluorescence occur from 25 % of excitons; however, phosphorescence occurs from 75 % of excitons. Difference in spin symmetries of excited state and ground state make the phosphorescence forbidden for organic molecules due to lack of spin-flip mechanism. Very efficient LEDs can be processed via harvesting triplet excitons [103–105].

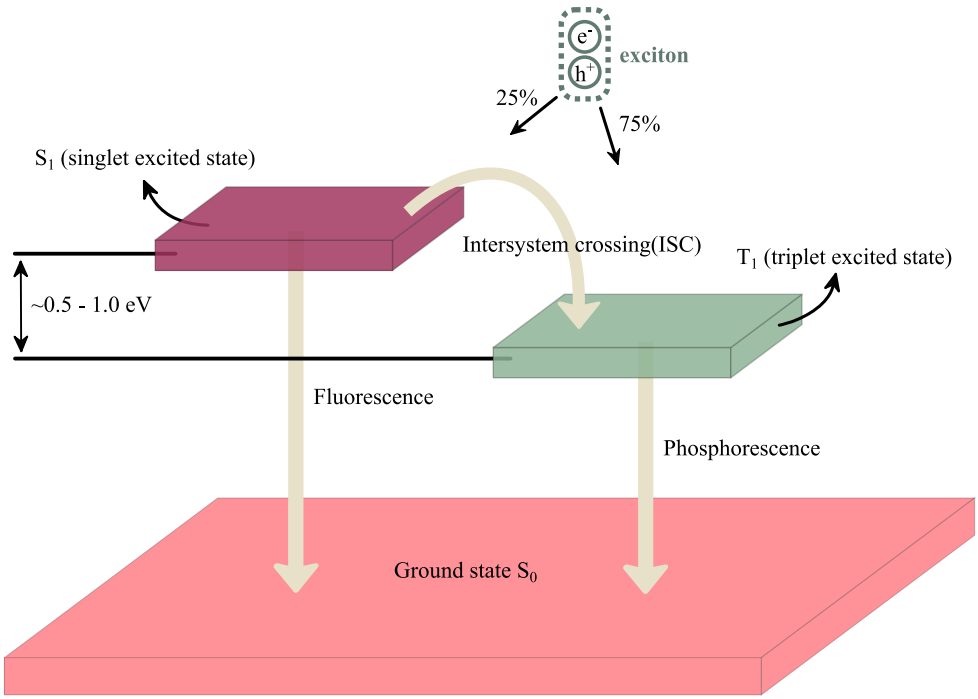

Figure 1.27: Electroluminescence of fluorescent and phosphorescent materials.

1.8.2 Device construction and working principle of OLEDs

Typical OLED device consists of transparent and highly conductive anode material which is usually ITO [106], an emissive layer, a conductive layer and a properly chosen cathode material according to work function alignment [107]. As depicted in Figure 1.28, when an external potential is applied through electrodes, electrons are injected from cathode and holes are injected from anode. Hole transport layer which is PEDOT:PSS enables movement of holes through

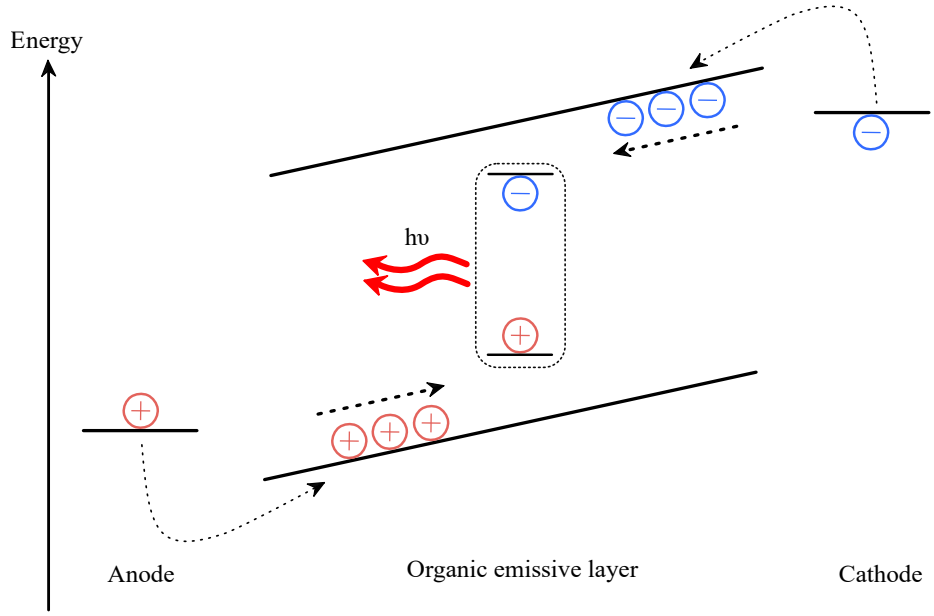

Figure 1.28: Operational principle of an OLED.

emissive layer. Due to coulombic attraction, electron and hole combine and produce exciton in the emissive layer. Since hole has higher mobility than electron, they recombine near emissive layer. Lastly, radiative decay occurs in emissive layer which has visible light frequency.

1.9 Aim of the Study

As it is mentioned before, getting maximum efficiency from sun is very crucial for both academia and the industry. In order to fulfill this aim, donor-acceptor

approach is preferred for the design of active layer materials for OPVs. This approach enables to obtain low band gap polymers which will result in enhanced PCEs. By the light of these information, two novel conducting polymers were synthesized by Stille polycondensation as shown in Figure 1.29. Benzotriazole was used as the electron acceptor unit due to its high electron transporting ability. Moreover, benzodithiophene was chosen as the electron donating moiety due to its strong intramolecular charge transfer ability and planar structure. Furthermore, in order to enhance conjugation length, thiophene and bithiophene units were incorporated between donor and acceptor moieties as a π-bridge. Electrochemical and spectroelectrochemical and kinetic studies were performed. Moreover, organic solar cell devices were constructed for both P1 and P2. Electroluminescence properties of P1 was also investigated.

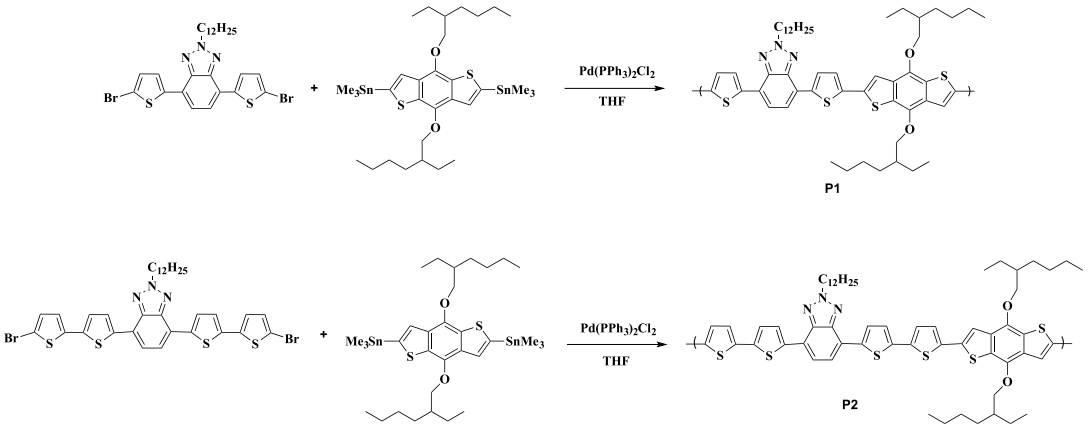

Figure 1.29: Synthetic route for copolymers, P1 and P2.

CHAPTER 2

EXPERIMENTAL

2.1 Materials

1H-Benzotriazole, 1-bromododecane, potassium tert-butoxide, tributyltin chloride, ammonium chloride, bis(triphenyl- phosphine)palladium(II) dichloride, N-bromosuccinimide, sodium bicarbonate, bromine, hydrobromic acid, thiophene, magnesium sulfate, acetic acid, methanol, dichloromethane, hexane, chloroform, and 2,6-bis(trimethylstannyl)-4,8-bis(2-ethyl-hexyloxy)benzo[1,2-b:4,5-b']dithiophene were purchased from Sigma Aldrich Chemical Co. Ltd and were used without further purification. $PC_{71}BM$ was obtained from Solenne. All reactions were carried out under an argon atmosphere unless otherwise mentioned. Tetrahydrofuran (THF) was freshly distilled over Na/benzophenone ketyl. Tributyl(thiophene-2-yl)stannane, 2-dodecylbenzotriazole and 2-dodecyl-4,7-di(thiophen-2-yl)-2H- benzo[d][1,2,3]triazole (TBT) were synthesized according to previously described methods [108].

2.2 Syntheses of Monomers

The synthetic routes towards monomers were shown in Figure 2.1. Compound 2 was synthesized according to reported procedures in literature [45]. Compound 2 was coupled via Stille polycondensation with compound 3 and 4 to obtain 2-dodecyl-4,7-di(thiophen-2-yl)-2H- benzo[d][1,2,3]triazole (5) and 2-dodecyl-4,7-di(bithiophen-2-yl)-2H-benzo[d][1,2,3]triazole (6), respectively. The resultant

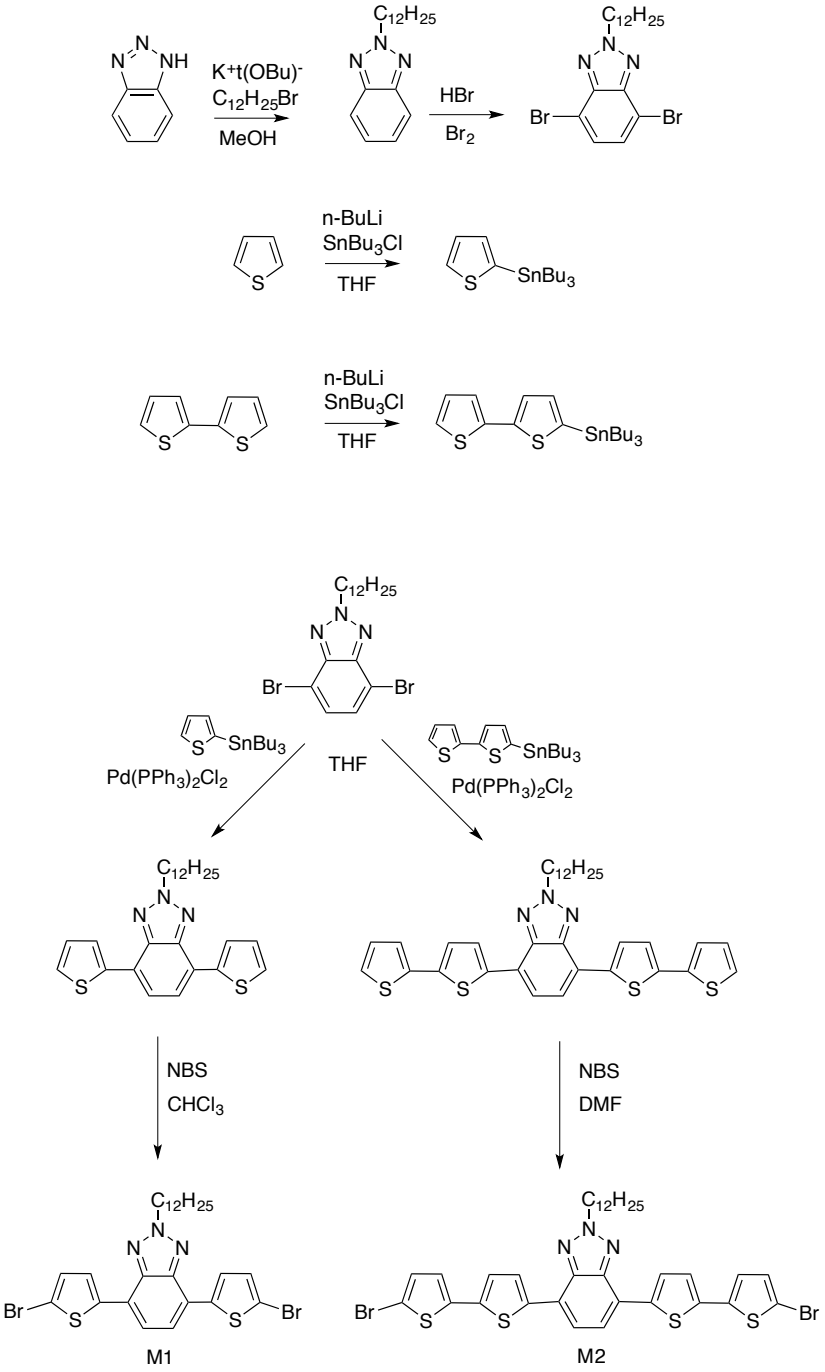

Figure 2.1: Synthetic route of monomer 1 and monomer 2.

products were brominated in the presence of N-bromosuccinimide (NBS), $CHCl_3$ and DMF, to obtain monomer 1 and monomer 2, respectively.

2.2.1 Synthesis of tributyl(thiophen-2-yl)stannane

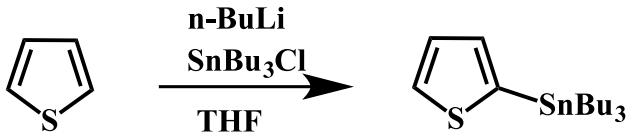

Figure 2.2: Synthesis of tributyl(thiophen-2-yl)stannane.

Thiophene (2.00 g, 23.8 mmol) and freshly distilled THF (25 mL) were added in a 100 mL three-necked flask under argon atmosphere. n-Butyl lithium (9.50 mL, 2.5 M in hexane, 23.8 mmol) was added drop wise to the solution at −78 °C. Subsequently, the solution was stirred for 1 h at room temperature. After cooling to −78 °C, tributyltin chloride (23.8 mL, 28.5 mmol) was added drop wise. The mixture was allowed to reach room temperature gradually and stirred overnight. After evaporation of solvent under reduced pressure, dichloromethane was added and the mixture was washed with NH_4Cl(saturated), brine(saturated) and distilled water until a clear organic layer was obtained. The organic layer was dried over anhydrous $MgSO_4$. After removal of solvent, a light yellow liquid was obtained [109]. The product was used without further purification. (8.35 g, yield: 94 %).

^{1}H NMR (400 MHz, $CDCl_3$, ppm): δ 7.67 (d, J = 4.6 Hz, 1H), 7.27 (t, J = 3.2 Hz, 1H), 7.21 (d, J = 3.2 Hz, 1H), 1.59 (m, 6H), 1.37 (m, 6H), 1.12 (t, J = 8.3 Hz, 6H), 0.91 (t, J = 7.0 Hz, 9H).

^{13}C NMR (100 MHz, $CDCl_3$): δ 136.2, 135.2, 130.6, 127.8, 28.98, 27.28, 13.68, 10.82.

2.2.2 Synthesis of [2,2'-bithiophen]-5-yltributylstannane

2-2'-Bithiophene (3.00 g, 18.0 mmol) was dissolved in anhydrous THF (30 mL) in a 100 mL three-necked round bottom flask and kept under argon atmosphere. The reaction temperature was cooled to −78 °C, n-butyl lithium (7.22 mL, 2.5 M in hexane, 18.0 mmol) was added drop wise. Afterwards, the solution was stirred

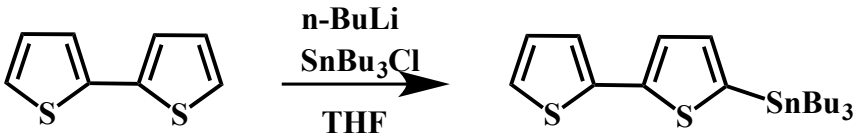

Figure 2.3: Synthesis of [2,2'-bithiophen]-5-yltributylstannane.

at this temperature for 1 h. Tributyltin chloride (5.87 mL, 21.6 mmol) was added drop wise at −78 °C. After completion tributyltin chloride addition, the solution was gradually warmed room temperature and stirred overnight under argon atmosphere. After 12 hours, solvent was evaporated under reduced pressure and dichloromethane was added and the mixture was washed with $NaHCO_3$ (saturated), brine (saturated) and distilled water. Subsequently, the organic layer was dried over anhydrous $MgSO_4$. After evaporation of solvent, green colored liquid was attained. The product was used without further purification. (2.46 g, yield 30 %).

^{1}H NMR (400 MHz, $CDCl_3$, ppm): δ 7.32 (d, J = 3.3 Hz, 1H), 7.21 (d, J = 5.1 Hz, 1H), 7.09 (d, J = 3.3 Hz, 1H), 7.09 (d, J = 3.5 Hz, 1H), 7.03 (d, J = 3.6 Hz, 1H), 1.43-1.34 (m,6H), 1.16 (t, J = 8.4 Hz, 6H), 1.16 (t, J = 8.3 Hz, 6H), 0.98-0.93 (m, 9H) .

^{13}C NMR (100 MHz, $CDCl_3$): δ 136.1, 127.8, 127.7, 125.0 124.3, 123.9, 123.8, 123.5, 29.00, 27.30, 10.70, 10.92.

2.2.3 Synthesis of 2-dodecyl-2H-benzo[d][1,2,3]triazole

1H-benzo[d][1,2,3]triazole (5.02 g, 42.1 mmol) was added into two-necked round bottom flask, dissolved and refluxed in methanol (30 mL). After 30 minutes of reflux, KOtBu (4.73 g, 42.2 mmol) was added to reaction medium followed by, 1-Bromododecane (12.6 g, 50.6 mmol). The reaction was allowed to reflux overnight. The completion of the reaction was controlled by TLC. Methanol

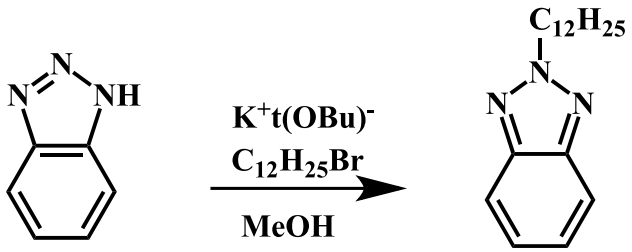

Figure 2.4: Synthesis of 2-dodecyl-2H-benzo[d][1,2,3]triazole.

was evaporated and chloroform was added to crude product. After that, the organic layer was washed with brine (saturated) and distilled water until a clear organic phase was obtained. The organic phase was dried over $MgSO_4$ and the solvent was evaporated under reduced pressure. Column chromatography was performed with $CHCl_3$: Hexane (2:1) as the eluent. Product was obtained as a colorless oil [108]. (3.63 g, yield: 30 %).

^{1}H NMR (400 MHz, $CDCl_3$, ppm): δ 7.87 (m, 2H), 7.39 (m, 2H), 4.74 (t, J = 7.2 Hz, 2H), 2.15-2.08 (quin, J =7.3 Hz, 2H), 1.34-1.24 (m,18H), 0.87 (t, J = 6.6 Hz, 3H).

^{13}C NMR (100 MHz, $CDCl_3$): δ 144.28, 126.12, 117.95, 56.67, 31.90, 30.07, 29.59, 29.50, 29.37, 29.32, 29.03, 29.56, 22.67, 14.10.

2.2.4 Synthesis of 4,7-dibromo-2-dodecyl-2H-benzo[d][1,2,3]triazole

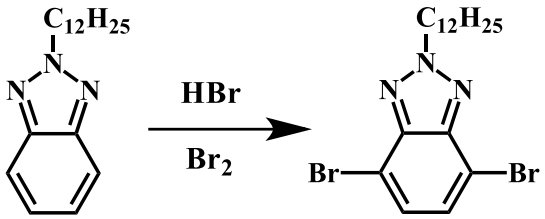

Figure 2.5: Synthesis of 4,7-dibromo-2-dodecyl-2H-benzo[d][1,2,3]triazole.

2-Dodecylbenzotriazole (3.00 g, 10.4 mmol) was dissolved in hydrobromic acid (5.8 M, 11.9 mL) and heated to 110 °C for 1 hour in a three-necked round bottom

flask. Afterwards, bromine (1.5 mL, 28.6 mmol) was added to reaction medium and the mixture was stirred and refluxed at 135 °C overnight. After completion of reaction, the mixture was cooled to room temperature and $NaHCO_3$ (saturated) was added to mixture and excess bromine was quenched with saturated $NaHCO_3$. After that, chloroform was added and the mixture washed with distilled water. Organic layer dried with $MgSO_4$ and chloroform was evaporated under reduced pressure. For further purification, column chromatography was performed with DCM:Hexane(1:1). The product was obtained as white solid. (3.47 g, yield: 75 %).

1^1H NMR (400 MHz, $CDCl_3$, ppm): δ 7.44 (s, 2H), 4.75 (t, J = 7.4 Hz, 2H), 2.14 (quin, J = 7.3 Hz, 2H), 1.36-1.24 (m, 18H), 0.87 (t, J = 6.7 Hz, 3H).

^{13}C NMR (100 MHz, $CDCl_3$): δ 143.7, 129.5, 109.9, 57.5, 31.91, 30.23, 30.22, 29.59, 29.49, 29.34, 28.98, 26.51, 22.68, 14.11.

2.2.5 Synthesis of 2-dodecyl-4,7-di(thiophen-2-yl)-2H-benzo[d][1,2,3]-triazole 4,7-Dibromo-2-dodecylbenzotriazole

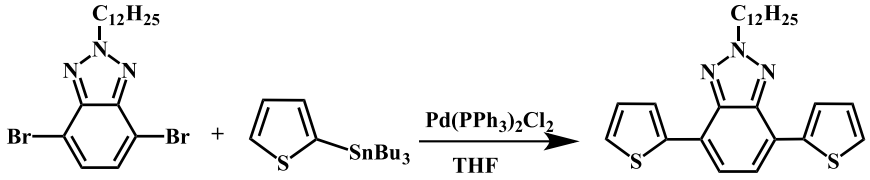

Figure 2.6: Synthesis of 2-dodecyl-4,7-di(thiophen-2-yl)-2H-benzo[d][1,2,3]triazole 4,7-Dibromo-2-dodecylbenzotriazole.

4,7-Dibromo-2-dodecyl-2H-benzo[d][1,2,3]triazole (600 mg, 1.35 mmol), and tributyl(thiophen-2-yl) stannane (1.39 g, 4.05 mmol) were added into three-necked round bottom flask under Ar atmosphere. Continuous argon flow was provided into reaction medium. Anhydrous THF (40 mL) and bis(triphenylphosphine)-palladium(II) dichloride were added to the reaction. The mixture was refluxed for 2 days under inert atmosphere at 125 °C. Completion of reaction was controlled with the TLC analysis and then solvent was evaporated under vacuum.

The crude product was purified by column chromatography (DCM:Hexane(1:2)) on silica gel to obtain green solid as the product. (1.37 g, yield 75 %).

1^1H NMR (400 MHz, $CDCl_3$, ppm): δ 8.10 (d, J = 2.6 Hz, 2H), 7.63 (s, 2H), 7.38 (d, J = 4.0 Hz, 2H), 7.18 (t, J = 3.7 Hz, 2H), 4.82 (t, J = 7.3 Hz, 2H), 2.20 (quin, J = 7.3 Hz, 2H), 1.45-1.24 (m, 18H), 0.82 (t, J = 6.6 Hz, 3H).

^{13}C NMR (100 MHz, $CDCl_3$): δ 142.1, 140.0, 128.1, 127.0, 125.5, 123.6, 122.8, 56.88, 32.00, 30.13, 29.71, 29.64, 29.53, 29.44, 29.13, 26.67, 22.58, 14.23. HRMS results; calculated mass: 452.2194, found mass: 452.2192

2.2.6 Synthesis of 4,7-di([2,2'-bithiophen]-5-yl)-2-dodecyl-2H-benzo[d][1,2,3]triazole

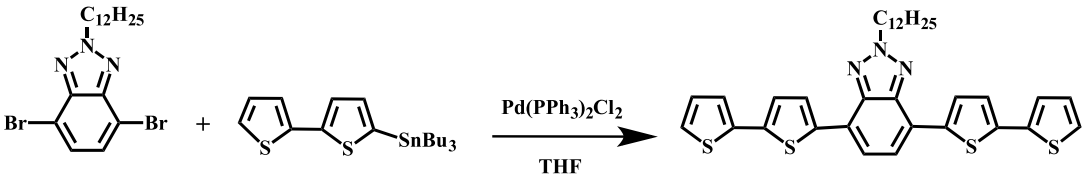

Figure 2.7: Synthesis of 4,7-di([2,2'-bithiophen]-5-yl)-2-dodecyl-2H-benzo[d][1,2,3]triazole.

4,7-Dibromo-2-dodecylbenzotriazole (489 mg, 1.10 mmol) and [2,2'-bithiophen]-5-yltributylstannane (2.50 g, 5.50 mmol) were added into two-necked round bottom flask. The reaction was kept under Argon atmosphere for 1h at room temperature. Then, freshly distilled THF (25 mL) was added to reaction medium at room temperature under argon atmosphere. After 30 minutes, bis(triphenylphosphine)palladium(II) dichloride (5 mol %) was added to reaction medium and the mixture was refluxed overnight at 125 °C. The completion of the reaction was controlled with TLC analysis. The solvent was evaporated under reduced pressure and column chromatography on silica was performed with DCM:Hexane(1:2) to obtain orange color solid product. (0.64 g, yield 94 %).

1^1H NMR (400 MHz, $CDCl_3$, ppm): δ 8.02 (d, J = 3.8 Hz, 2H), 7.59 (s, 2H), 7.27 (m, J = 1.1 , 2H), 7.26 (d, J = 1.5 Hz, 2H), 7.24 (d, J = 1.5 Hz, 2H), 7.06

(dd, J = 3.6 Hz, 2H), 4.85 (t, J = 7.2 Hz, 2H), 2.21 (quin, J = 7.6 Hz, 2H), 1.46-1.24 (m, 18H), 0.88 (t, J = 6.6 Hz, 3H).

^{13}C NMR (100 MHz, $CDCl_3$): δ 141.9, 138.8, 137.5, 137.5, 127.94, 127.9, 127.8, 124.8, 124.6, 124.4, 123.9, 123.9, 123.3, 122.4, 56.88, 31.94, 0.09, 29.66, 29.60, 29.49, 29.37, 29.07, 26.64, 22.71, 14.14. HRMS results; calculated mass: 615.1949, found mass: 615.1956.

2.2.7 Synthesis of 4,7-bis(5-bromothiophen-2-yl)-2-dodecyl-2H-benzo-[d][1,2,3]triazole

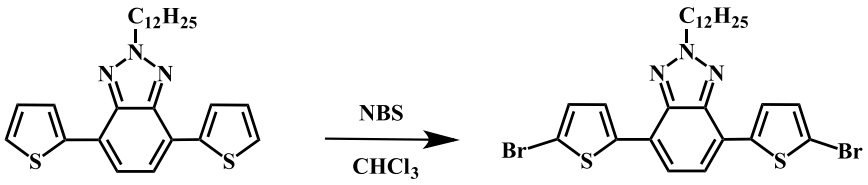

Figure 2.8: Synthesis of 4,7-bis(5-bromothiophen-2-yl)-2-dodecyl-2H-benzo[d]-[1,2,3]triazole.

2-Dodecyl-4,7-di(thiophen-2-yl)-2H-benzo[d][1,2,3]triazole (450 mg, 1.0 mmol) was dissolved in a mixture of chloroform (20 mL) and glacial acetic acid (20 mL). N-bromosuccinimide (445 mg, 2.5 mmol) was added to the mixture in several portions in the dark at room temperature. The mixture was stirred overnight at room temperature in the dark. $NaHCO_3$ (saturated) was added to the mixture and the organic layer was washed with distilled water. The organic phase was dried over $MgSO_4$. After filtration and solvent removal, the crude product was recrystallized from ethanol to obtain a yellow solid. (0.47 g, yield: 78 %).

1^1H NMR (400 MHz, $CDCl_3$, ppm): δ 7.79 (d, J = 3.9 Hz, 2H), 7.52 (s, 2H), 7.13 (d, J = 3.9 Hz, 2H), 4.80 (t, J = 7.3 Hz, 2H), 2.17 (quin, J = 6.6 Hz, 2H), 1.42-1.24 (m, 18H), 0.87 (t, J = 6.6 Hz, 3H).

^{13}C NMR (100 MHz, $CDCl_3$): δ 141.3, 130.9, 126.9, 123.0, 122.2, 115.3, 113.2, 56.96, 31.92, 30.06, 29.63, 29.60, 29.55, 29.44, 29.35, 29.02, 28.99, 22.70.

2.2.8 Synthesis of 4,7-Bis(5'-bromo-[2,2'-bithiophen]-5-yl)-2-dodecyl-2H-benzo[d][1,2,3]triazole

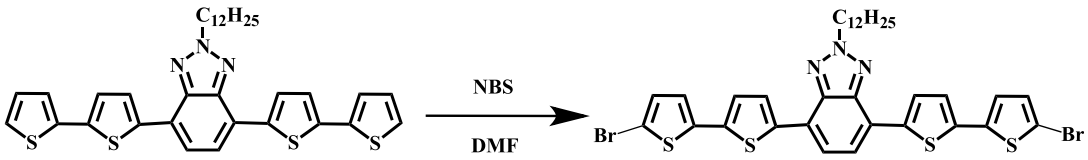

Figure 2.9: Synthesis of 4,7-Bis(5'-bromo-[2,2'-bithiophen]-5-yl)-2-dodecyl-2H-benzo[d][1,2,3]triazole.

4,7-di([2,2'-bithiophen]-5-yl)-2-dodecyl-2H-benzo[d][1,2,3]triazole (320 mg, 0.52 mmol) was dissolved in DMF (6 mL) in a round bottom flask. Then, N--bromosuccinimide (212 mg, 1.2 mmol) was added to reaction medium in several portions. The solution was stirred for 12 hours at room temperature. Solvent was evaporated under reduced pressure. Ethyl acetate was added to the crude product and organic layer washed with brine and distilled water. Organic layer was dried over Na_2SO_4 and the solvent was removed under reduced pressure. For further purification column chromatography was carried out using $CHCl_3$:Hexane(1:2) system as eluent. The product was obtained as a dark orange. (0.10 g, yield: 25 %).

^{1}H NMR (400 MHz, $CDCl_3$, ppm): δ 8.0 (d, J = 3.9 Hz, 2H), 7.58 (s, 2H), 7.18 (d, J= 3.9 Hz, 2H), 7.01 (s, 4H), 4.83 (t, J = 7.2 Hz, 2H), 2.24 (quin, J= 7.1 Hz, 2H), 1.46-1.24 (m, 18H), 0.87 (t, J = 6.5 Hz, 3H).

^{13}C NMR (100 MHz, $CDCl_3$, ppm): δ 141.9, 139.2, 138.9, 136.4, 130.7, 127.9, 124.9, 123.9, 123.25, 122.5, 111.2, 56.91, 31.91, 30.06, 29.63, 29.57, 29.46, 29.34, 29.03, 26.60, 22.68, 14.11.

2.3 Synthesis of poly(4-(5-(4,8-bis((2-ethylhexyl)oxy)-6-methylbenzo-[1,2-b:4,5-b']dithiophen-2-yl)thiophen-2-yl)-2-dodecyl-7-(5-methyl-thiophen-2-yl)-2H-benzo[d][1,2,3]triazole)

4,7-Bis(5-bromothiophen-2-yl)-2-dodecyl-2H-benzo[d][1,2,3]triazole (250 mg, 0.41 mmol), 2,6-bis(trimethylstannyl)-4,8-bis(2-ethylhexyloxy)benzo[1,2-b:4,5-b']di-

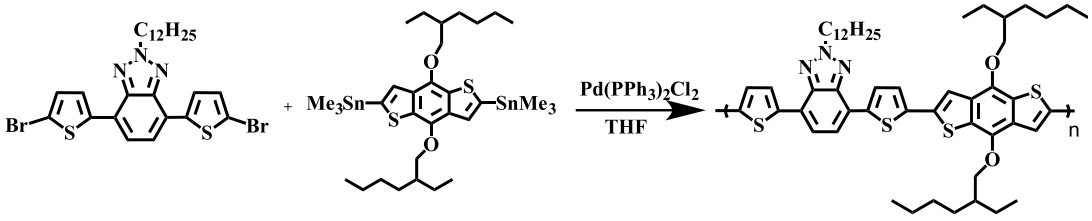

Figure 2.10: Synthesis f poly(4-(5-(4,8-bis((2-ethylhexyl)oxy)-6-methylbenzo-[1,2-b:4,5-b']dithiophen-2-yl)thiophen-2-yl)-2-dodecyl-7-(5-methylthiophen-2--yl)-2H-benzo[d][1,2,3]triazole).

thiophene (316.8 mg, 0.41 mmol) and bis(triphenylphosphine)palladium(II) dichloride (0.02 mmol) were mixed and refluxed at 110 °C under an argon atmosphere for 2 days in THF. The solvent was removed under reduced pressure. To remove oligomers, the crude product was washed with methanol, acetone, and hexane using Soxhlet extractor. Chloroform was used to extract polymer. Polymer was obtained as a red solid after precipitation from cold methanol. Yield: 37 %.

^{1}H NMR (400 MHz, $CDCl_3$, δ: ppm) 7.56 (BTz), 7.31 (BDT), 7.66 (thiophene), 4.77(-OCH_2), 3.23 (N-CH_2), 2.27 (-CH), 1.96-1.68 (-CH_2), 1.18-0.79 (–CH_3).

Mn: 34 kDa, Mw: 42 kDa, PDI: 1.2.

2.4 Synthesis of poly(4-(5'-(4,8-bis((2-ethylhexyl)oxy)-6-methylbenzo-[1,2-b:4,5-b']dithiophen-2-yl)-[2,2'-bithiophen]-5-yl)-2-dodecyl-7-(5'-methyl-[2,2'-bithiophen]-5-yl)-2H-benzo[d][1,2,3]triazole)

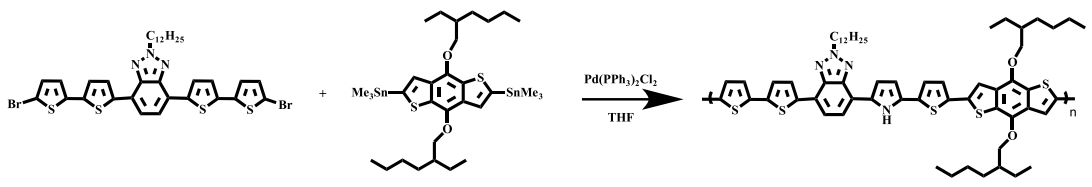

Figure 2.11: Synthesis of poly(4-(5'-(4,8-bis((2-ethylhexyl)oxy)-6-methylbenzo-[1,2-b:4,5-b']dithiophen-2-yl)-[2,2'-bithiophen]-5-yl)-2-dodecyl-7-(5'-methyl--[2,2'-bithiophen]-5-yl)-2H-benzo[d][1,2,3]triazole).

4,7-Bis(5'-bromo-[2,2'-bithiophen]-5-yl)-2-dodecyl-2H-benzo[d][1,2,3]triazole (76.3 mg, 0.098 mmol) was added into three necked round bottom flask and the reaction medium was purged with Argon gas for 1 hour. 2,6-bis(trimethylstannyl)-4,8-bis(2- ethylhexyloxy)benzo[1,2-b:4,5-b']dithiophene (75.9 mg, 0.098 mmol) was added to reaction medium was purged with argon atmosphere. After, freshly distilled THF (10 mL) was added to reaction mixture and the solution was heated to 125 °C. The reaction was allowed to refluxed at 125 °C and bis(triphenylphosphine)palladium(II) dichloride (4.93 mmol, 3.5 mg) was added to reaction medium, in the dark under argon atmosphere. The polymerization reaction was kept for 40 hours, chlorobenzene was added and after 6h stannylated thiophene was added as end cappers to the reaction medium. The solvent was evaporated and methanol added to the crude product. Later, methanol, acetone and hexane were used, respectively in soxhlet to remove oligomers. The polymer was extracted with chloroform, the solvent was removed and the product was precipitated in methanol to give the pure polymer. A green solid was obtained. The low solubility of monomer led to obtain low number average molecular weight of the polymer. Yield 20 %.

Mn: 5 kDa, Mw: 7 kDa, PDI: 1.4.

2.5 Methods and Equipment

^{1}H NMR and ^{13}C NMR spectra were recorded using a Bruker SpectroSpin Avance DPX-400 spectrometer, with tetramethylsilane (TMS) as the internal reference; chemical shifts were recorded in ppm. The UV-Vis spectra were recorded on Varian Cary 5000 UV-Vis spectrophotometer at room temperature. Cyclic voltammetry studies were carried out in a solution of 0.1 M of tetrabutylammonium hexafluorophosphate ($TBAPF_6$) in acetonitrile (ACN) solution at a scan rate of 100 mV s^{-1}. A Gamry 600 potentiostat was used with a three-electrode system in a quartz cell. Molecular weights and polydispersity indexes of the polymers were determined by gel permeation chromatography (GPC). Surface of ITO substrates were cleaned in Bandelin Sonorex Ultrasonic Bath. For further cleaning of anode surfaces Harrick Plasma Cleaner was used.

Organic layers of OPV and OLED devices were spin coated SAWATEC Spinner in MBraun glove box system. Evaporation of metal cathode was performed in the glove box MBRAUN MB EVAPORATOR. Current/Luminance-Voltage characteristics were performed with Keithley 2400 Source, Maya2000PRO Spectrophotometer and a Newport fiber optic.

2.6 Electrochemical Studies

For cyclic voltammetry studies, polymers were dissolved in $CHCl_3$ (5 mg/mL) and spray coated onto ITO coated glass substrate using an Omni spray coating gun. A three electrode system was constructed; ITO substrate was used as the working electrode, Pt wire as the counter electrode and Ag wire as the reference electrode which was calibrated against Fc/Fc^+ reference electrode. 0.1 M $TBAPF_6$ was used as the supporting electrolyte. In order to conduct electrochemical studies, polymers were coated on ITO electrodes and dipped into monomer free solutions.

Cyclic voltammetry studies were performed in order to investigate redox properties of the polymers. Since polymers have ambipolar (both p and n dopable) character, HOMO and LUMO energy levels were calculated from the onset of the oxidation of p-doping states and onset of the reduction of n-doping states, respectively.

2.7 Spectroelectrochemical Studies

Polymer films were coated on ITO electrodes and dipped into monomer free solutions of 0.1 M $TBAPF_6$/ACN. In order to investigate the electronic transitions and optical changes upon doping, benzotriazole bearing copolymers were subjected to incrementally increasing applied potential while recording UV–Vis spectra.

2.8 Kinetic Studies

Kinetic studies were performed to determine switching times and percent transmittance changes (ΔT%) of the polymers. The measurements were performed between the neutral and fully oxidized states of the polymers with 5 s time intervals.

2.9 Organic Solar Cell and Organic Light Emitting Diode Fabrications

2.9.1 Anode Cleaning: ITO

ITO glass substrates were purchased from Visiontek Systems and the substrates were etched with acid solution (12 M HCl acid) to avoid a short-circuit. Cleaning step is a very crucial step affecting fabrication of other layers. ITO substrates are sonicated for 15 minutes with toluene, detergent (Hellmanex III), distilled water, and isopropanol, consecutively. After this process, N_2 gas was used to dry substrates. In order to remove small organic impurities from the surface, ITO substrates were subjected to oxygen plasma for 5 minutes. Moreover, plasma cleaning increases the work function of the ITO surface and enable to create more hydrophilic surface for PEDOT:PSS layer.

2.9.2 Coating Hole Transport Layer (PEDOT: PSS) and Active Layer

Poly (3,4-ethylenedioxythiophene) (PEDOT-PSS) solution is filtered from 0.45 µm PVDF membrane and spin-coated on cleaned ITO surface with a thickness of 40 nm to obtain a smooth, clean and hydrophilic hole transport layer [110]. Since PEDOT:PSS is dispersed in water, residual water is removed by annealing for 10 minutes at 150 °C.

Active layer contribution is different for OSC and OLED devices. In OSC, active layer consists of polymer PCBM blend in an organic solvent. However, in OLED applications active layer comprises of only polymer in a solvent. In OSC

applications; Polymer-$PC_{70}BM$ blends, were prepared at different weight ratios and spin-coated under N_2 atmosphere.

2.9.3 Thermal Evaporation of Cathode Material

0.8 nm LiF and 100 nm Al were thermally evaporated with an average rate of 0.08 and 1 $\text{Å}\,\text{s}^{-1}$, respectively in the glove box system. A very thin layer of LiF buffer layer lowers the work function of Al layer and protects the active layer from increasing temperature during Al deposition hence it increases the open circuit value and fill factor of the device [111].

2.9.4 Characterization of OSC

J–V curves were recorded with a Keithley 2400 source meter under simulated AM 1.5 G illumination of 100 $\text{m}\,\text{W}\,\text{cm}^{-2}$ with a Newport solar simulator. Incident photon to current efficiencies (IPCE) of solar cells were recorded by the Oriel Quantum Efficiency Measurement system and as a reference monosilicon diode was used which have response between 300 nm-900 nm

2.9.5 Characterization of OLED

Spectra-Suite Software was connected to Maya2000PRO spectrophotometer and the electroluminescence (EL) spectra was measured upon applied potential. Keithley 2400 source-meter was used to record the current density-voltage and luminance-voltage curves.

CHAPTER 3

RESULTS AND DISCUSSION

3.1 Electrochemical Studies

Electrochemical studies were performed to determine electronic band gap, HOMO - LUMO energy levels and redox behavior of the polymers. For cyclic voltammetry studies, polymers were dissolved in $CHCl_3$ (5 mg/mL) and spray coated onto ITO coated glass substrate using Omni spray coating gun. The thicknesses of the polymers were less than a micron to study their electrochromic properties. Three electrode system was constructed in a quartz cell. 0.1 M $TBAPF_6$ was used as the supporting electrolyte and ACN as a solvent. All cyclic voltammetry experiments performed at 100 mV/s scan rate.

Since polymers have ambipolar (both p and n dopable) character, HOMO and LUMO energy levels were calculated from the onset of the oxidations of p-doping states and onset of the reductions of n-doping states, respectively. Cyclic voltammograms of polymers are shown in Figure 3.1. P1 has two reversible redox couples in the p-type doping/dedoping processes, P2 has one reversible redox couple. First redox couple of P1 was at 0.89 V and 0.57 V and the second one was seen at 1.19 V and 0.89 V, redox couple of P2 is at 1.00 V and 0.58 V. The respective n-type doping/dedoping redox couples were located at −1.57 Vand −1.59 V for P1 and for P2, respectively. The onset of the oxidation at p-doping state was 0.63 V for P1 and onset of the reduction at n-doping state was −1.95 V. From (3), HOMO-LUMO energy levels were calculated as −5.38 eV and −3.16 eV, respectively and electronic band gap for P1 was found as 2.22 eV. For P2, the

onset of the oxidation at p-doping state and the onset of the reduction at n-doping state were found as 0.63 V and −1.93 V, respectively. HOMO-LUMO energy levels were calculated as −5.38 eV and −3.14 eV, respectively. Electronic band gap was found as 2.24 eV. Relatively low HOMO energy level is beneficial to obtain high open circuit voltage (V_{oc}) value, since V_{oc} is proportional to the difference between the LUMO of the acceptor and the HOMO of the donor. Table 3.1 summarizes optoelectronic properties of the polymers.

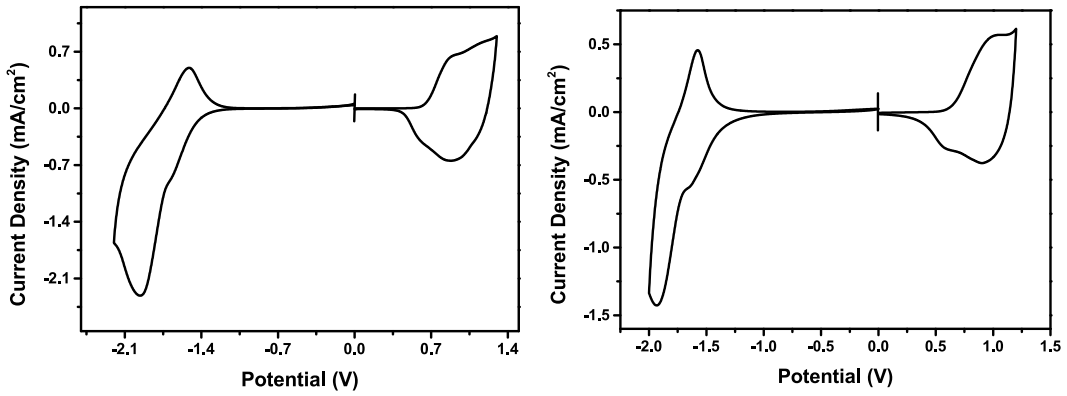

Figure 3.1: Cyclic voltammograms of P1 and P2 in a solution of 0.1 M $TBAPF_6$-/ACN.

$$HOMO = -(E_{ox}, onset + 4.75)eV \tag{3.1}$$

$$LUMO = -(E_{red}, onset + 4.75)eV \tag{3.2}$$

Table 3.1: Summary of electrochemical studies.

	E p-doping (V)	E p-dedoping (V)	E^{ox} onset (V)	E n-doping (V)	E n-dedoping (V)	E^{red} onset (V)	HOMO (eV)	LUMO (eV)	Eg el (eV)
P1	0.89/ 1.19	0.57/ 0.89	0.63	-1.95	-1.51	-1.59	-5.38	-3.16	2.22
P2	1.00	0.58	0.63	-1.93	-1.57	-1.61	-5.38	-3.14	2.24

Incorporation of conjugated π-bridge into polymer backbone influences electronic and optical properties of the polymers. π-bridge does not affect LUMO energy level however, it has strong influence on HOMO energy level [112]. Although, low lying HOMO level increase the V_{oc} value, it reduces the light harvesting of OSC device. LUMO values of the polymers are effective enough for good charge transfer where energy level diagram of P1 and P2 are given in Figure 3.1.

In order to investigate stabilities of the polymers and to prove non diffusion controlled mass transfer during redox process, current density vs. potential data were collected at different scan rates. Randles-Sevcik equation given in Equation 3.3 explains relationship between the current and scan rate. Linearity of current density vs scan rate proves there was non-diffusion controlled mass transfer between anion of electrolyte and polymer film surface. This situation suggests that anions of supporting electrolyte create anion layer on polymer chains and mass transfer occurs between these two layers. Figure 3.2 shows change in cyclic voltammograms at different scan rate for both P1 and P2.

$$i_p = 0.4463nFAC\left(\frac{nF\upsilon D}{RT}\right)^{\frac{1}{2}} \tag{3.3}$$

where

- i_p = current in amps,
- n = number of electrons transferred in the redox event,
- A = electrode area in cm^2,
- F = Faraday Constant in C/mol,
- D = diffusion coefficient in cm^2/s,
- C = concentration in mol/cm^3,
- υ = scan rate in V/s,
- R = gas constant in $J\,K^{-1}\,mol^{-1}$ and

- T = temperature in K.

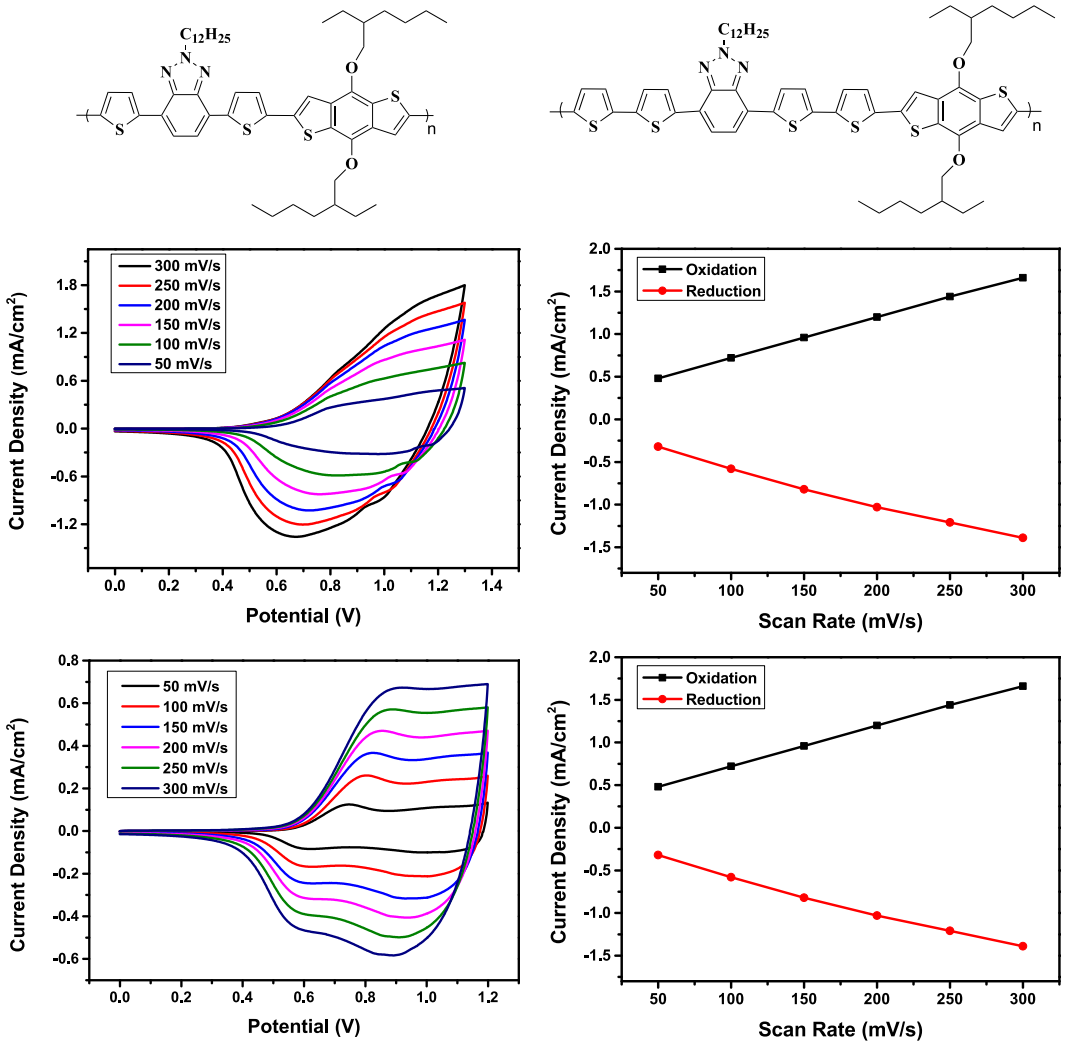

Figure 3.2: Cyclic voltammograms of P1 and P2 in 0.1 M $TBAPF_6$/ACN electrolyte/solvent couple at different scan rates.

3.2 Spectroelectrochemical Studies

In order to investigate electronic transitions and optical changes upon doping, benzotriazole and benzodithiophene bearing copolymers P1 and P2 were subjected to incrementally increasing applied potential while recording UV–Vis spectra. Polymer films were coated on ITO electrodes and dipped into solutions

of 0.1 M $TBAPF_6$/ACN supporting electrolyte solvent couple. Polymers showed electrochromic properties. They show reversible color change upon external potential. As shown in Figure 3.3 and Figure 3.4, maximum absorption bands were observed at 500 nm and 495 nm at the neutral state which corresponds to π-π*

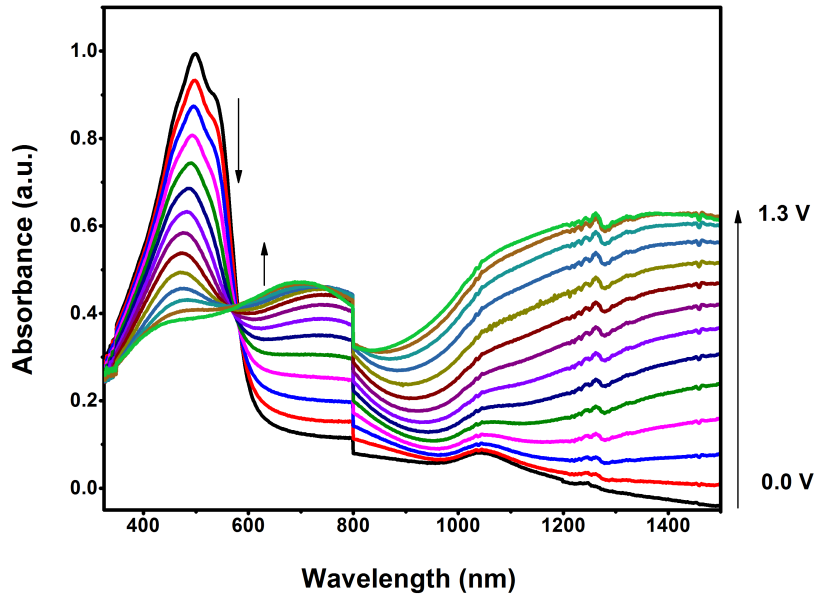

Figure 3.3: Change in the electronic absorption spectra of P1 in 0.1 M $TBAPF_6$-/ACN electrolyte/solvent couple upon oxidative doping at potentials between 0.0/1.3 V.

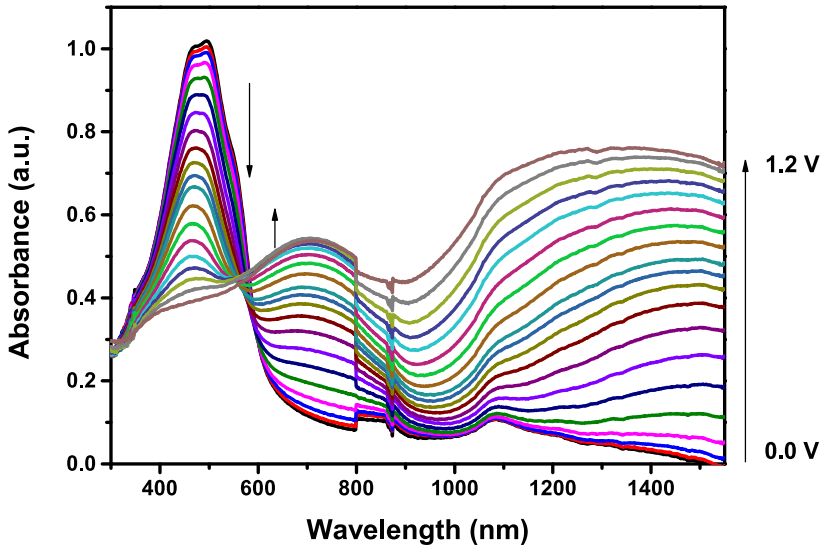

Figure 3.4: Change in the electronic absorption spectra of P2 in 0.1 M $TBAPF_6$-/ACN electrolyte/solvent couple upon oxidative doping at potentials between 0.0/1.2 V.

inter band transition for copolymers P1 and P2, respectively. While applied potential was increasing, the absorption of π-π^* transition decreased meanwhile new absorption bands started to form at around 700 nm and 1370 nm for P1, 720 nm and 1450 nm for P2. The formation of these new bands at longer wavelengths are due to the formation of polaronic (radical cation) and bipolaronic (dication) charge carriers on the polymer backbone. 5 nm red shift in absorbance spectra was observed for P1 compared to P2 due to stronger π-π stacking between polymer chains which leads to higher intermolecular interaction. P2 was expected to have red shifted absorption due to enhanced conjugation length through by bithiophene unit. Since P1 has high molecular weight compared to P2 a red shifted absorption was observed for P1. The number average molecular weight of P1 is 34 kDa whereas 5 kDa for P2.

Optical band gap of the polymers were calculated from the onset of the neutral state absorption. As summarized in Table 3.2, these onsets are located at 653 nm and 645 nm for respective polymers. For the polymers optical band gaps were calculated as 1.90 eV and 1.92 eV from Equation 3.4. Electronic band gap is higher than optical band gap due to incorporation of electron binding energy. Spectroelectrochemical studies upon n-doping were conducted and shown in Figure 3.5. Polymers showed quite stable character upon n-doping process. Moreover, from claret red to greenish color change for P1 and from claret red to gray color change for P2 were observed at n-doping state.

$$E_g^{op} = \frac{1241}{\lambda_{onset}} \tag{3.4}$$

Table 3.2: Summary of the Spectroelectrochemical studies.

	λ_{max} (nm)	λ_{max}^{onset} (nm)	E_g^{op} (eV)
P1	500	653	1.90
P2	495	645	1.92

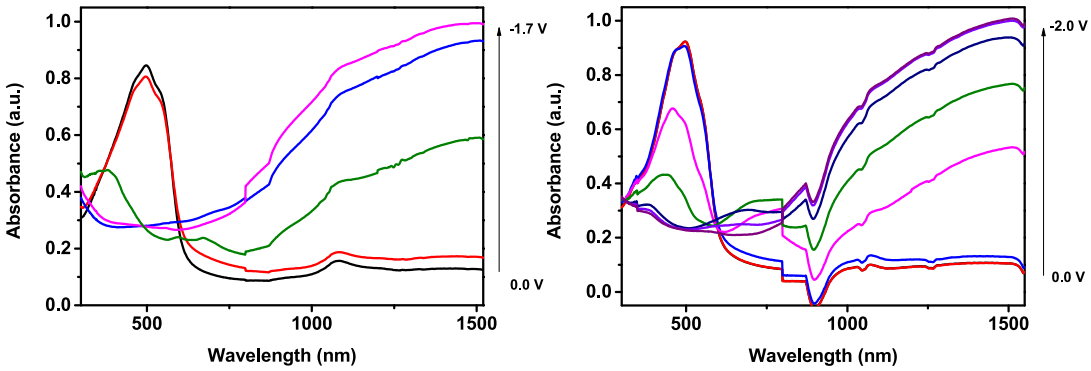

Figure 3.5: Change in the electronic absorption spectra of P1 and P2 upon oxidative doping at potentials between 0.0/-1.7 V, 0.0/-2.0 V, respectively.

3.2.1 Colorimetry Studies

Colorimetry studies were conducted to report scientific colors of the polymers upon applied potential. International Commission on Illumination created CIE color space to be used as a reference. L indicates luminance and a, b indicate color opponent dimensions. Related data were summarized in Table 3.3. Moreover, reversible color changes of polymers upon oxidation and reduction also recorded and depicted in Figure 3.6.

Table 3.3: Colors of the polymers at different voltages.

	Applied Potential (V)	**L**	**a**	**b**
P1	-2.0	52	-4	-1
	0.0	45	36	2
	0.9	45	36	2
	1.1	48	0	3
	1.3	45	-1	-3
P2	-1.9	63	-1	-1
	0.0	51	27	1
	0.9	56	5	0
	1.2	62	0	-6

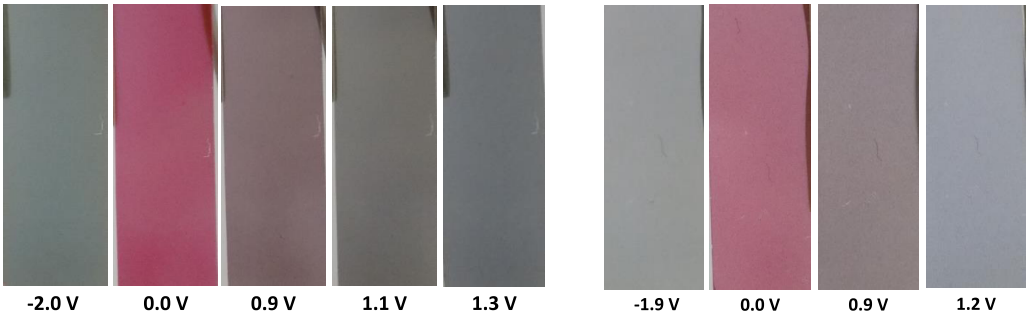

Figure 3.6: Color changes of P1 and P2, respectively.

3.3 Kinetic Studies

Kinetic studies were performed to determine switching times and percent transmittance changes (ΔT%) of the polymer.

The measurement was done between the neutral and fully oxidized states of the polymers with 5 seconds time intervals. As shown in Figure 3.7 and summarized in Table 3.4, the copolymer P1 film revealed 18 % optical contrast with a switching time of 0.4 s at 500 nm, 14 % optic contrast with a switching time of 0.5 s at 700 nm, 36 % optical contrast with 0.4 s switching time at 1370 nm. P2 showed better results at VIS and NIR regions. 20 % optic contrast with a switching time of 0.6 s at 495 nm, 14 % with a 0.6 s switching time at 720 nm and lastly, 48 % optic contrast at 1450 nm with a 0.3 s switching time. P2 was quite stable at NIR region with a very short short switching time due to more quinoid-structure formation at this region.

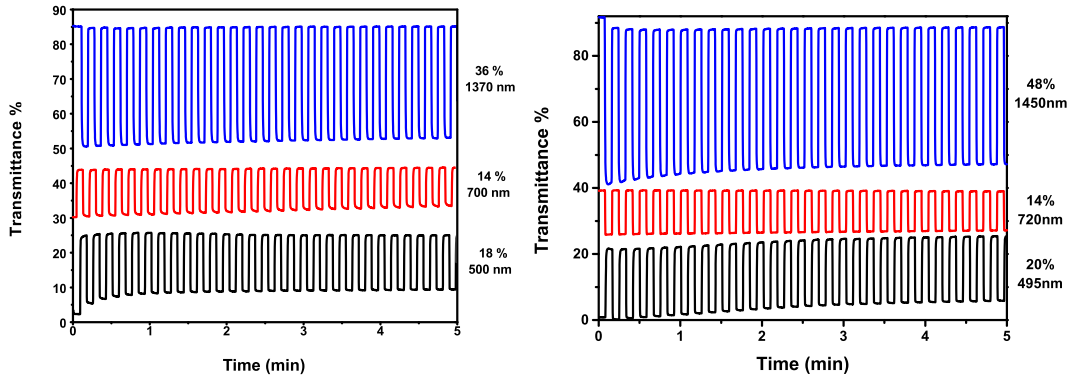

Figure 3.7: Changes in the percent transmittances for P1 and P2.

Table 3.4: Electrochromic switching and changes in % transmittance of the P1 and P2 on ITO electrode in 0.1 M ACN/$TBAPF_6$ solvent/electrolyte system.

	λ (nm)	**Optical Contrast (%)**	**Switching Time (s)**
P1	500	18	0.4
	700	14	0.5
	1370	36	0.4
P2	495	20	0.6
	720	14	0.6
	1450	48	0.3

3.4 Photovoltaic Studies

Two novel benzotriazole and benzodithiophene bearing alternating copolymers were synthesized and thiophene (P1) and bithiophene (P2) conjugated units were incorporated between donor and acceptor units. Our aim was to enhance PCE via the incorporation of π-bridges resulting in enhanced charge carrier mobility. Exciton dissociation and charge transport properties are affected by charge carrier mobility.

In order to investigate photovoltaic properties of the polymers, bulk heterojunction solar cells were fabricated with a device architecture of ITO/PEDOT:PSS (Clevios) (40 nm)/Polymer:$PC_{71}BM$/LiF(0.8 nm)/Al(100 nm). The performance of P1 and P2 based devices was optimized via changing the ratio of donor acceptor, spin coating speed (thickness of the active layer), thermal annealing treatment and addition of an additive. Since organic solar cell applications highly depend on solubility and film formation of the polymer fullerene blend, optimization of solvent is a crucial step in organic solar cell applications [113]. In this context, dissolving polymer $PC_{71}BM$ blend in o-DCB resulted in the best morphology. $PC_{71}BM$ was used as the acceptor to enhance absorption of the blend due to broad absorption range of $PC_{71}BM$ in visible region. Current density/voltage (J/V) characteristics of the optimized OSCs are shown in Figure 3.8

for P1 and Figure 3.9 for P2.

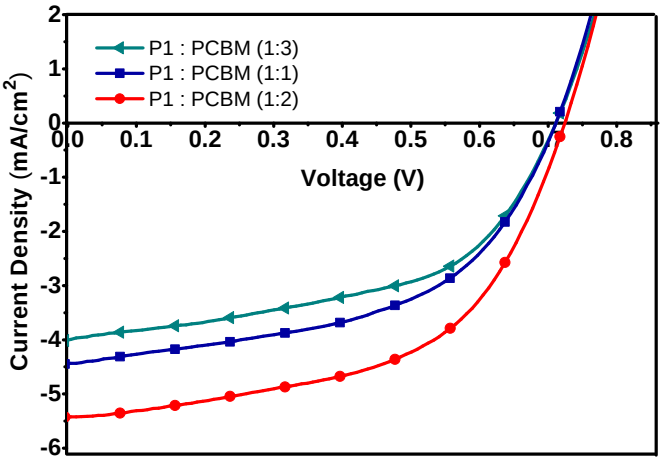

Figure 3.8: J–V curve of bulk heterojunction OSCs based on P1:$PC_{71}BM$ for 1:1, 1:2, and 1:3 blends.

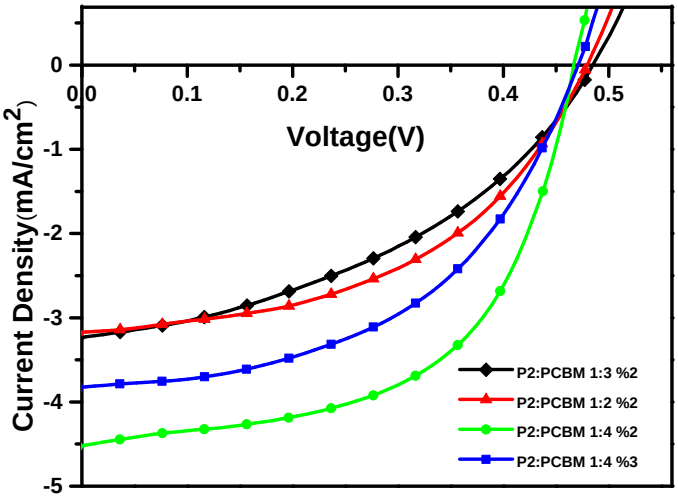

Figure 3.9: J–V curve of bulk heterojunction OSCs based on P2:$PC_{71}BM$ for 1:2, 1:3 and 1:4 blends.

The best performance was obtained with device construction of 1:2 P1:$PC_{71}BM$ ratio and 1:4 P2: $PC_{71}BM$. As summarized in Table 3.5 for P1, increasing $PC_{71}BM$ ratio from 1:1 to 1:2 was improved charge transport as a result power conversion efficiency (PCE) was enhanced [114]. However, increasing $PC_{71}BM$ ratio from 1:2 to 1:3 was decreased the short circuit current (J_{sc}) due to less contribution of the polymer on absorption. Moreover, it decreased the hole transport ability of the active layer [115]. Hereby, as depicted in Table 3.6 optimum ratio was found as 1:2 polymer:$PCB_{71}M$. In the case of P2 1:4 polymer $PCB_{71}M$ ratio was found as the optimum ratio. Increase in $PCB_{71}M$ amount led to enhancement of film formation and charge transport ability resulting in increase in J_{sc} and FF.

Table 3.5: Summarized Photovoltaic properties of P1*annealed at 110 °C for 10 minutes.

	Thickness (nm)	V_{oc} (V)	J_{sc} ($mA\,cm^{-2}$)	FF (%)	PCE (%)
P1:PCBM 1:1	102	0.71	4.45	52	1.64
P1:PCBM 1:2	116	0.72	5.45	54	2.12
P1:PCBM 1:3	125	0.71	4.00	52	1.48
P1:PCBM 1:2	108	0.73	5.34	50	1.82
P1:PCBM 1:3	108	0.74	4.70	57	2.00
P1:PCBM* 1:2	113	0.76	3.37	59	1.53

Normalized absorption spectra of P1: $PC_{71}BM$ (1:2) and P2: $PC_{71}BM$ (1:4) was demonstrated in Figure 3.10. The maximum absorption peaks of P1 and $PC_{71}BM$ blend in solution and in thin film were located at 473/510 nm and 493/530 nm, respectively. Due to enhanced intermolecular interactions through the polymer chains in the solid state, 20 nm a red shift was observed in UV-VIS absorption spectra of P1. Moreover, maximum absorption peaks of P2 and $PC_{71}BM$ blend in solution were located at 468/501 nm and in thin film at 495/533 nm around 30 nm red shift was observed resulting from increased π-π stacking and aggregation tendency through polymer chains in thin film form.

Table 3.6: Summarized photovoltaic properties of P2.

	V_{oc} (V)	J_{sc} (mA cm^{-2})	FF (%)	PCE (%)
P2:PCBM 1:2	0.48	3.17	48	0.73
P2:PCBM 1:3	0.49	3.24	41	0.66
P2:PCBM 1:4	0.47	4.52	56	1.20
P2:PCBM 1:4	0.47	4.51	43	0.91
P2:PCBM 1:4 1 % w/DIO	0.57	3.04	54	0.94
P2:PCBM 1:4 1 % w/DIO (MeOH) treatment	0.60	2.94	65	1.16

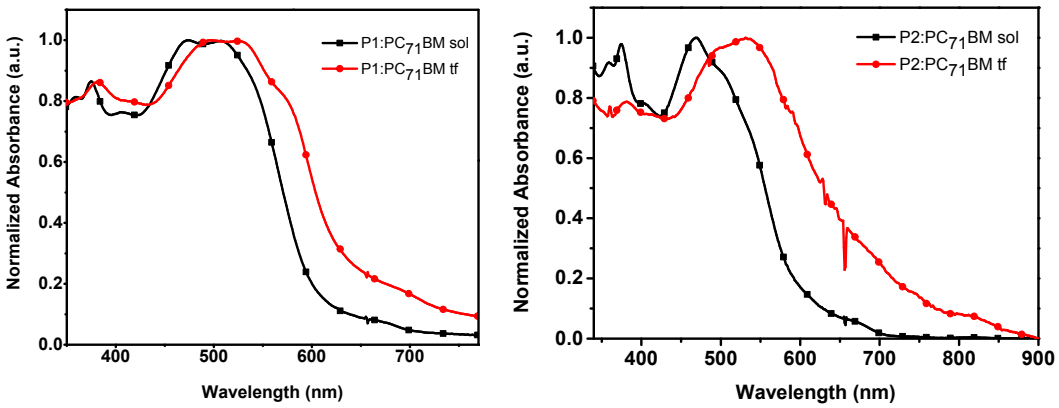

Figure 3.10: Normalized film and solution absorbance spectra for polymer:-$PC_{71}BM$ blends.

Active layer thickness should be optimized to balance the absorption and charge transport. Since the absorption of sun light is enhanced within active layer, thickness increases and this results in higher charge production. On the other hand, active layer thickness is limited to few hundreds of nanometers due to low diffusion length of organic materials which is around 10-20 nm [116]. The optimum active layer thickness for P1 based device was found as 116 nm, P2 based device 95 nm which was determined by AFM (Atomic Force Microscopy) (Figure 3.11 (a,b) and Figure 3.12 (a,b)). PSCs showed the highest photovoltaic performance of 2.12 % with V_{oc} of 0.72 V, J_{sc} of 5.45 mA/cm^2 and FF of 54 % for P1. The results of P2 were 1.20 % PCE with V_{oc} of 0.47 V, J_{sc} of 4.53 mA/cm^2 and 56 % for P1.

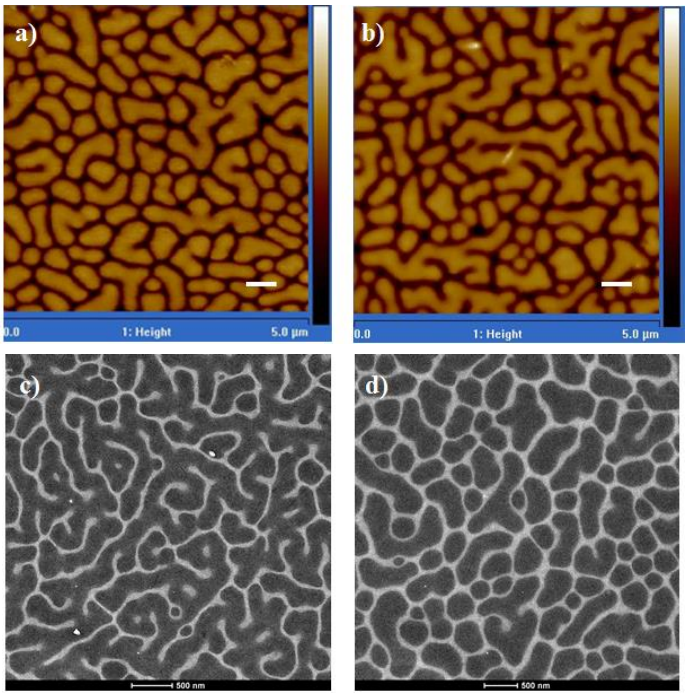

Figure 3.11: a) AFM height image of P1: $PC_{71}BM$ blend on ITO/PEDOT: PSS. b) AFM height image of P1: $PC_{71}BM$ blend on ITO/PEDOT: PSS annealed at 110 °C for 10 minutes. c) TEM image of P1:$PC_{71}BM$ blend d) TEM image of P1:$PC_{71}BM$ blend annealed at 110 °C for 10 minutes. Scale bars in AFM and TEM images are 500 nm.

Pre and post annealing treatments, addition of additive were carried out to improve the morphology of the active layer of P1 and P2 based devices. For the optimization of P1 based devices, active layer coated ITO substrates were annealed at different temperatures for different time periods. However, power conversion efficiency decreased from 2.12 % to 1.53 %. To investigate the effect of pre-annealing treatment on morphology, Transmission Electron Microscopy (TEM) and Atomic Force Microscopy (AFM) measurements were carried out. Due to the higher electron density of $PC_{71}BM$ compared to polymer, the dark areas correspond to $PC_{71}BM$ domains in TEM images. As depicted in Figure 3.11 (c,d), nanoscale morphology was adversely affected with thermal annealing. J_{sc} value was decreased from 5.45 mA/cm^2 to 3.37 mA/cm^2 due to the formation of less interconnected donor-acceptor network upon annealing. As a result PCE

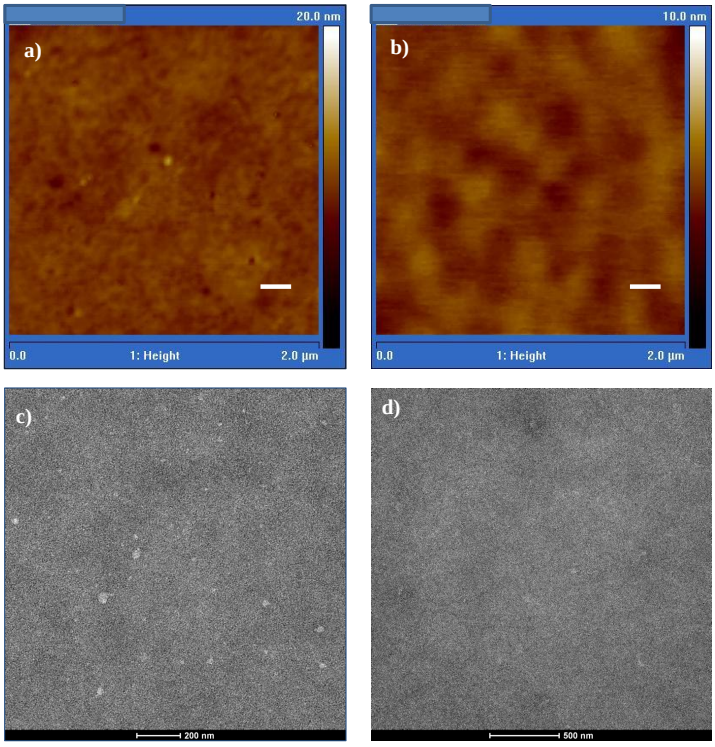

Figure 3.12: a) AFM height image of P2: $PC_{71}BM$ blend on ITO/PEDOT: PSS. b) AFM height image of P2: $PC_{71}BM$ blend with 1 % DIO with methanol treatment on ITO/PEDOT: PSS c) TEM image of P2:$PC_{71}BM$ blend d) TEM image of P2:$PC_{71}BM$ blend with 1 % DIO with methanol treatment. Scale bars in AFM and TEM images are 400 nm.

of the device decreased [117]. According to AFM results of the P1 blend film root mean square roughness (Rms) were determined as 6.79 nm and 6.47 nm annealed and not annealed devices, respectively. For further optimization for P1, addition of 1 % 1,8-diiodooctane (DIO) to polymer PCBM blend did not make any improvement on PCE.

Although, the addition of 1 % DIO decreased the PCE, methanol treatment on active layer surface improved the FF and V_{oc} of P2 based solar cell devices. Since DIO selectively dissolve PCBM molecules and has higher boiling point than o-DCB it can affect the formation of charge transfer states [118]. Since methanol removes residual additive from the surface of the active layer, enhances the stability of morphology. Methanol was chosen due to its low boiling point and

poor solvation capacity for polymers [119]. As a result, FF of the devices was improved from 56 % to 65 % and V_{oc} values from 0.47 V to 0.60 V. AFM and TEM images of P2 based organic solar cell devices are shown in Figure 3.12.

Incident photon to electron conversion efficiency (IPCE) measurements were performed and 40 % and 25 % IPCE values were obtained for the devices with the best results as shown in Figure 3.13 . External quantum efficiencies of P1 and P2 based devices as a function of wavelength from 350 nm to 750 nm match well with UV-Vis absorbance range of polymer $PC_{71}BM$ blend.

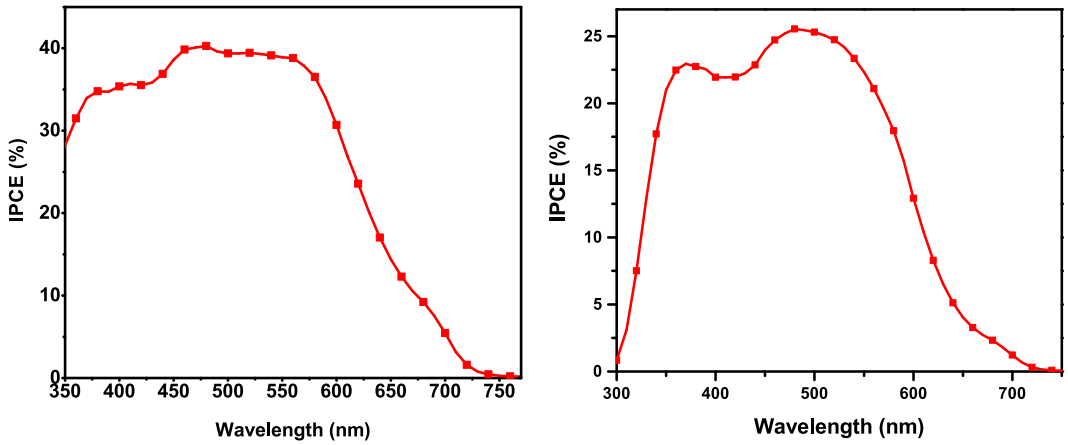

Figure 3.13: IPCE curve of the best performance solar cells of P1 and P2.

Molecular weight has very strong influence on molecular packing, charge carrier mobilities and blend morphology. Increasing molecular weight enhances the light absorption and hence increases the short circuit current. Moreover, it leads to higher hole mobilities with enhanced fill factor as a result higher power conversion efficiencies. Low molecular weight means lower in conjugation length and results in higher band gap. Lower V_{oc}, J_{sc} and PCE values are correlated with low molecular weight of P2 compared to P1. [120].

3.5 OLED Studies of P1

Emission studies were performed using Perkin Elmer Fluorescence Spectrometer. Thin films were prepared with spin-coater with a speed of 1500 rpm for

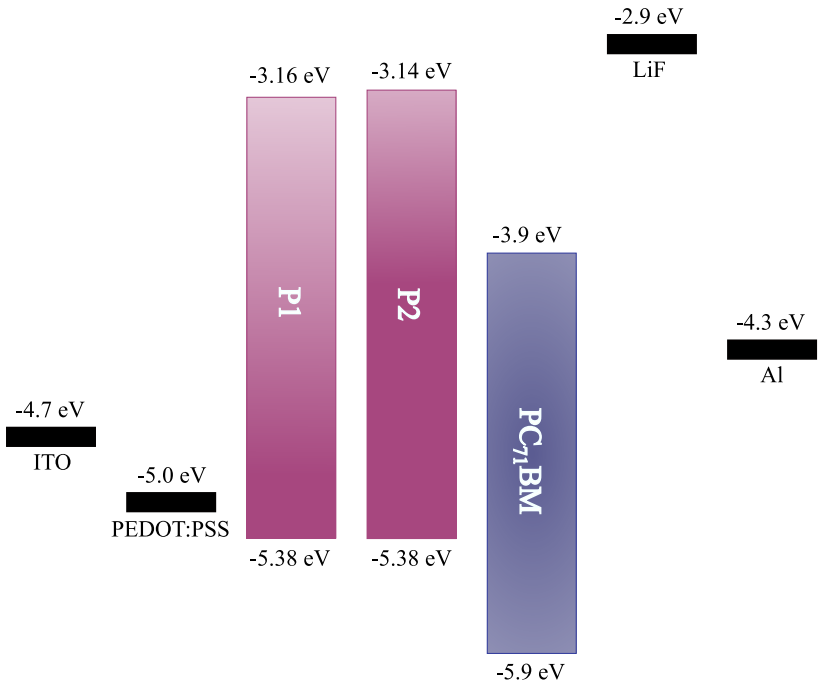

Figure 3.14: Energy level diagram of organic solar cell devices for P1 and P2.

60 seconds duration. Photoluminescence spectra of the polymer thin films and solution which were excited at 480 nm are depicted in Figure 3.15.

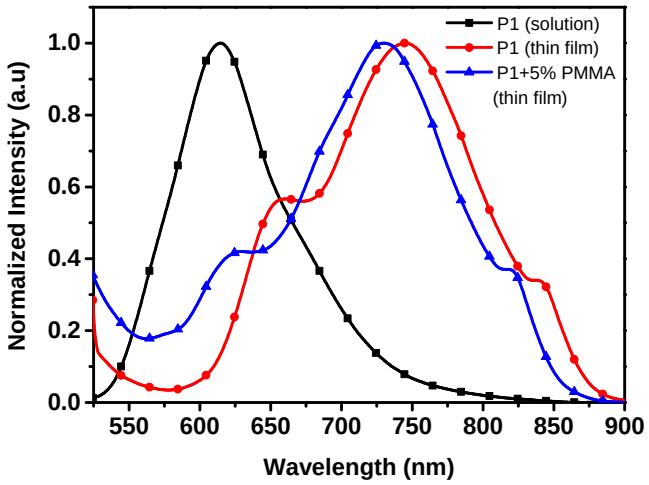

Figure 3.15: Photoluminescence spectra of P1.

The emission properties of P1 are shown in Figure 3.15. When electrons and

holes are recombined light is emitted. The maximum emission of P1 in chloroform located at 614 nm and thin film emission maximum at 745 nm. The excited state emission mechanism is highly affected by inter-chain interactions and hence broad red shift was observed in PL spectra of thin film compared to that of the one in solution. In solid state, the red shift in emission was observed due to π-π^* interaction and aggregation caused increase in the conjugation length.

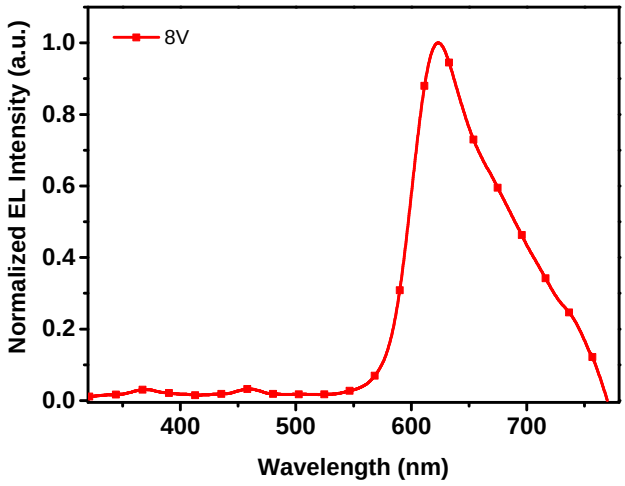

Figure 3.16: Electroluminescence spectra for ITO/PEDOT:PSS/P1/LiF/Al devices.

Electroluminescence is the light emission from the device under external voltage. Figure 3.16 demonstrates EL intensity of the OLED at 8 V. The maximum EL emission was at 624 nm which was blue shifted compared to PL emission.

Current density-voltage relationship was demonstrated in Figure 3.17. Luminance vs. voltage data were given in Figure 3.18. Highest luminance value was obtained as 60 cd/m^2 at 9 V. P1 based OLED revealed a low turn at 3.6 V.

As depicted in Figure 3.19, three parameters luminance, hue and saturation were demonstrated in the CIE Chromaticity coordinates and they were given for red polymer light emitting diode as x = 0.65, y = 0.34. At 8 V, the constructed device image was given in Figure 3.20.

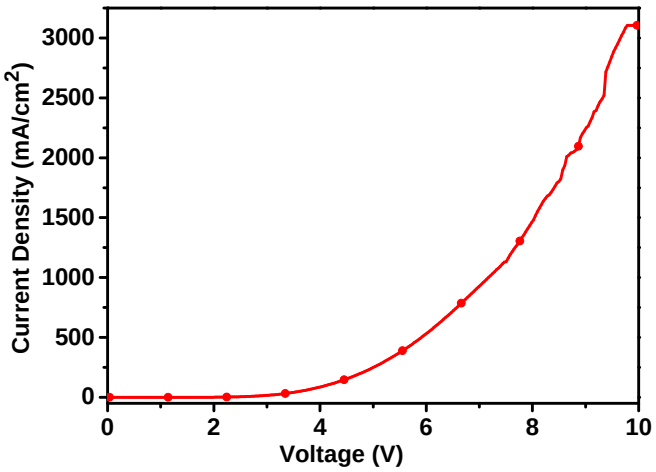

Figure 3.17: Current density vs. applied voltage for ITO/PEDOT:PSS/P1/-LiF/Al devices.

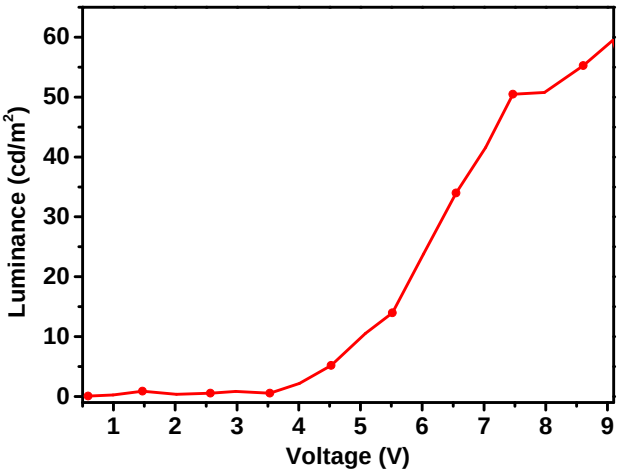

Figure 3.18: Luminance vs. applied voltage for ITO/PEDOT:PSS/P1/LiF/Al devices.

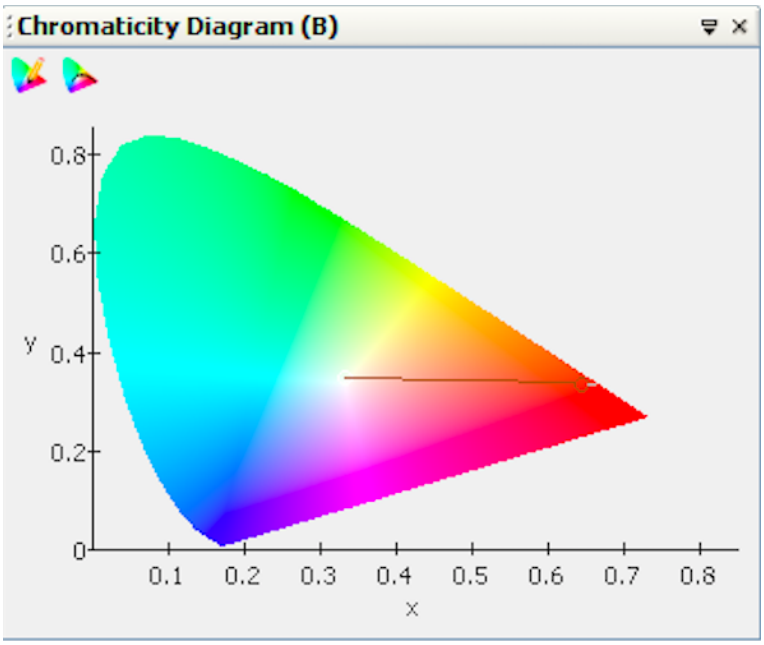

Figure 3.19: CIE chromaticity diagram for ITO/PEDOT:PSS/P1/LiF/Al devices.

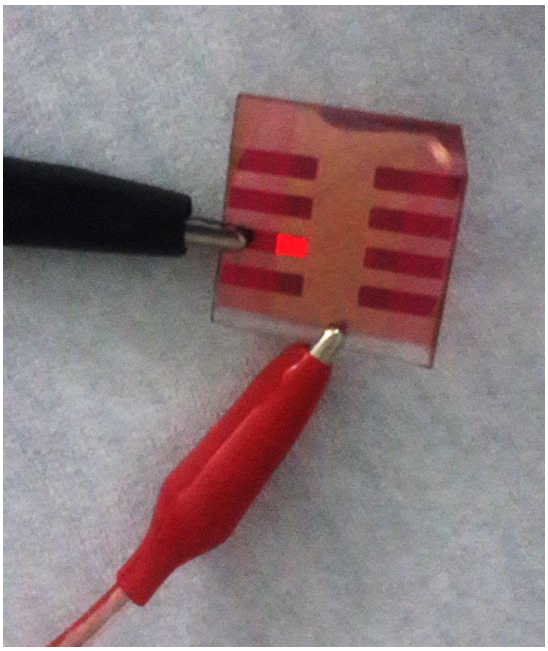

Figure 3.20: Constructed red emissive OLEDs.

CHAPTER 4

CONCLUSION

Two novel D-A type copolymers were synthesized by Stille polycondensation. Monomers and polymers were fully characterized by Nuclear Magnetic Resonance. Benzotriazole was used beacuse of its high electron transportin ability and benzodithiophene was also utilized due to its strong electron donating ability, planar structure and enhanced intramolecular charge transfer. Alkyl chains on the both benzotriazole and benzodithiophene units increased the solubility of the copolymers in different organic solvents which ease their further applications. Previously, Zou and coworkers synthesized benzotriazole coupled with benzodithiophene based copolymer with a shorter alkyl chain and they obtained maximum 1.7 % PCE [121]. Our aim was to investigate π-bridge effect on electrochemical, optical, OPV and OLED applications. Therefore, thiophene and bithiophene units were incorporated into polymer backbone to enhance the charge transfer and conjugation length and 2.12 % PCE was obtained which is higher than the previously synthesized similar structure polymer.

Gel permeation chromatography was used to determine molecular weight and polydispersity index of the polymers. The number average molecular weight of P1 was 34 kDa with a PDI of 1.2 whereas, the number average molecular weight of P2 was 5 kDa with a PDI of 1.4. Electrochemical, spectroelectrochemical and kinetic characterizations were performed. Since both polymers revealed ambipolar character HOMO-LUMO energy levels were calculated from cyclic voltammograms as -5.38 eV for both P1 and P2. -3.16 and -3.14 were the LUMO energy levels of the respective polymers. Electronic band gaps were

found as 2.22 and 2.24 eV for P1 and P2, respectively. Optical band gaps of the polymers were found from spectroelectrochemical experiments. The onset of the π-π^* of the neutral film gives optical band gap as 1.90 eV and 1.92 eV for P1 and P2, respectively. Kinetic studies were performed, good stabilities and low switching times were recorded around 0.4 s and 0.3 s with a 36 % and 48 %optical contrast at NIR region for P1 and P2, respectively. Due to increasing conjugation length, P2 should show red shifted character; however, due to its low molecular weight compared to P1, in other words less repeating units, optical properties of the polymers were very similar.

Organic photovoltaic applications of the polymers were conducted with a device structure of ITO/PEDOT:PSS/POLYMER:$PC_{71}BM$/LiF/Al. The active layer morphologies were analyzed with AFM studies and 1,2-dichlorobenzene was selected as the solvent both P1 and P2. Several optimization studies were performed and the best results were supported by AFM and TEM studies. As a result of optimization studies, 1:2 ratio of polymer:$PC_{71}BM$ was determined for P1 and, 0.72 V V_{oc}, 5.45 mA/cm^2 J_{sc}, 54 % FF, 2.12 % of PCE were achieved. The bicontinuous active layer morphology was negatively affected by annealing treatment and supported with TEM studies. Polymer: $PC_{71}BM$ ratio was found as 1:4 for P2. After several optimization studies such as annealing, addition of DIO and methanol treatment with DIO, highest PCE was obtained as 1.20 % with a V_{oc} of 0.47 V, J_{sc} of 4.52 mA/cm^2 J_{sc} and FF of 56 %. Moreover, Incident photon to electron conversion efficiency (IPCE) measurements were performed and 40 % and 25 % IPCE values were obtained for P1 and P2, respectively.

P1 was used as the active layer for further studies and red emissive OLEDs were constructed with a device structure of ITO/PEDOT:PSS/P1/LiF/Al. Red emissive OLED device gave CIE coordinates (x,y) of 0.65, 0.34, respectively. Maximum PL emission in solution was at 614 nm and in thin film was at 745 nm. EL absorption maximum was located at 624 nm. The OLED device has low turn on voltage which was 3.6 V and reached maximum brightness of 60 cd/m^2 at 9 V. According to these results, benzotriazole and benzodithiophene based alternating copolymer with incorportaion of thiophene moiety (P1) was a good candidate for OLED applications.

Electrochemical, Spectroelectrochemical and organic solar cell studies of P1 were published in New Journal of Chemistry in 2015 [122].

REFERENCES

[1] W. Ni, X. Wan, M. Li, Y. Wang, and Y. Chen, "A-D-A small molecules for solution-processed organic photovoltaic cells," *Chemical communications*, vol. 51, p. im Druck, 2015.

[2] Y. Li and Y. Zou, "Conjugated polymer photovoltaic materials with broad absorption band and high charge carrier mobility," *Advanced Materials*, vol. 20, no. 15, pp. 2952–2958, 2008.

[3] M. Jorgensen, K. Norrman, and F. C. Krebs, "Stability/degradation of polymer solar cells," *Solar Energy Materials and Solar Cells*, vol. 92, no. 7, pp. 686–714, 2008.

[4] M. C. Scharber, D. Mühlbacher, M. Koppe, P. Denk, C. Waldauf, A. J. Heeger, and C. J. Brabec, "Design rules for donors in bulk-heterojunction solar cells - Towards 10 % energy-conversion efficiency," *Advanced Materials*, vol. 18, no. 6, pp. 789–794, 2006.

[5] M. a. Naik, M. Raghavendra, R. Bhaskar, K. Siram, and S. Patil, "Polymer solar cells : design of materials by donor – acceptor approach," *Materials*, pp. 1115–1123, 2013.

[6] A. Facchetti, "π-Conjugated polymers for organic electronics and photovoltaic cell applications," *Chemistry of Materials*, vol. 23, no. 3, pp. 733–758, 2011.

[7] H. Spanggaard and F. C. Krebs, "A brief history of the development of organic and polymeric photovoltaics," *Solar Energy Materials and Solar Cells*, vol. 83, no. 2-3, pp. 125–146, 2004.

[8] S. Gunes, H. Neugebauer, and N. S. Sariciftci, "Conjugated Polymer-Based Organic Solar Cells," *Chemical Reviews*, pp. 1324–1338, 2007.

[9] A. Cirpan, Z. Ayse Aroguz, and F. E. Karasz, "Efficient light emitting diodes from ternary blends of PPV-based copolymers," *Journal of Applied Polymer Science*, vol. 102, no. 3, pp. 2509–2511, 2006.

[10] S. Setayesh, A. C. Grimsdale, T. Weil, V. Enkelmann, K. M??llen, F. Meghdadi, E. J. W. List, and G. Leising, "Polyfluorenes with polyphenylene dendron side chains: Toward non-aggregating, light-emitting polymers," *Journal of the American Chemical Society*, vol. 123, no. 5, pp. 946–953, 2001.

[11] R. Mondal, H. a. Becerril, E. Verploegen, D. Kim, J. E. Norton, S. Ko, N. Miyaki, S. Lee, M. F. Toney, J.-L. Brédas, M. D. McGehee, and Z. Bao, "Thiophene-rich fused-aromatic thienopyrazine acceptor for donor–acceptor low band-gap polymers for OTFT and polymer solar cell applications," *Journal of Materials Chemistry*, vol. 20, no. 28, p. 5823, 2010.

[12] G. a. Sotzing, J. L. Reddinger, A. R. Katritzky, J. Soloducho, R. Musgrave, J. R. Reynolds, and P. J. Steel, "Multiply Colored Electrochromic Carbazole-Based Polymers," *Chemistry of Materials*, vol. 9, no. 15, pp. 1578–1587, 1997.

[13] G. Sonmez, H. B. Sonmez, C. K. F. Shen, R. W. Jost, Y. Rubin, and F. Wudl, "A processable green polymeric electrochromic," *Macromolecules*, vol. 38, no. 3, pp. 669–675, 2005.

[14] C. K. Chiang, C. R. Fincher, Y. W. Park, A. J. Heeger, H. Shirakawa, E. J. Louis, S. C. Gau, and A. G. MacDiarmid, "Electrical conductivity in doped polyacetylene," *Physical Review Letters*, vol. 39, no. 17, pp. 1098–1101, 1977.

[15] C. M. Mikulski, P. J. Russo, M. S. Saran, A. McDiarmid, A. F. Garito, and A. J. Heeger, "Synthesis and Structure of Metallic Polymeric Sulfur Nitride, (SN)„ and Its Precursor, Disulfur Dinitride,," *Journal of the American Chemical Society*, vol. 29, no. 28, pp. 6358–6363, 1975.

[16] R. L. Greene, G. B. Street, and L. J. Suter, "Superconductivity in polysulfur nitride (SN)X," *Physical Review Letters*, vol. 34, no. 10, pp. 577–579, 1975.

[17] H. Shirakawa, E. J. Louis, A. G. MacDiarmid, C. K. Chiang, and A. J. Heeger, "Synthesis of electrically conducting organic polymers: halogen derivatives of polyacetylene, (CH)," *Journal of the Chemical Society, Chemical Communications*, no. 16, pp. 578–580, 1977.

[18] H. Shirakawa, T. Ito, and S. Ikeda, "Electrical Properties of Polyacetylene with Various Cis-Eans Compositions," *Die Makromolekulare Chemie*, vol. 179, no. 6, pp. 1565–1573, 1978.

[19] P. Bernier, M. Rolland, M. Galtier, A. Montaner, M. Candille, M. Aldissi, C. Linaya, F. Schu, P. Bernier, M. Rolland, M. Galtier, and A. Montaner, "Electronic properties of non-doped and doped polyacetylene films studied by E . S . R .," vol. 40, no. 13, pp. 297–301, 1979.

[20] A. Heeger, A. G. MacDiarmid, and H. Shirakawa, "The Nobel Prize in chemistry, 2000: conductive polymers," *Stockholm, Sweden: Royal Swedish Academy of Sciences*, pp. 1–16, 2000.

[21] J. K. Stille, "The Palladium-Catalyzed Cross-Coupling Reactions of Organotin Reagents with Organic Electrophiles," *Angewandte Chemie*, vol. 25, pp. 508–524, 1986.

[22] Z. Bao, W. K. Chan, and L. Yu, "Exploration of the Stille Coupling Reaction for the Synthesis of Functional Polymers," *Journal of the American Chemical Society*, vol. 117, no. 50, pp. 12426–12435, 1995.

[23] C. Cordovilla, C. Bartolomé, J. M. Martínez-Ilarduya, and P. Espinet, "The stille reaction, 38 years later," *ACS Catalysis*, vol. 5, no. 5, pp. 3040–3053, 2015.

[24] G. Zotti, G. Schiavon, A. Berlin, and G. Pagani, "Thiophene oligomers as polythiophene Models .1. Anodic coupling of thiophene oligomers to dimers - A kinetic investigation," *Chemistry of Materials*, vol. 5, no. 4, pp. 430–436, 1993.

[25] Y. Wei, C. C. Chan, J. Tian, G. W. Jang, and K. F. Hsueh, "Electrochemical polymerization of thiophenes in the presence of bithiophene or terthiophene: kinetics and mechanism of the polymerization," *Chemistry of Materials*, vol. 3, no. 5, pp. 888–897, 1991.

[26] G. Sabouraud, S. Sadki, and N. Brodie, "The mechanisms of pyrrole electropolymerization," *Chemical Society Reviews*, vol. 29, no. 5, pp. 283–293, 2000.

[27] M. G. Bamfield, P, Hutchings, "Chromic Phenomena," *Spring*, pp. 1–8, 2010.

[28] P. M. S. Monk, R. J. Mortimer, D. R. Rosseinsky, H. Gerischer, C. W. T. Eds, and J. Wang, "Fundamentals and Applications Further Titles of Interest by VCH Frontiers of Electrochemistry,"

[29] C.-g. Granqvist, "Electrochromic Metal Oxides : An Introduction to Materials," 2015.

[30] K. C. Cheng, F. R. Chen, and J. J. Kai, "Electrochromic property of nanocomposite Prussian Blue based thin film," *Electrochimica Acta*, vol. 52, no. 9, pp. 3330–3335, 2007.

[31] C. L. Bird and a. T. Kuhn, "Electrochemistry of the viologens," *Chemical Society Reviews*, vol. 10, no. 1, p. 49, 1981.

[32] A. G. MacDiarmid and W. Zheng, "Electrochemistry of conjugated polymers and electrochemical applications," *MRS Bull.*, vol. June, p. 24, 1997.

[33] P. R. Somani and S. Radhakrishnan, "Electrochromic Materials and Devices: present and future," *Materials Chemistry and Physics*, vol. 77, pp. 117–133, 2002.

[34] S. Tarkuc, E. K. Unver, Y. A. Udum, and L. Toppare, "Multi-colored electrochromic polymer with enhanced optical contrast," *European Polymer Journal*, vol. 46, no. 11, pp. 2199–2205, 2010.

[35] R. J. Mortimer, "Electrochromic materials," vol. 26, pp. 147–156, 1997.

[36] N. M. Rowley and R. J. Mortimer, "New electrochromic materials.," *Science progress*, vol. 85, no. Pt 3, pp. 243–262, 2002.

[37] J. Bredas and G. Street, "Polarons, bipolarons, and solitons in conducting polymers," *Accounts of Chemical Research*, vol. 1305, no. 4, pp. 309–315, 1985.

[38] J. Roncali, "Synthetic Principles for Bandgap Control in Linear π-Conjugated Systems," *Chemical Reviews*, vol. 97, no. 1, pp. 173–206, 1997.

[39] A. A. Argun, P. H. Aubert, B. C. Thompson, I. Schwendeman, C. L. Gaupp, J. Hwang, N. J. Pinto, D. B. Tanner, A. G. MacDiarmid, and J. R. Reynolds, "Multicolored electrochromisin in polymers: Structures and devices," *Chemistry of Materials*, vol. 16, no. 23, pp. 4401–4412, 2004.

[40] F. Garnier, G. Tourillon, M. Gazard, and J. Dubois, "Organic conducting polymers derived from substituted thiophenes as electrochromic material," *Journal of Electroanalytical Chemistry and Interfacial Electrochemistry*, vol. 148, no. 2, pp. 299–303, 1983.

[41] L. D. Talley, "On the Production of a Blue Substance by the Electrolpsis of Sulyhate of Aniline," vol. 101, no. 161, pp. 161–163, 1996.

[42] R. M. Walczak and J. R. Reynolds, "Poly(3,4-alkylenedioxypyrroles): The PXDOPs as versatile yet underutilized electroactive and conducting polymers," *Advanced Materials*, vol. 18, no. 9, pp. 1121–1131, 2006.

[43] L. Groenendaal, F. Jonas, D. Freitag, H. Pielartzik, and J. R. Reynolds, "Poly(3,4-ethylenedioxythiophene) and its derivatives: past, present, and future," *Advanced Materials*, vol. 12, no. 7, pp. 481–494, 2000.

[44] H. W. Heuer, R. Wehrmann, and S. Kirchmeyer, "Electrochromic Window Based on Conducting Poly (3, 4-ethylenedioxythiophene),ÄìPoly (styrene sulfonate)," *Advanced Functional Materials*, vol. 12, no. 2, pp. 89–94, 2002.

[45] A. Balan, G. Gunbas, A. Durmus, and L. Toppare, "Donor-acceptor polymer with benzotriazole moiety: Enhancing the electrochromic properties of the "donor unit"," *Chemistry of Materials*, vol. 20, no. 24, pp. 7510–7513, 2008.

[46] S. Tarkuc, Y. A. Udum, and L. Toppare, "Tuning of the neutral state color of the π-conjugated donor-acceptor-donor type polymer from blue to

green via changing the donor strength on the polymer," *Polymer*, vol. 50, no. 15, pp. 3458–3464, 2009.

[47] G. E. Gunbas, A. Durmus, and L. Toppare, "A unique processable green polymer with a transmissive oxidized state for realization of potential RGB-based electrochromic device applications," *Advanced Functional Materials*, vol. 18, no. 14, pp. 2026–2030, 2008.

[48] A. L. Dyer, M. R. Craig, J. E. Babiarz, K. Kiyak, and J. R. Reynolds, "Orange and Red to Transmissive Electrochromic Polymers Based on Electron-Rich Dioxythiophenes," *Macromolecules*, vol. 43, no. 10, pp. 4460–4467, 2010.

[49] G. E. Gunbas, A. Durmus, and L. Toppare, "Could green be greener? Novel donor-acceptor-type electrochromic polymers: Towards excellent neutral green materials with exceptional transmissive oxidized states for completion of RGB color space," *Advanced Materials*, vol. 20, no. 4, pp. 691–695, 2008.

[50] J. A. Kerszulis, C. M. Amb, A. L. Dyer, and J. R. Reynolds, "Follow the yellow brick road: Structural optimization of vibrant yellow-to-transmissive electrochromic conjugated polymers," *Macromolecules*, vol. 47, no. 16, pp. 5462–5469, 2014.

[51] C. M. Amb, A. L. Dyer, and J. R. Reynolds, "Navigating the Color Palette of Solution-Processable Electrochromic Polymers," *Chemistry of Materials*, vol. 23, no. 3, pp. 397–415, 2011.

[52] J. Xue, "Perspectives on Organic Photovoltaics," *Polymer Reviews*, vol. 50, no. 4, pp. 411–419, 2010.

[53] M. T. Kibria, A. Ahammed, S. M. Sony, and F. Hossain, "A Review : Comparative studies on different generation solar cells technology," *International Conference on Environmental Aspects of Bangladesh*, pp. 51–53, 2014.

[54] F. Krebs, S. Gevorgyan, and J. Alstrup, "A roll-to-roll process to flexible polymer solar cells: model studies, manufacture and operational stability studies," *Journal of Materials Chemistry*, pp. 5442–5451, 2009.

[55] F. C. Krebs, T. Tromholt, and M. Jørgensen, "Upscaling of polymer solar cell fabrication using full roll-to-roll processing.," *Nanoscale*, vol. 2, no. 6, pp. 873–886, 2010.

[56] C. J. Brabec and J. R. Durrant, "Solution-processed organic solar cells," *MRS bulletin*, vol. 33, no. 7, pp. 670–675, 2008.

[57] C. J. Brabec, "Organic photovoltaics: Technology and market," *Solar Energy Materials and Solar Cells*, vol. 83, no. 2-3, pp. 273–292, 2004.

[58] T. Lei, J.-y. Wang, and J. Pei, "Roles of Flexible Chains in Organic Semiconducting Materials," *Chemistry of Materials*, vol. 26, no. 1, pp. 594–603, 2014.

[59] K. M. Coakley and M. D. McGehee, "Conjugated polymer photovoltaic cells," *Chemistry of Materials*, vol. 16, no. 23, pp. 4533–4542, 2004.

[60] A. J. MouleÃÅ, J. B. Bonekamp, and K. Meerholz, "The effect of active layer thickness and composition on the performance of bulk-heterojunction solar cells," *Journal of Applied Physics*, vol. 100, no. 9, p. 094503, 2006.

[61] G. Yu, J. Gao, J. C. Hummelen, F. Wudl, and A. J. Heeger, "Polymer Photovoltaic Cells - Enhanced Efficiencies Via a Network of Internal Donor-Acceptor Heterojunctions," *Science*, vol. 270, no. 5243, pp. 1789–1791, 1995.

[62] N. Li, D. Baran, K. Forberich, M. Turbiez, T. Ameri, F. C. Krebs, and C. J. Brabec, "An efficient solution-processed intermediate layer for facilitating fabrication of organic multi-junction solar cells," *Advanced Energy Materials*, vol. 3, no. 12, pp. 1597–1605, 2013.

[63] N. Li, D. Baran, K. Forberich, F. Machui, T. Ameri, M. Turbiez, M. Carrasco-Orozco, M. Drees, A. Facchetti, F. C. Krebs, and C. J. Brabec, "Towards 15% energy conversion efficiency: a systematic study of the solution-processed organic tandem solar cells based on commercially available materials," *Energy & Environmental Science*, vol. 6, no. 12, pp. 3407–3413, 2013.

[64] T. Ameri, N. Li, and C. J. Brabec, "Highly efficient organic tandem solar cells: a follow up review," *Energy & Environmental Science*, vol. 6, no. 8, p. 2390, 2013.

[65] T. Ameri, P. Khoram, J. Min, and C. J. Brabec, "Organic ternary solar cells: A review," *Advanced Materials*, vol. 25, no. 31, pp. 4245–4266, 2013.

[66] A. C. Mayer, S. R. Scully, B. E. Hardin, M. W. Rowell, and M. D. McGehee, "Polymer-based solar cells," *Materials Today*, vol. 10, no. 11, pp. 28–33, 2007.

[67] H. Hoppe and N. S. Sariciftci, "Organic solar cells: An overview," *Journal of Materials Research*, vol. 19, no. 07, pp. 1924–1945, 2004.

[68] B. Kippelen and J.-L. Brédas, "Organic photovoltaics," *Energy & Environmental Science*, vol. 2, no. 3, p. 251, 2009.

[69] A. B. Halls, J. J. M.; Walsh, C. A.; Greenham, N. C.; Marseglia, E. A.; Friend, R. H.; Moratti, S. C.; Holmes, "Efficient photodiodes from interpenetrating polymer networks," *Nature*, vol. 376, pp. 498–500., 1995.

[70] G. Yu, J. Gao, J. C. Hummelen, F. Wudl, and A. J. Heeger, "Polymer Photovoltaic Cells - Enhanced Efficiencies Via a Network of Internal Donor-Acceptor Heterojunctions," *Science*, vol. 270, no. 5243, pp. 1789–1791, 1995.

[71] C. J. Brabec, A. Cravino, D. Meissner, N. Serdar Sariciftci, T. Fromherz, M. T. Rispens, L. Sanchez, and J. C. Hummelen, "Origin of the open circuit voltage of plastic solar cells," *Advanced Funtional Materials*, vol. 11, no. 5, pp. 374–380, 2001.

[72] T. L. Benanti and D. Venkataraman, "Organic solar cells: An overview focusing on active layer morphology," *Photosynthesis Research*, vol. 87, no. 1, pp. 73–81, 2006.

[73] Y. Li, "Molecular design of photovoltaic materials for polymer solar cells: Toward suitable electronic energy levels and broad absorption," *Accounts of Chemical Research*, vol. 45, no. 5, pp. 723–733, 2012.

[74] I. Etxebarria, J. Ajuria, and R. Pacios, "Solution-processable polymeric solar cells: A review on materials, strategies and cell architectures to overcome 10%," *Organic Electronics: physics, materials, applications*, vol. 19, pp. 34–60, 2015.

[75] T. Xu and L. Yu, "How to design low bandgap polymers for highly efficient organic solar cells," *Biochemical Pharmacology*, vol. 17, no. 1, pp. 11–15, 2014.

[76] H. Zhang and J. Hou, "Molecular design strategies for voltage modulation in highly efficient polymer solar cells," *Polymer International*, vol. 64, no. February, pp. 957–962, 2015.

[77] J. Chen and Y. Cao, "Development of Novel Conjugated Donor Heterojunction Photovoltaic Devices," *Accounts of Chemical Research*, vol. 42, no. 11, pp. 1709–1718, 2009.

[78] Z. B. Henson, K. Müllen, and G. C. Bazan, "Design strategies for organic semiconductors beyond the molecular formula," *nature chemistry*, vol. 4, no. September, pp. 699–704, 2012.

[79] P. M. Beaujuge and J. M. J. Fr, "Molecular Design and Ordering Effects in π -Functional Materials for Transistor and Solar Cell Applications," *Journal of American Chemical Society*, vol. 133, pp. 20009–20029, 2011.

[80] Y.-j. Cheng, S.-h. Yang, and C.-s. Hsu, "Synthesis of Conjugated Polymers for Organic Solar Cell Applications," *Chem.Rev.*, vol. 109, pp. 5868–5923, 2009.

[81] M. C. Scharber, D. Mühlbacher, M. Koppe, P. Denk, C. Waldauf, A. J. Heeger, and C. J. Brabec, "Design rules for donors in bulk-heterojunction solar cells - Towards 10 % energy-conversion efficiency," *Advanced Materials*, vol. 18, no. 6, pp. 789–794, 2006.

[82] B. F. Padinger, R. S. Rittberger, and N. S. Sariciftci, "Effects of Postproduction Treatment on Plastic Solar Cells," *Advanced Functional Materials*, vol. 13, no. 1, pp. 85–88, 2003.

[83] C. Duan, F. Huang, and Y. Cao, "Recent development of push-pull conjugated polymers for bulk-heterojunction photovoltaics : rational design and fine tailoring of molecular structures," *Journal of Materials Chemistry*, vol. 22, pp. 10416–10434, 2012.

[84] M. Svensson, M.; Zhang, F.; Veenstra, S. C.; Verhees, W. J. H.; Hummelen, J.C.;Kroon, J.M.;InganasÃà, O.;Andersson, "High-Performance Polymer Solar Cells of an Alternating Polyfluorene Copolymer and a Fullerene Derivative **," *Advanced Materials*, vol. 15, no. 12, pp. 988–991, 2003.

[85] J. Hou, M.-H. Park, S. Zhang, Y. Yao, L.-M. Chen, J.-H. Li, and Y. Yang, "Bandgap and Molecular Energy Level Control of Conjugated Polymer Photovoltaic Materials Based on Benzo[1,2-b:4,5-b']dithiophene," *Macromolecules*, vol. 41, no. 16, pp. 6012–6018, 2008.

[86] Y. Liang, D. Feng, Y. Wu, S.-T. Tsai, G. Li, C. Ray, and L. Yu, "Highly efficient solar cell polymers developed via fine-tuning of structural and electronic properties.," *Journal of the American Chemical Society*, vol. 131, no. 22, pp. 7792–7799, 2009.

[87] Y. Liang, Y. Wu, D. Feng, S.-t. Tsai, H.-j. Son, G. Li, and L. Yu, "Development of New Semiconducting Polymers for High Performance Solar," *Journal of American Chemical Society Communications*, vol. 131, pp. 56–57, 2009.

[88] C. J. Neef, I. D. Brotherston, and J. P. Ferraris, "Synthesis and Electronic Properties of Poly(2-phenylthieno [3,4-b]thiophene): A New Low Band Gap Polymer," *Chemistry of Materials*, vol. 11, pp. 1957–1958, 1999.

[89] M. Pomerantz and X. Gu, "A New Soluble Low-Bandgap Conducting Polymer," *Synthetic Metals*, vol. 84, pp. 243–244, 1997.

[90] J. Subbiah, B. Purushothaman, M. Chen, T. Qin, M. Gao, D. Vak, F. H. Scholes, X. Chen, S. E. Watkins, G. J. Wilson, A. B. Holmes, W. W. H.

Wong, and D. J. Jones, "Organic Solar Cells Using a High-Molecular-Weight Benzodithiophene and Benzothiadiazole Copolymer with an Efficiency of 9.4%," *Advanced Materials*, vol. 27, pp. 702–705, 2015.

[91] D. G. Parnum, G. Mehta, G. G. I. Moore, and F. P. Siegal, "Attempted Refdrmatskii Reaction of Benzdnitrile, 1,4-diketo-3,6-diphenylpyrrolo[3,4-c]pyrrole. A Lactam Anagolue of Pentalene," *Tetrahedron Letters*, vol. 29, pp. 2549–2552, 1974.

[92] L. Dou, J. You, J. Yang, C.-C. Chen, Y. He, S. Murase, T. Moriarty, K. Emery, G. Li, and Y. Yang, "Tandem polymer solar cells featuring a spectrally matched low-bandgap polymer," *Nature Photonics*, vol. 6, no. 3, pp. 180–185, 2012.

[93] Y. Huang, X. Guo, F. Liu, L. Huo, Y. Chen, T. P. Russell, C. C. Han, Y. Li, and J. Hou, "Improving the Ordering and Photovoltaic Properties by Extending π – Conjugated Area of Electron-Donating Units in Polymers with D-A Structure," *Advanced Materials*, vol. 24, pp. 3383–3389, 2012.

[94] L. Lu, T. Zheng, Q. Wu, A. M. Schneider, D. Zhao, and L. Yu, "Recent Advances in Bulk Heterojunction Polymer Solar Cells," *Chemical Reviews*, vol. 115, no. 23, pp. 12666–12731, 2015.

[95] T. Lei, J.-y. Wang, and J. Pei, "Roles of Flexible Chains in Organic Semiconducting Materials," *Chemistry of Materials*, vol. 26, no. 1, pp. 594–603, 2014.

[96] S. Zhang, M. A. Uddin, W. Zhao, L. Ye, H. Y. Woo, D. Liu, B. Yang, H. Yao, Y. Cui, and J. Hou, "Optimization of side chains in alkylthiothiophene-substituted benzo[1,2-b:4,5-b']dithiophene-based photovoltaic polymers," *Polymer Chemistry*, vol. 6, no. 14, pp. 2752–2760, 2015.

[97] S.-h. Liao, H.-j. Jhuo, Y.-s. Cheng, and S.-a. Chen, "Fullerene Derivative-Doped Zinc Oxide Nanofi lm as the Cathode of Inverted Polymer Solar Cells with Low-Bandgap Polymer (PTB7-Th) for High Performance," *Advanced Materials*, vol. 25, pp. 4766–4771, 2013.

[98] K. Li, Z. Li, K. Feng, X. Xu, L. Wang, and Q. Peng, "Development of large band-gap conjugated copolymers for efficient regular single and tandem organic solar cells," *Journal of the American Chemical Society*, vol. 135, no. 36, pp. 13549–13557, 2013.

[99] C. W. Tang, S. A. Vanslyke, and C. H. Chen, "Electroluminescence of doped organic thin films," *Journal of Applied Physics*, vol. 65, no. 9, pp. 3610–3616, 1989.

[100] B. Valeur and M. N. Berberan-Santos, "A brief history of fluorescence and phosphorescence before the emergence of quantum theory," *Journal of Chemical Education*, vol. 88, no. 6, pp. 731–738, 2011.

[101] S. E. Braslavsky, "Glossary of terms used in photochemistry, 3rd edition," *Pure Applied Chemistry*, vol. 79, no. 3, pp. 293 – 465, 2007.

[102] J. R. Lakowicz, *Principles of Fluorescence Spectroscopy Principles of Fluorescence Spectroscopy*. Springer, 2006.

[103] D. Since, "Triplet Harvesting and Singlet Harvesting," no. Iii, pp. 1–6.

[104] J. Kalinowski, "Electroluminescence in organics," *J. Phys. D: Appl. Phys.*, vol. 179, 1999.

[105] B. A. Köhler, J. S. Wilson, and R. H. Friend, "Fluorescence and Phosphorescence in Organic Materials," *Advanced Engineering Materials*, vol. 4, no. 7, pp. 453–459, 2002.

[106] R. Schlaf, H. Murata, and Z. H. Kafafi, "Work function measurements on indium tin oxide films," *Journal of Electron Spectroscopy*, vol. 120, pp. 149–154, 2001.

[107] M. Stössel, J. Staudigel, F. Steuber, J. Simmerer, and A. Winnacker, "Impact of the cathode metal work function on the performance of vacuum-deposited organic light emitting-devices," *Applied Physics A.*, vol. 390, pp. 387–390, 1999.

[108] A. Balan, D. Baran, G. Gunbas, A. Durmus, F. Ozyurt, and L. Toppare, "One polymer for all: benzotriazole containing donor-acceptor type polymer as a multi-purpose material.," *Chemical communications (Cambridge, England)*, vol. 60, no. 44, pp. 6768–6770, 2009.

[109] G. Hızalan, A. Balan, D. Baran, and L. Toppare, "Spray processable ambipolar benzotriazole bearing electrochromic polymers with multi-colored and transmissive states," *Journal of Materials Chemistry*, vol. 21, no. 6, p. 1804, 2011.

[110] J. H. Cook, H. A. Al-Attar, and A. P. Monkman, "Effect of PEDOT-PSS resistivity and work function on PLED performance," *Organic Electronics: physics, materials, applications*, vol. 15, no. 1, pp. 245–250, 2014.

[111] C. J. Brabec, S. E. Shaheen, C. Winder, N. S. Sariciftci, and P. Denk, "Effect of LiF/metal electrodes on the performance of plastic solar cells," *Applied Physics Letters*, vol. 80, no. 7, pp. 1288–1290, 2002.

[112] J.-h. Kim, B. Park, F. Xu, D. Kim, and J. Kwak, "Environmental Science E ff ect of p -conjugated bridges of TPD-based medium bandgap conjugated

copolymers for e ffi cient tandem organic photovoltaic cells ,Ä†," *Energy & Environmental Science*, vol. 7, pp. 4118–4131, 2014.

[113] R. Badrou Aïch, Y. Zou, M. Leclerc, and Y. Tao, "Solvent effect and device optimization of diketopyrrolopyrrole and carbazole copolymer based solar cells," *Organic Electronics: physics, materials, applications*, vol. 11, no. 6, pp. 1053–1058, 2010.

[114] Y. Yang, J. Zhang, Y. Zhou, G. Zhao, C. He, Y. Li, M. Andersson, O. Inganäs, and F. Zhang, "Solution-processable organic molecule with triphenylamine core and two benzothiadiazole-thiophene arms for photovoltaic application," *Journal of Physical Chemistry C*, vol. 114, no. 8, pp. 3701–3706, 2010.

[115] T. Kietzke, R. Y. C. Shin, D. A. M. Egbe, Z.-K. Chen, and A. Sellinger, "Effect of Annealing on the Characteristics of Organic Solar Cells:¬† Polymer Blends with a 2-Vinyl-4,5-dicyanoimidazole Derivative," *Macromolecules*, vol. 40, no. 13, pp. 4424–4428, 2007.

[116] R. L. Uy, S. C. Price, and W. You, "Structure-property optimizations in donor polymers via electronics, substituents, and side chains toward high efficiency solar cells," *Macromolecular Rapid Communications*, vol. 33, no. 14, pp. 1162–1177, 2012.

[117] J. Z. Jie Min, Zhi-Guo Zhang, Siyuan Zhang, Maojie Zhang and Y. Li, "Synthesis and photovoltaic properties of copolymers based on 2,2-(1,5-pentamethylene)-2H-benzimidazole," *Macromoleculs*, vol. 44, no. 1-2, p. 7632, 2011.

[118] H. C. Liao, C. C. Ho, C. Y. Chang, M. H. Jao, S. B. Darling, and W. F. Su, "Additives for morphology control in high-efficiency organic solar cells," *Materials Today*, vol. 16, no. 9, pp. 326–336, 2013.

[119] S. Guo, B. Cao, W. Wang, J.-F. Moulin, and P. Müller-Buschbaum, "Effect of alcohol treatment on the performance of PTB7:PC71BM bulk heterojunction solar cells.," *ACS applied materials {&} interfaces*, vol. 7, no. 8, pp. 4641–4649, 2015.

[120] T. Y. Chu, J. Lu, S. Beaupré, Y. Zhang, J. R. Pouliot, J. Zhou, A. Najari, M. Leclerc, and Y. Tao, "Effects of the molecular weight and the side-chain length on the photovoltaic performance of dithienosilole/thienopyrrolodione copolymers," *Advanced Functional Materials*, vol. 22, no. 11, pp. 2345–2351, 2012.

[121] Z. Zhang, B. Peng, B. Liu, C. Pan, Y. Li, Y. He, K. Zhou, and Y. Zou, "Copolymers from benzodithiophene and benzotriazole: synthesis and photovoltaic applications," *Polymer Chemistry*, vol. 1, no. 9, p. 1441, 2010.

[122] C. Istanbulluoglu, S. Göker, G. Hizalan, S. O. Hacioglu, Y. A. Udum, E. D. Yildiz, A. Cirpan, and L. Toppare, "Synthesis of a benzotriazole bearing alternating copolymer for organic photovoltaic applications," *New Journal of Chemistry*, vol. 39, no. 8, pp. 6623–6630, 2015.

APPENDIX A

NMR DATA

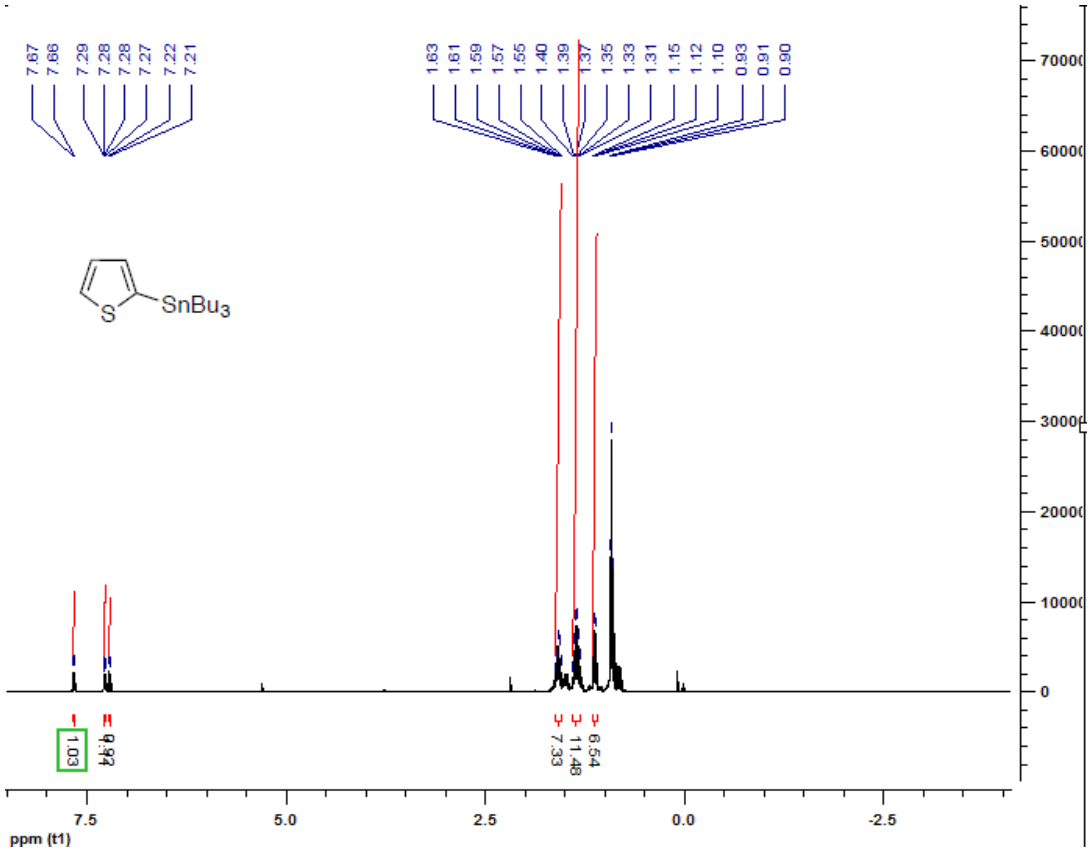

Figure A.1: ^{1}H-NMR data of tributyl[thiophen-2-yl]stannane

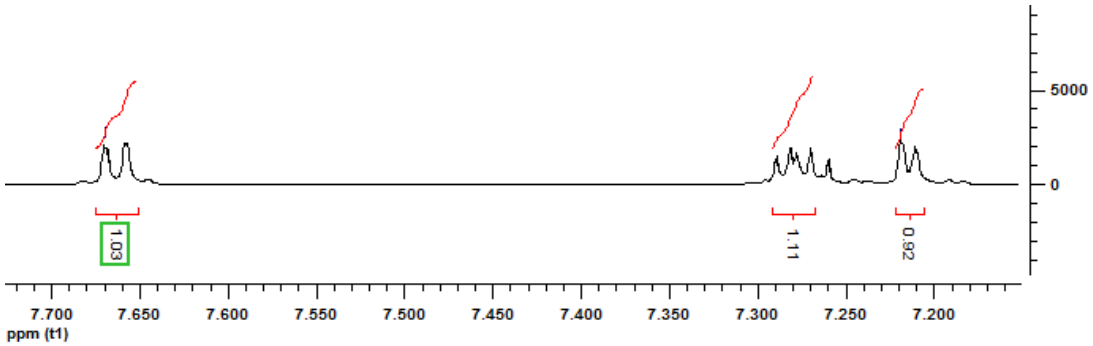

Figure A.2: ^{1}H-NMR data of tributyl[thiophen-2-yl]stannane-aromatic region

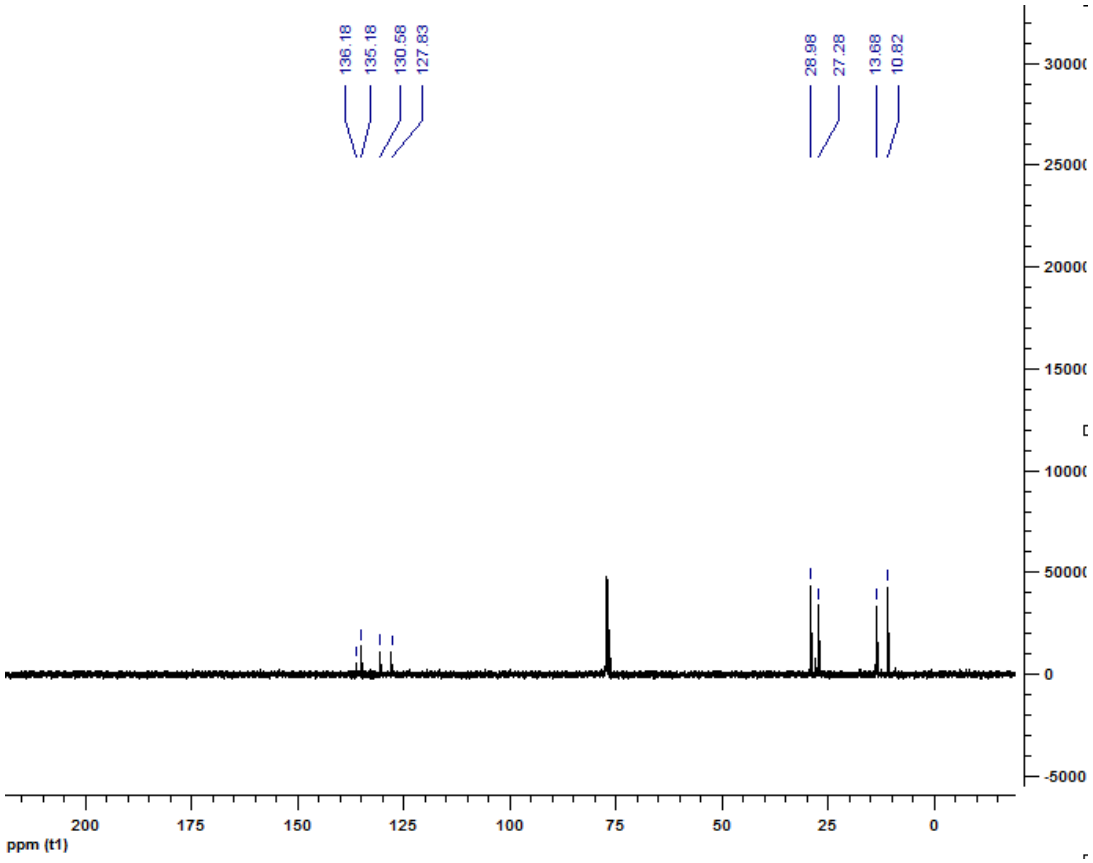

Figure A.3: ^{13}C-NMR data of tributyl[thiophen-2-yl]stannane

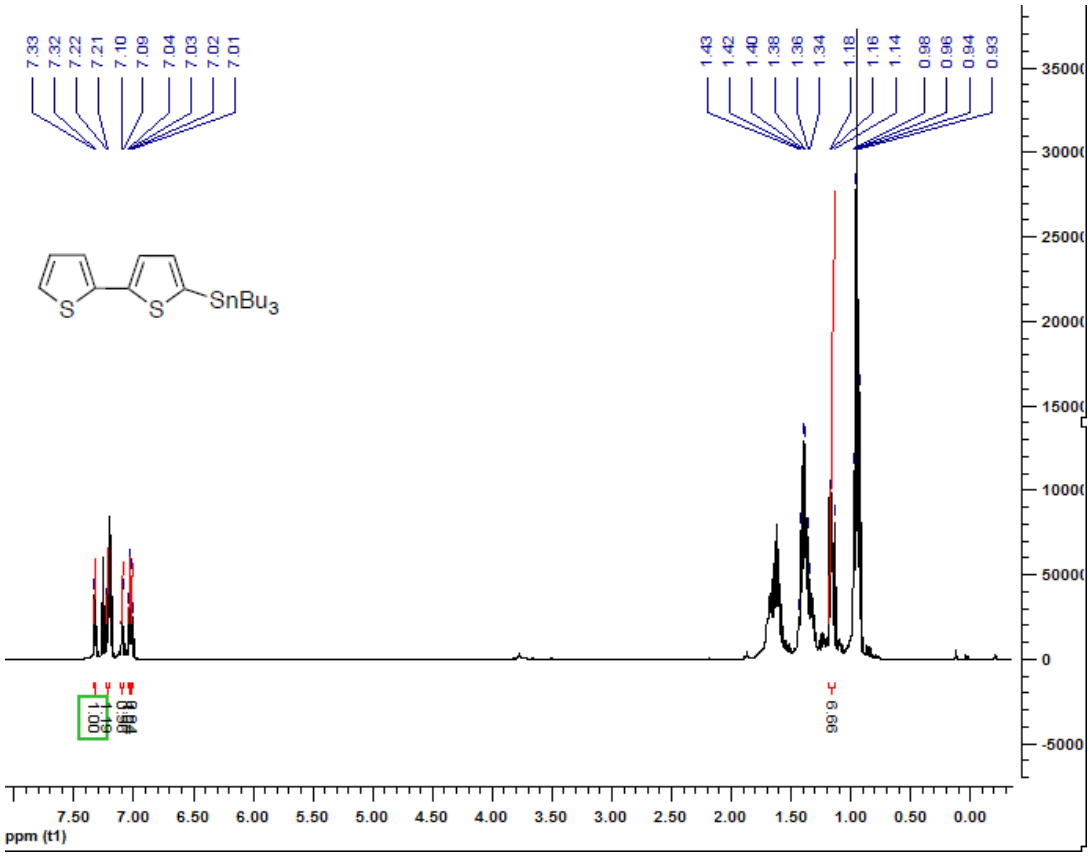

Figure A.4: ^{1}H-NMR data of [2,2'-bithiophen-5-yl]tributylstannane

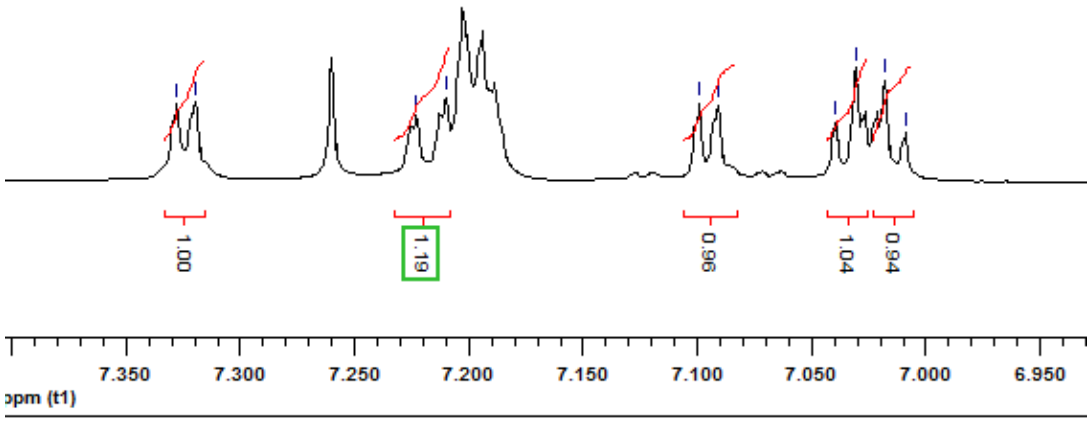

Figure A.5: ^{1}H-NMR data of [2,2'-bithiophen-5-yl]tributylstannane-aromatic region

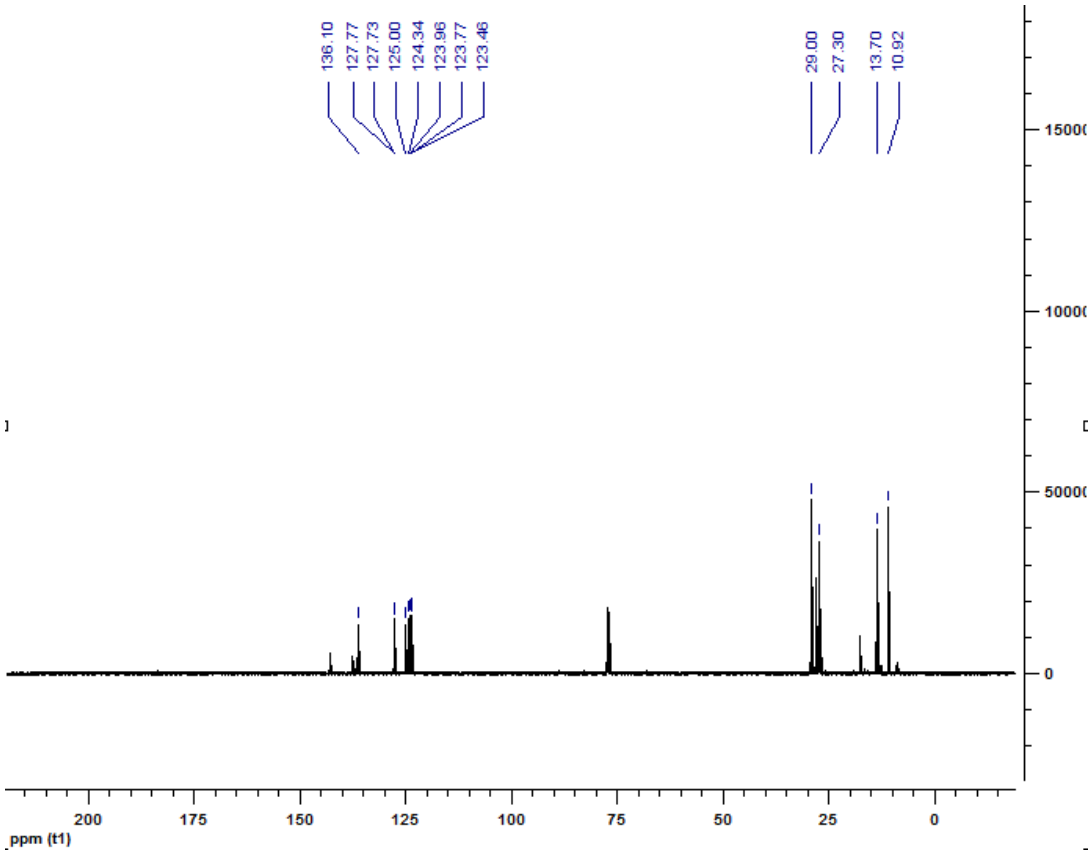

Figure A.6: ^{13}C-NMR data of 2,2'-bithiophen-5-yl]tributylstannane

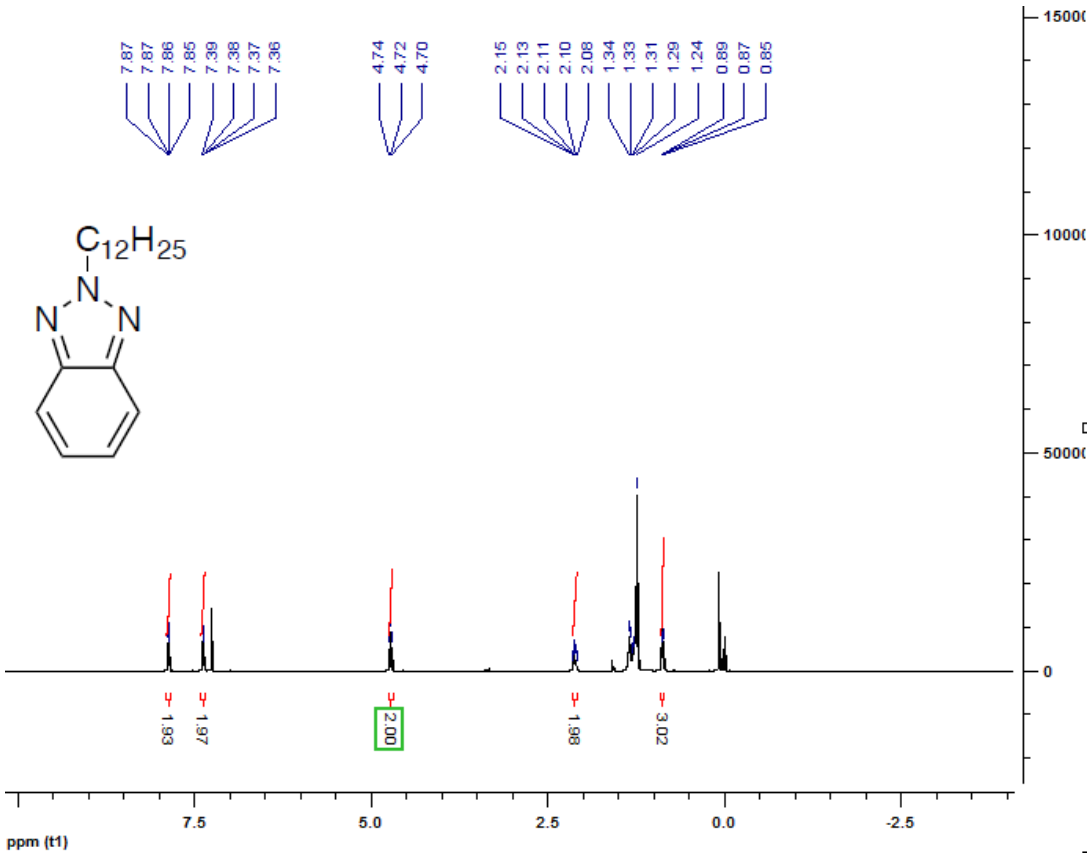

Figure A.7: ^{1}H-NMR data of 2-dodecyl-2H-benzo[d][1,2,3]triazole

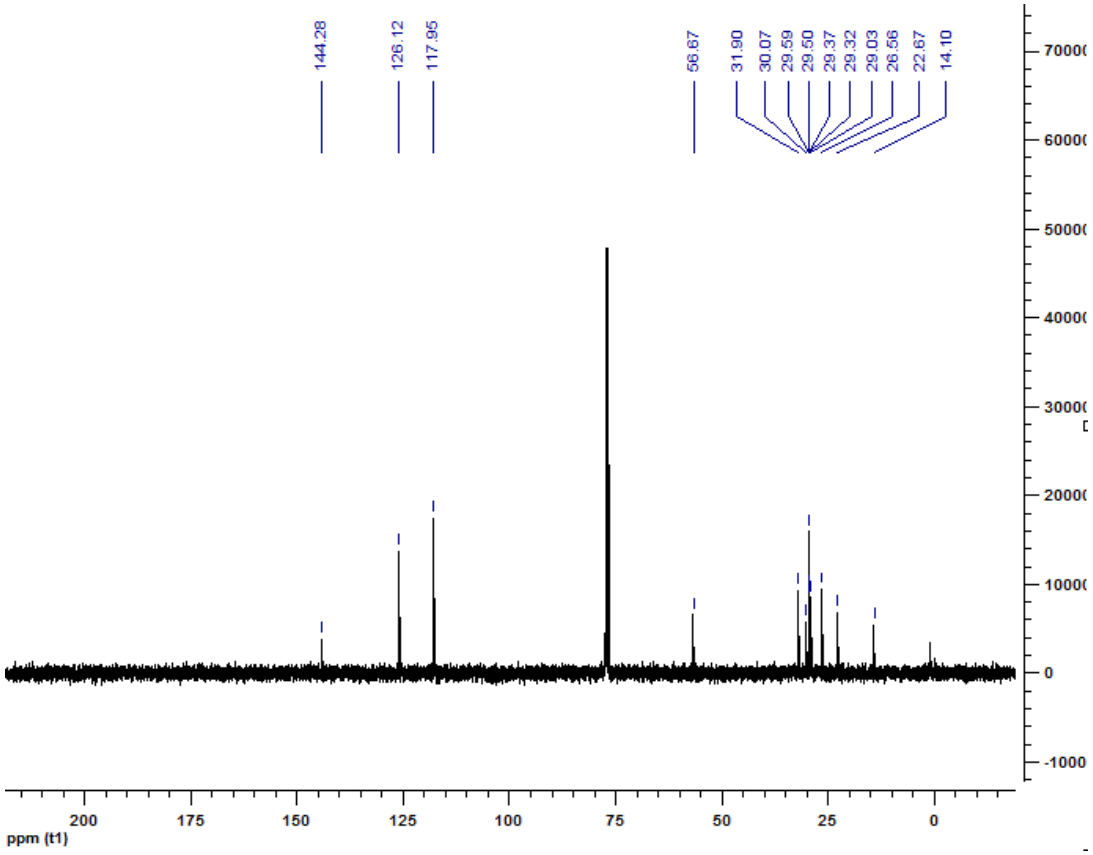

Figure A.8: ^{13}C-NMR data of 2-dodecyl-2H-benzo[d][1,2,3]triazole

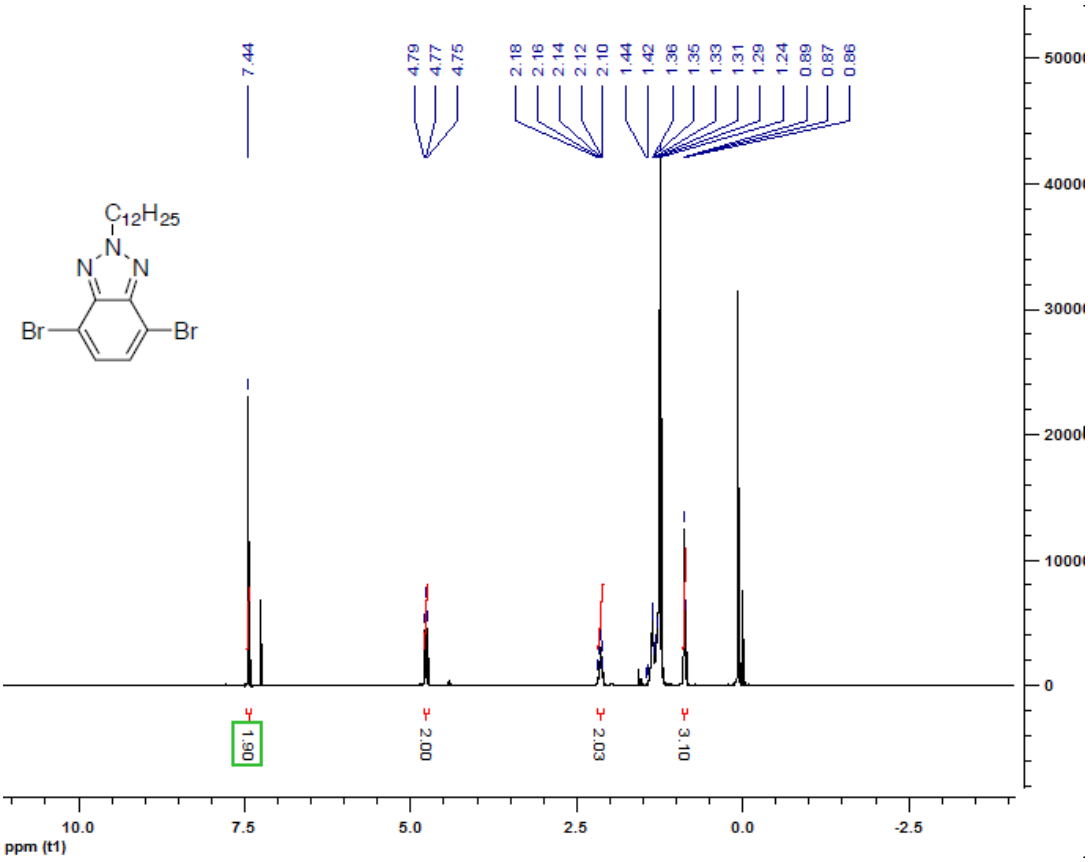

Figure A.9: ^{1}H-NMR data of 4,7-dibromo-2-dodecyl-2H-benzo[d][1,2,3]triazole

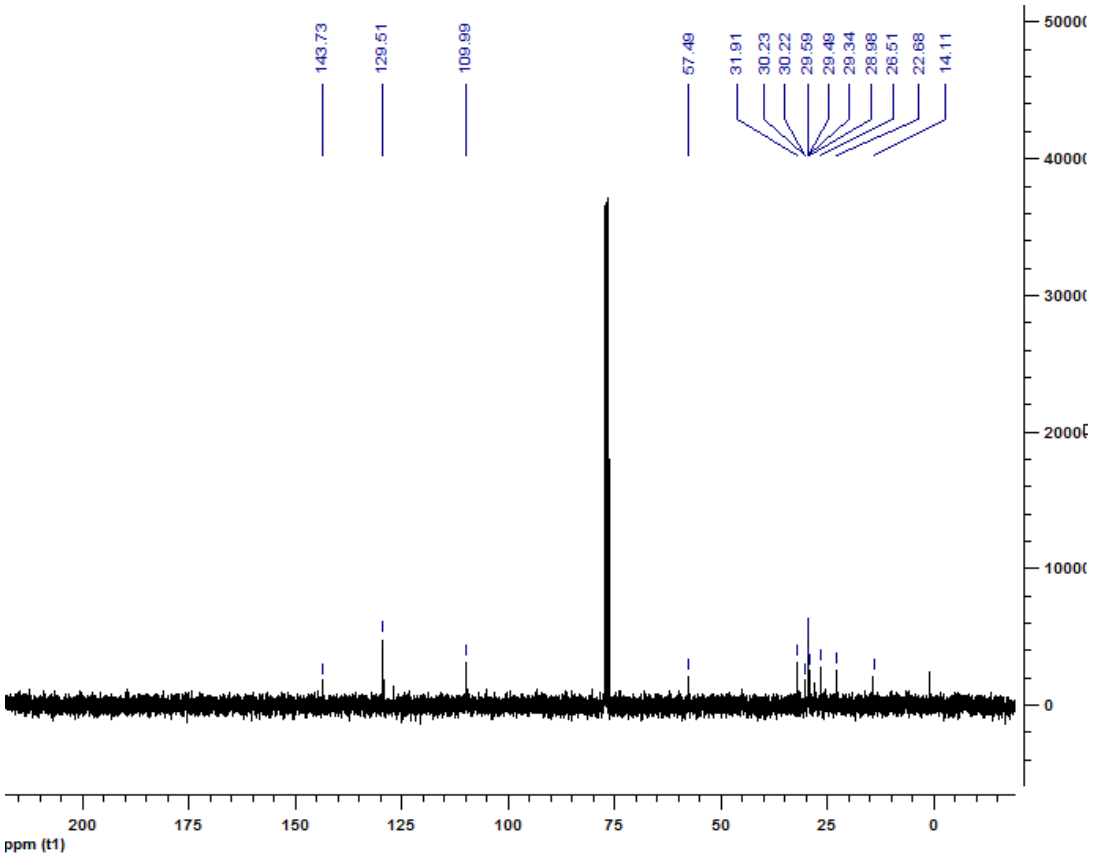

Figure A.10: ^{13}C-NMR data of 4,7-dibromo-2-dodecyl-2H-benzo[d][1,2,3]triazole

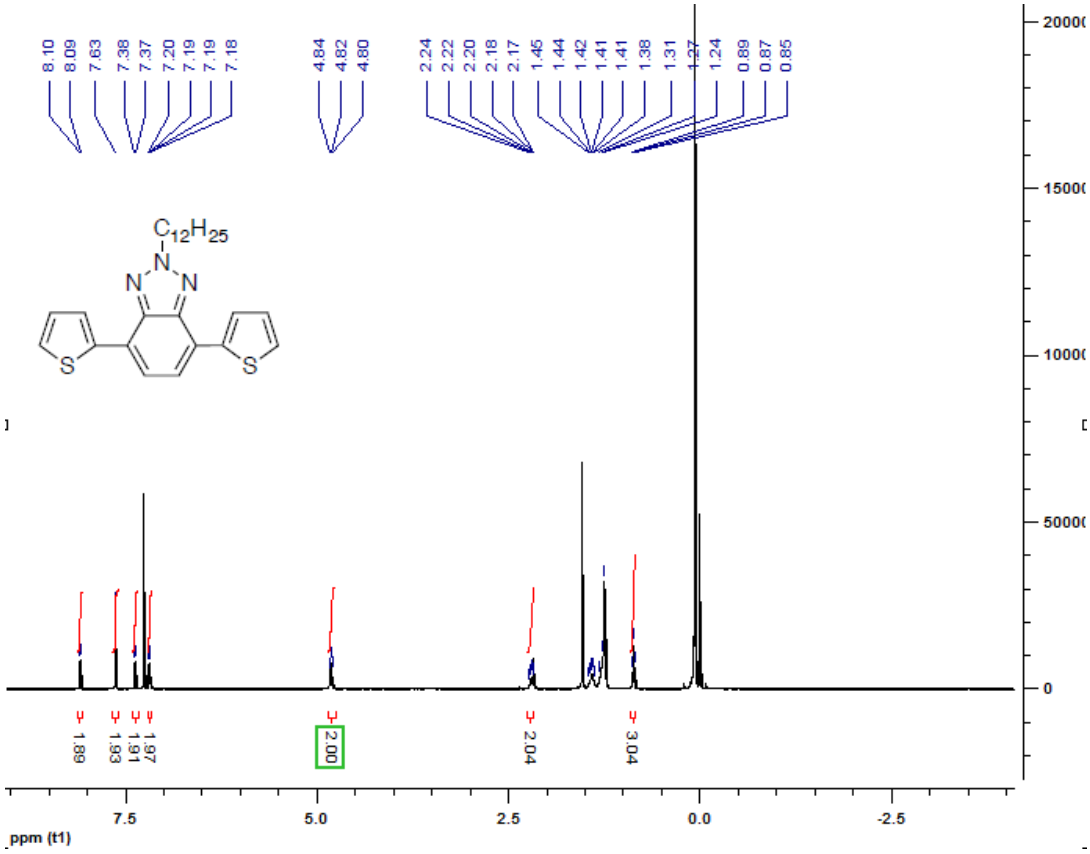

Figure A.11: ^{1}H-NMR data of 2-dodecyl-4,7-di(thiophen-2-yl)-2H-benzo[d]-[1,2,3]triazole 4,7-dibromo-2-dodecylbenzotriazole

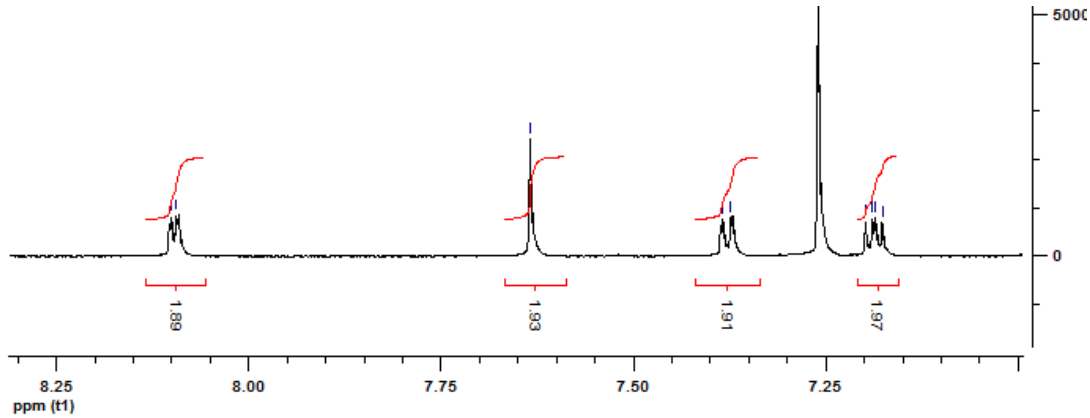

Figure A.12: ^{1}H-NMR data of 2-dodecyl-4,7-di(thiophen-2-yl)-2H-benzo[d]-[1,2,3]triazole 4,7-dibromo-2-dodecylbenzotriazole-aromatic region

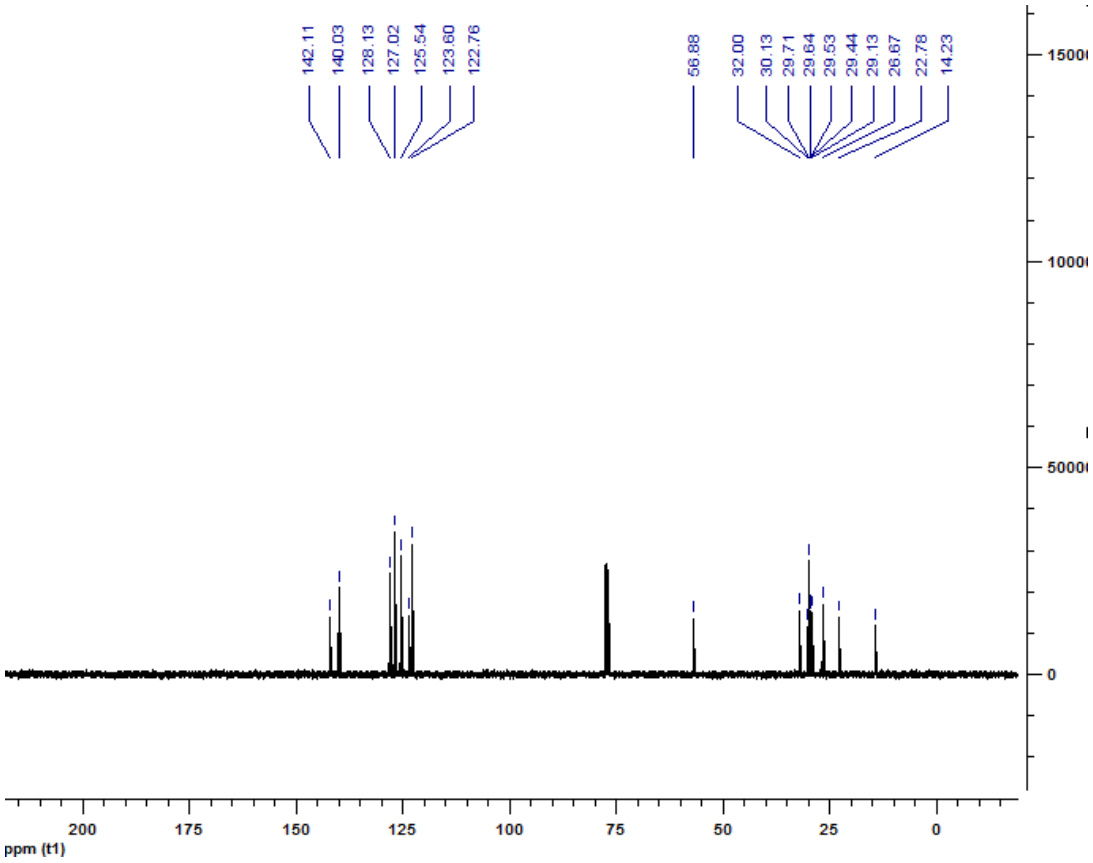

Figure A.13: ^{13}C-NMR data of 2-dodecyl-4,7-di(thiophen-2-yl)-2H-benzo[d]-[1,2,3]triazole 4,7-dibromo-2-dodecylbenzotriazole

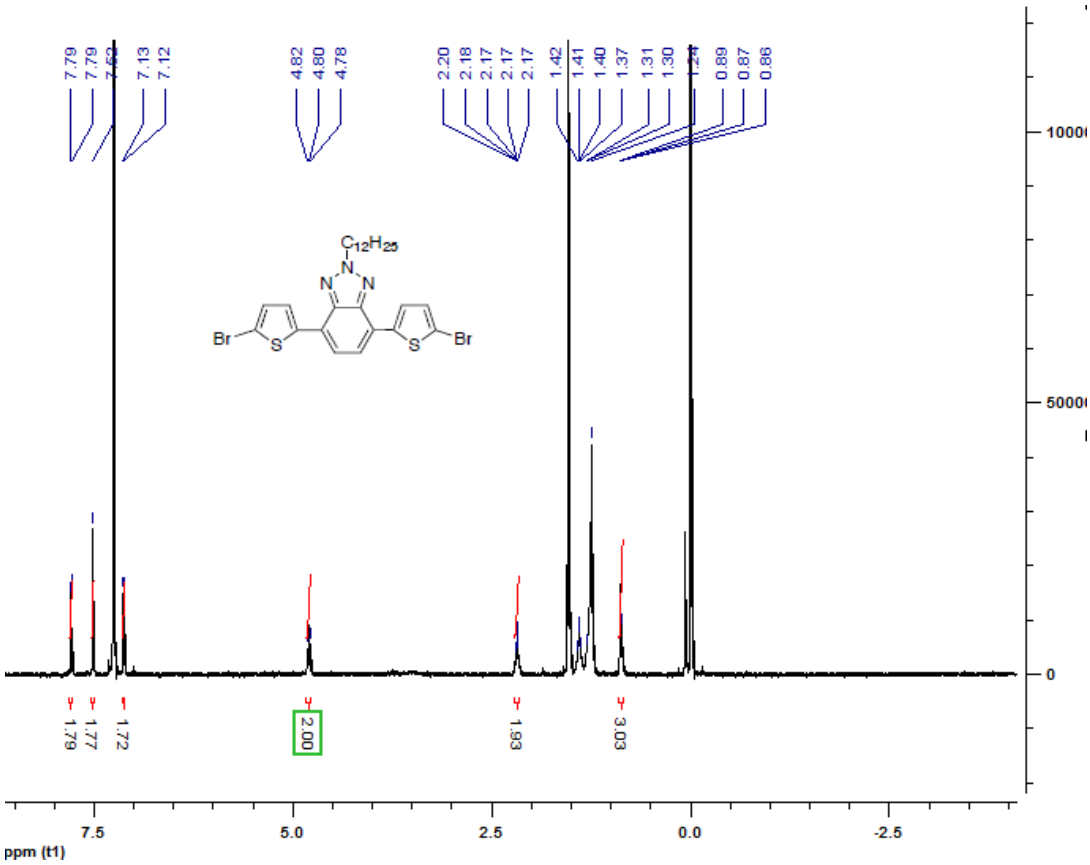

Figure A.14: ^{1}H-NMR data of 4,7-bis(5-bromothiophen-2-yl)-2-dodecyl-2H-benzo[d] [1,2,3]triazole

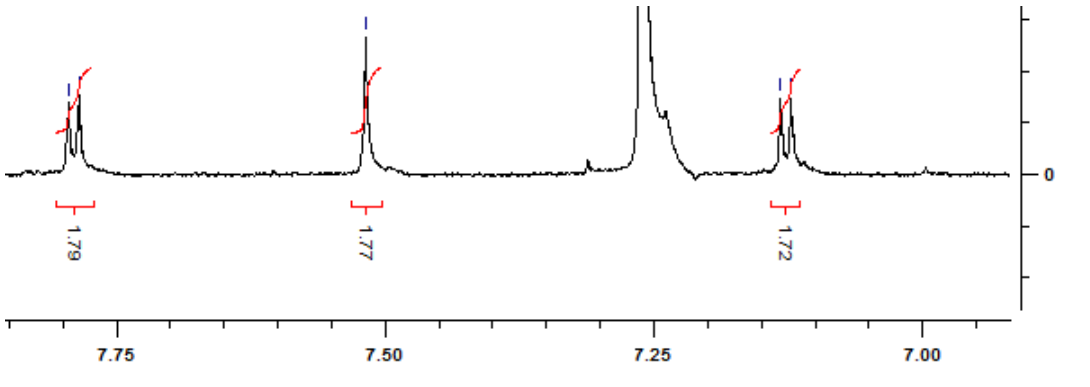

Figure A.15: ^{1}H-NMR data of 4,7-bis(5-bromothiophen-2-yl)-2-dodecyl-2H-benzo[d] [1,2,3]triazole-aromatic region

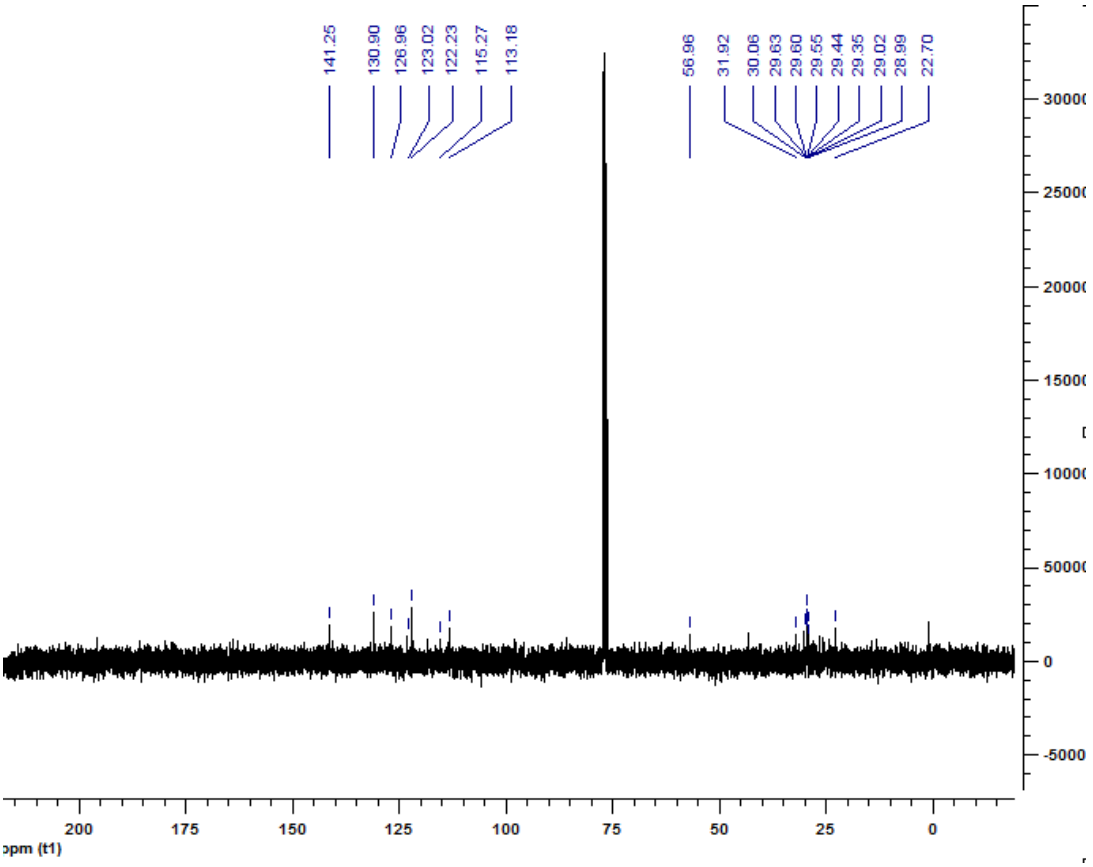

Figure A.16: ^{13}C-NMR data of 4,7-bis(5-bromothiophen-2-yl)-2-dodecyl-2H-benzo[d] [1,2,3]triazole

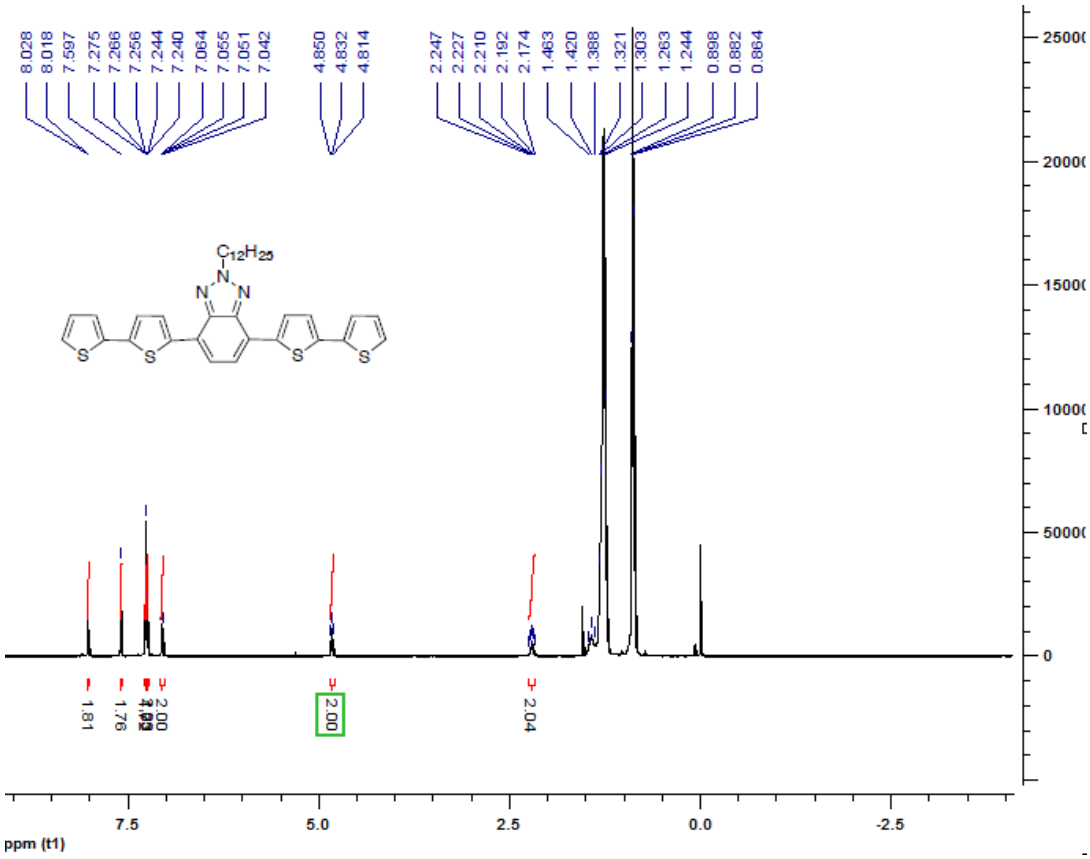

Figure A.17: ^{1}H-NMR data of 4,7-di([2,2'-bithiophen]-5-yl)-2-dodecyl-2H-benzo[d] [1,2,3]triazole

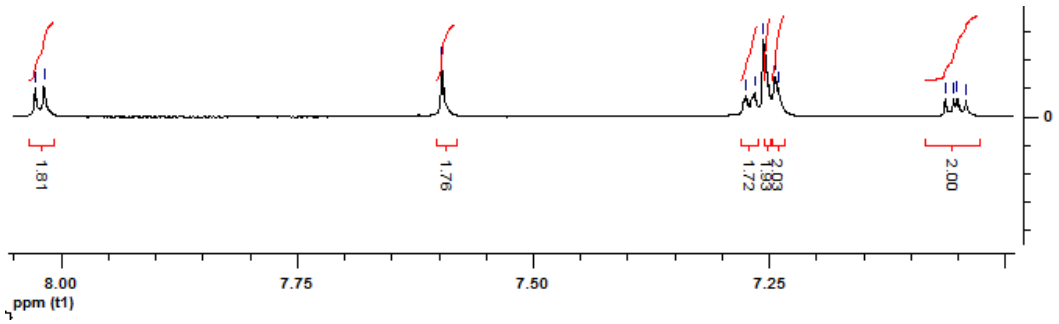

Figure A.18: ^{1}H-NMR data of 4,7-di([2,2'-bithiophen]-5-yl)-2-dodecyl-2H-benzo[d] [1,2,3]triazole-aromatic region

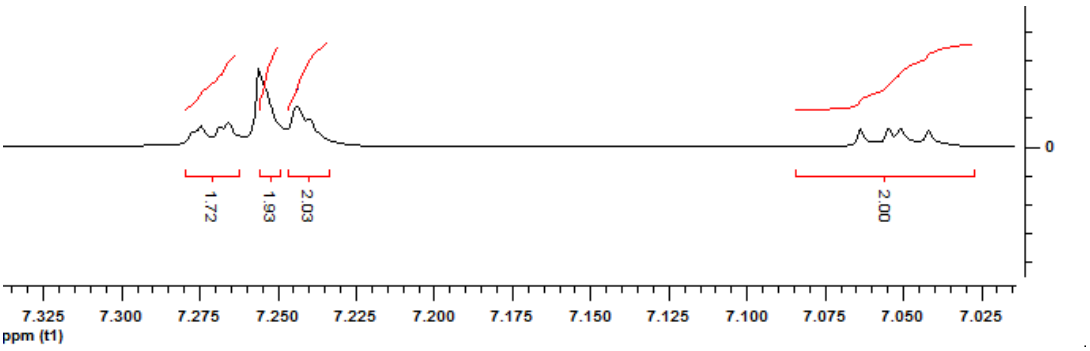

Figure A.19: ^{1}H-NMR data of 4,7-di([2,2'-bithiophen]-5-yl)-2-dodecyl-2H-benzo[d] [1,2,3]triazole-aromatic region-2

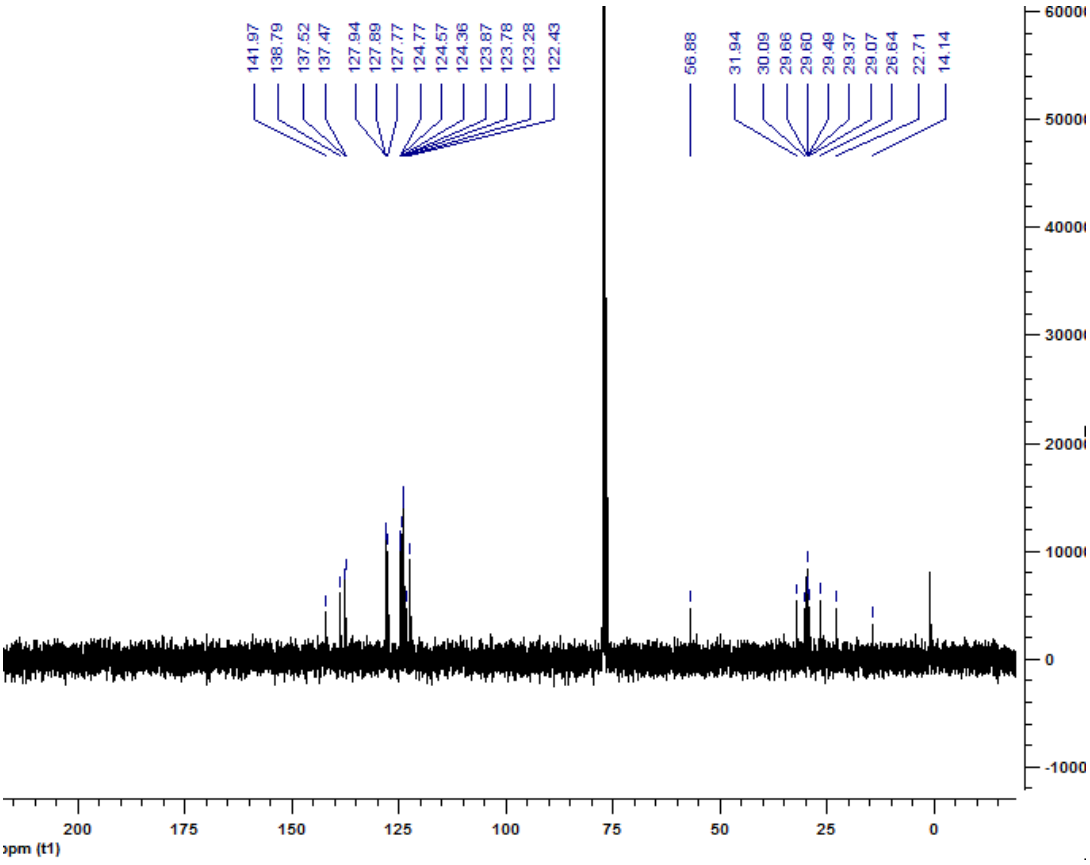

Figure A.20: ^{13}C-NMR data of 4,7-di([2,2'-bithiophen]-5-yl)-2-dodecyl-2H-benzo[d] [1,2,3]triazole

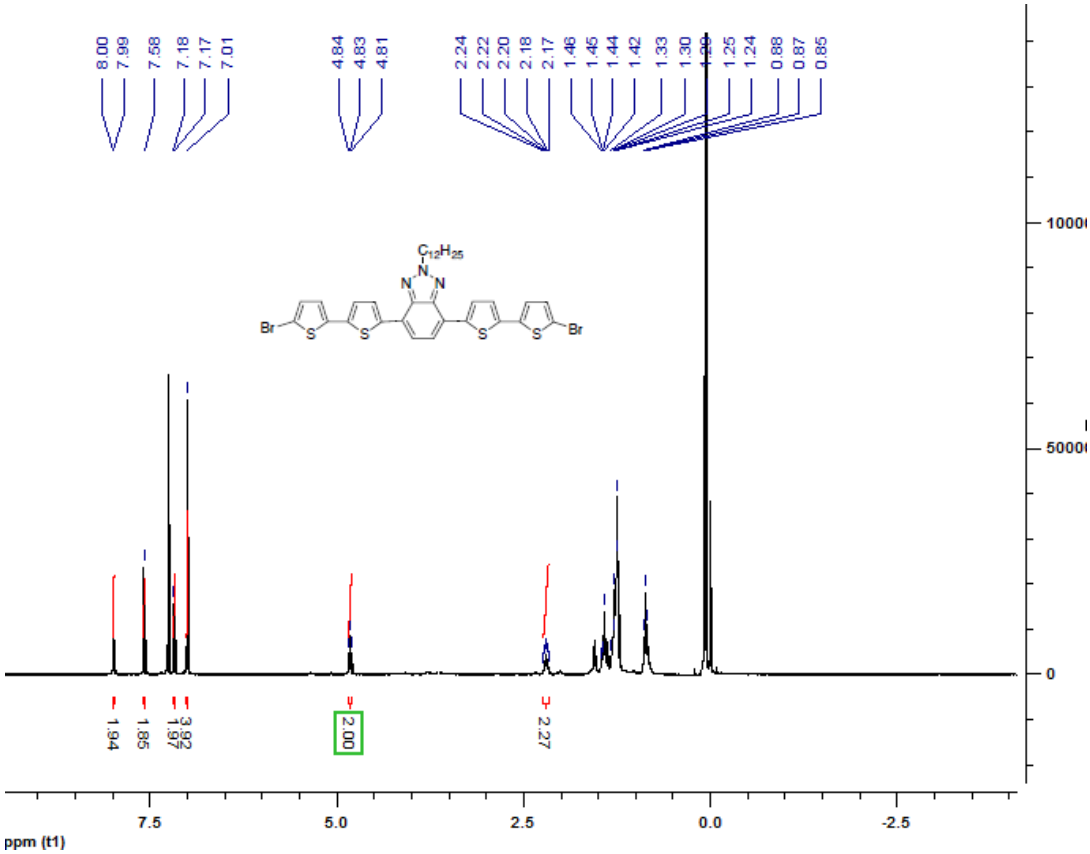

Figure A.21: ^{1}H-NMR data of 4,7-bis(5'-bromo-[2,2'-bithiophen]-5-yl)-2-dodecyl-2H-benzo[d][1,2,3]triazole

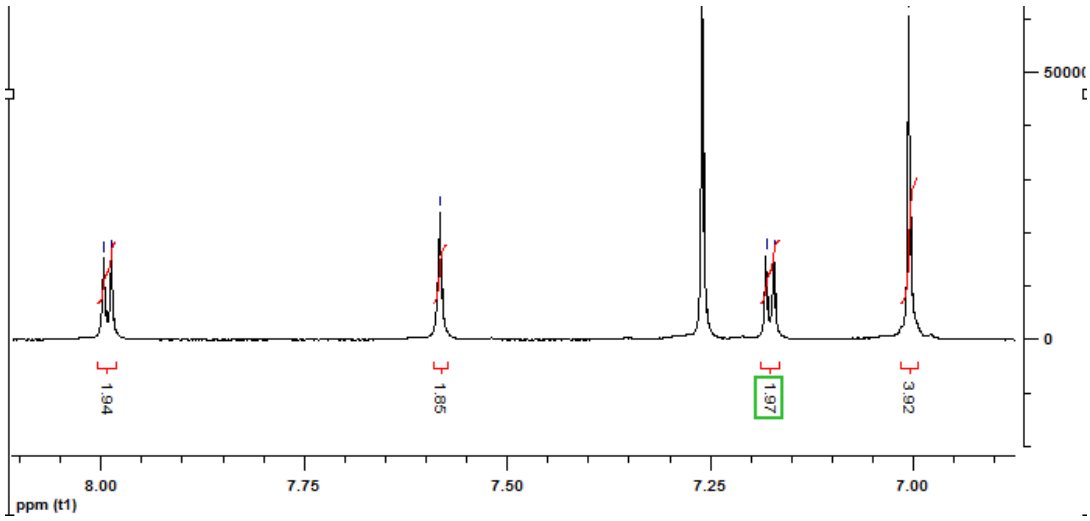

Figure A.22: ^{1}H-NMR data of 4,7-bis(5'-bromo-[2,2'-bithiophen]-5-yl)-2-dodecyl-2H-benzo[d][1,2,3]triazole-aromatic region

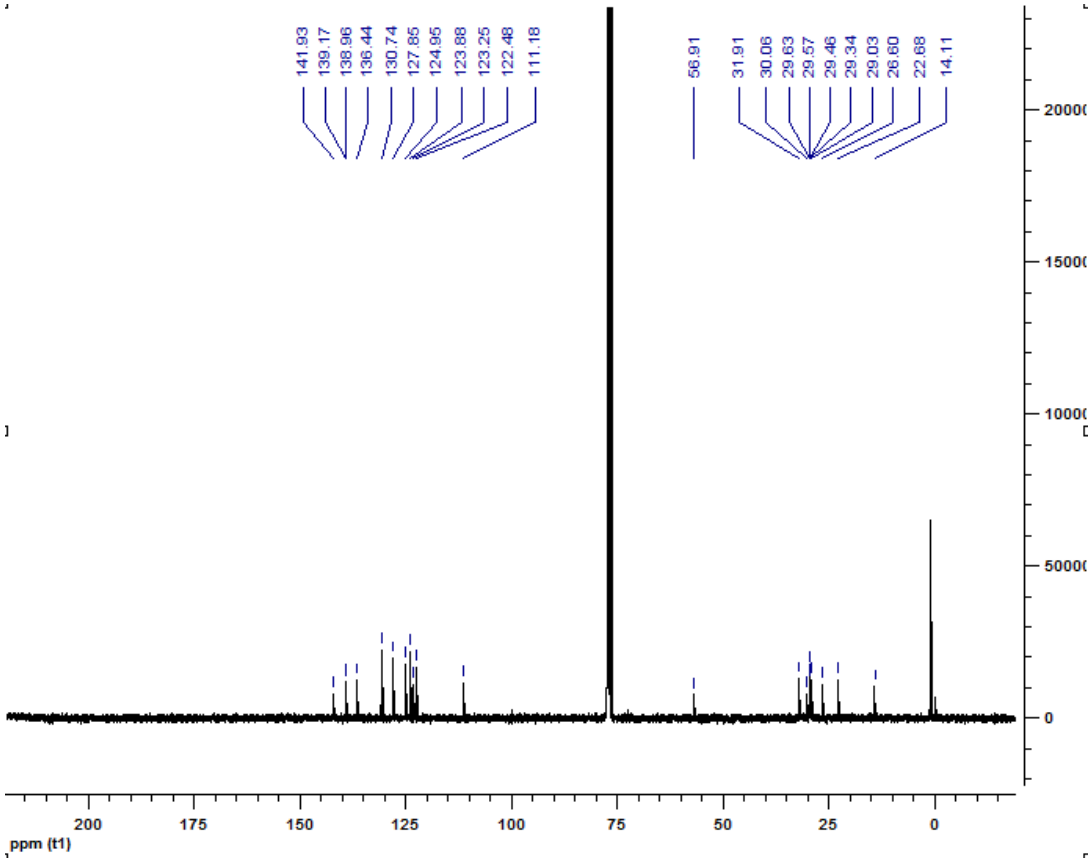

Figure A.23: ^{13}C-NMR data of 4,7-bis(5'-bromo-[2,2'-bithiophen]-5-yl)-2-dodecyl-2H-benzo[d][1,2,3]triazole

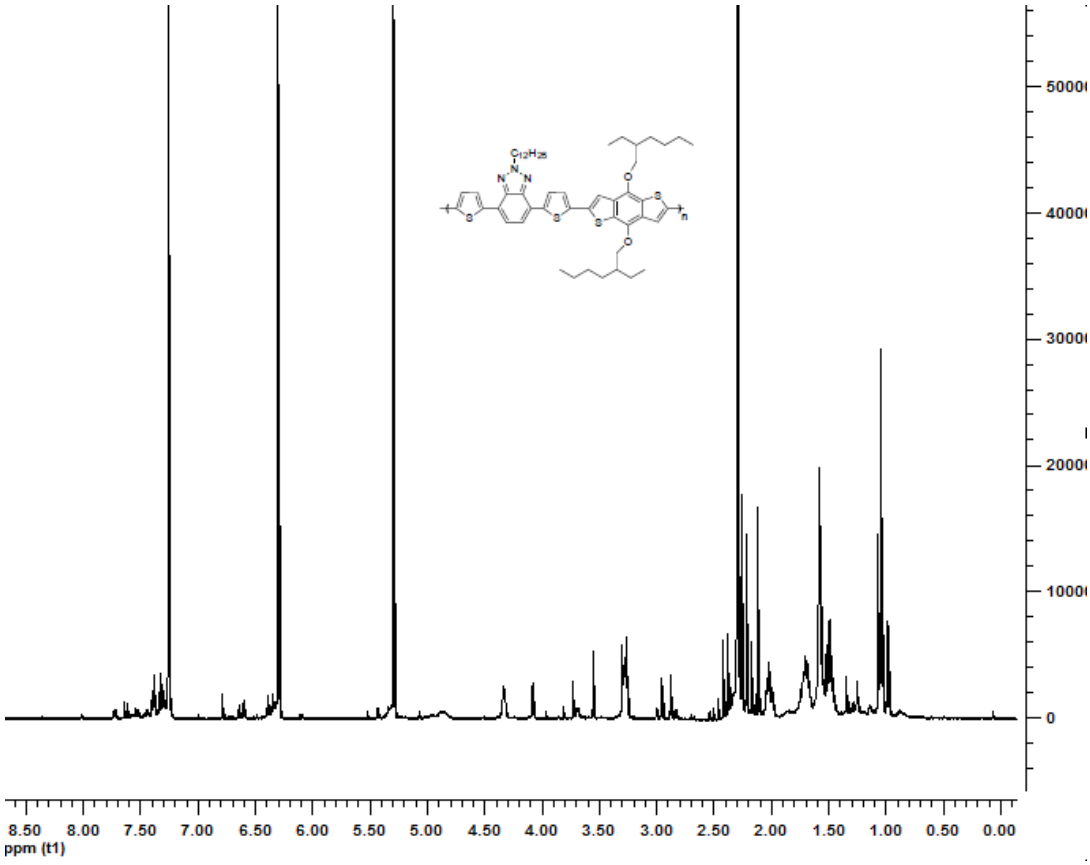

Figure A.24: ^{1}H-NMR data of poly(4-(5-(4,8-bis((2-ethylhexyl)oxy)-6-methylbenzo[1,2-b:4,5-b']dithiophen-2-yl)thiophen-2-yl)-2-dodecyl-7-(5-methylthiophen-2-yl)-2H-benzo[d][1,2,3]triazole).

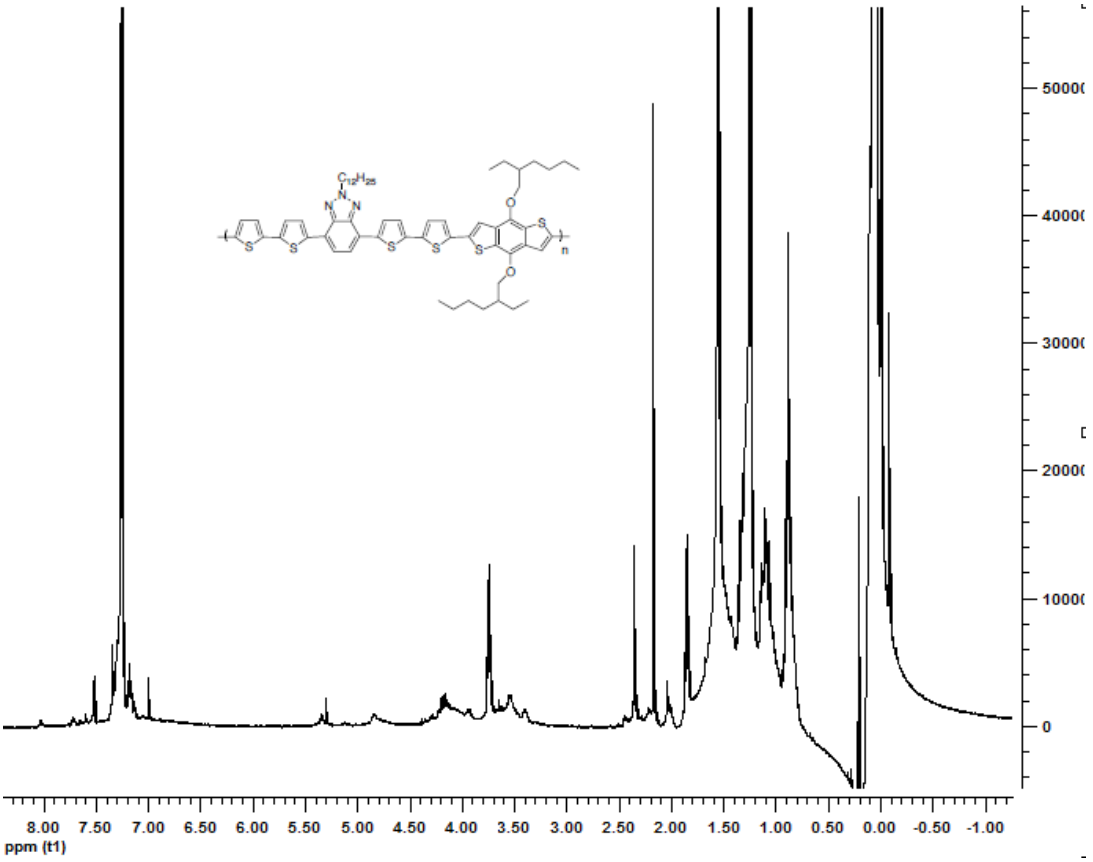

Figure A.25: ^{1}H-NMR data of poly(4-(5'-(4,8-bis((2-ethylhexyl)oxy)-6-methyl-benzo[1,2-b:4,5-b']dithiophen-2-yl)-[2,2'-bithiophen]-5-yl)-2-dodecyl-7-(5'--methyl-[2,2'-bithiophen]-5-yl)-2H-benzo[d][1,2,3]triazole).